ISTANBUL TECHNICAL UNIVERSITY ★ GRADUATE SCHOOL OF SCIENCE ENGINEERING AND TECHNOLOGY

STABILITY ANALYSIS OF CEMENTED SOIL SLOPES IN A GEOTECHNICAL CENTRIFUGE

M.Sc. THESIS

Hesam EBRAHIMISADR

Department of Civil Engineering

Soil Mechanics and Geotechnical Engineering Programme

JUNE 2020

ISTANBUL TECHNICAL UNIVERSITY ★ GRADUATE SCHOOL OF SCIENCE ENGINEERING AND TECHNOLOGY

STABILITY ANALYSIS OF CEMENTED SOIL SLOPES IN A GEOTECHNICAL CENTRIFUGE

M.Sc. THESIS

Hesam EBRAHIMISADR
(501161324)

Department of Civil Engineering

Soil Mechanics and Geotechnical Engineering Programme

Thesis Advisor: Assist. Prof. Dr. Berrak TEYMÜR

JUNE 2020

İSTANBUL TEKNİK ÜNİVERSİTESİ ★ FEN BİLİMLERİ ENSTİTÜSÜ

ÇİMENTOLU ZEMİN ŞEVLERİN GEOTEKNİK SANTRİFÜJ İLE STABİLİTE ANALİZİ

YÜKSEK LİSANS TEZİ

Hesam EBRAHIMISADR
(501161324)

İnşaat Mühendisliği Anabilim Dalı

Zemin Mekaniği Ve Geoteknik Mühendisliği Programı

Tez Danışmanı: Dr. Öğr. Üyesi Berrak TEYMÜR

HAZİRAN 2020

Hesam Ebrahimisadr, a M.Sc. student of ITU Graduate School of Science Enngineering and Technology student ID 501161324 successfully defended the thesis/dissertation entitled "STABILITY ANALYSIS OF CEMENTED SOIL SLOPES IN A GEOTECHNICAL CENTRIFUGE", which he prepared after fulfilling the requirements specified in the associated legislations, before the jury whose signatures are below.

Thesis Advisor :	**Asst. Prof. Dr. Berrak TEYMÜR** Istanbul Technical University	.....
Jury Members :	**Prof. Dr. Aykut ŞENOL** Istanbul Technical University	.....
	Asst. Prof. Dr. İ. Zeynep YILDIRIM Boğaziçi University	.....

Date of Submission : 12 June 2020
Date of Defense : 16 July 2020

To my family,

FOREWORD

I would like to express my gratitude to my Advisor Assis. Prof. Dr. Berrak Teymür, who supported me heartedly during my education at Istanbul Technical University. I would like to thank for her guidance, encouragement and valuable advices. This dissertation is a product of her confidence.

I would like to extend my special thanks to Prof. Dr. Eng- Wei Wu at University of Natural Resources and Life Sciences, Vienna, for his kindness, support, valuable advices and comments during my stay at this university for completing all experiments of this dissertation.

I would like to thank Martin Grogger and Dipl.-Ing. Dr. Markus Rauchecker for their kind assist and support during performing the experiments of my thesis at University of Natural Resources and Life Sciences, Vienna.

I also express my warm thanks to dear Jenny Lilian Allen, Secretary of Institute of Geotechnical Engineering and Mag. Ulrike Piringer, Coordinator of incoming students for their support during my stay at this university. I will never forget your kindness.

Last but not least, I offer my best regards and blessings to my family especially my dad, YAGHOUB EBRAHIMISADR, who always supported me during my life. Without you it would not have been possible for me to arrive at this stage. I owe this dissertation to your confidence and your never-ending support.

June 2020

Hesam EBRAHIMISADR
(Civil Engineer)

TABLE OF CONTENTS

FOREWORD ..... **ix**
TABLE OF CONTENTS ..... **xi**
ABBREVIATIONS ..... **xiii**
SYMBOLS ..... **xv**
LIST OF TABLES ..... **xvii**
LIST OF FIGURES ..... **xix**
SUMMARY ..... **xxiii**
ÖZET ..... **xxv**
1. INTRODUCTION **1**
1.1 Purpose of Thesis 1
1.2 Sections of Thesis 2
1.3 Slope Stability Analysis 2
1.3.1 Factor of safety 3
1.3.2 Critical slip surface 6
1.3.3 2D and 3D analyses 7
1. 4 Literature Review 8
1.4.1 Centrifugal studies 8
1.4.2 Non-centrifugal studies 15
2. GEOTECHNICAL CENTRIFUGE **19**
2.1 Introduction 19
2.2 Concept of Centrifuge Modelling 19
2.3. Scaling Rules of Centrifuge Modelling 20
2.4 Centrifuge Errors and Studying Scale Effect 22
2.4.1 Acceleration change error due to radius change 23
2.4.2 Soil particle size 25
2.4.3 Error of earth's 1g acceleration 25
2.4.4 Coriolis acceleration error 25
2.4.5 Error of gravitational acceleration direction unevenness 27
3. PARTICLE IMAGE VELOCIMETRY (PIV) **29**
3.1 PIV History 29
3.2 History of PIV Usage in Geotechnics 30
3.3 PIV Technique in Modelled Geotechnical Structures 32
3.3.1 Image texture 32
3.3.2 Particle Image Velocimetry 33
3.3.3 Centroiding 34
3.3.4 Close range photogrammetry 34
4. EXPERIMENTAL SETUP **37**
4.1 Description of IGT Beam Centrifuge 37
4.2 Model Box 39
4.3 Designing the Model 41
4.4 Soil 41
4.4.1 Soil 1 (S1) 41
4.4.2 Soil 2 (S2) 42
4.5 Sample Preparation 43
4.5.1 S1 sample preparation 43
4.5.2 S2 sample preparation 44

4.6 Slope Modelling 44
4.7 Instrumentation 45
4.8 Typical Test Procedure 46
5. RESULTS 53
5.1 Introduction 53
5.2 Experimental Results 53
5.2.1 Slopes with 70° inclination 54
5.2.2 Slopes with 90° inclination 74
5.3 Summary of Results 90
6. CONCLUSIONS AND RECOMMENDATIONS 93
6.1 Interpretation of the Results 93
6.2 Conclusions 95
6.3 Future Researches 96
REFERENCES 97
CURRICULUM VITAE 103

ABBREVIATIONS

CCD : Charge Coupled Device
DIN : Deutsches Institut für Normung (German Standards)
DPIV : Digital Particle Image Velocimetry
F_{2D} : Factor of Safety, Calculated By 3D Method
F_{3D} : Factor of Safety, Calculated By 3D Method
HPIV : Holographic Particle Image Velocimetry
LL : Liquid Limit
LSV : Laser Speckle Velocimetry
PDV : Particle Displacement Velocimetry
PIDV : Particle Image Displacement Velocimetry
PIV : Particle Image Velocimetry
PL : Plastic Limit
PLV : Pulsed Light Velocimetry
PPTV : Photogrammetric Particle Tracking Velocimetry
PSV : Particle Streak Velocity
PTV : Particle Tracing Velocimetry
S1 : Soil 1
S2 : Soil 2
USCS : The Unified Soil Classification System

SYMBOLS

a	: Centripetal acceleration
a_c	: Coriolis acceleration
c, ϕ	: Cohesion and Friction angle of soil
Cc	: Coefficient of Curvature
c_d, ϕ_d	: Cohesion and Friction angle on critical failure surface
Cu	: Coefficient of Uniformity
D	: Depth
Dr	: Relative density
e	: Void ratio
e_{max} ,e_{min}	: Maximum and Minimum Void ratio
F_c	: Factor of safety relative to cohesion
F_s	: Factor of safety
F_ϕ	: Factor of safety relative to friction angle
g	: Earth's gravitational acceleration
Gs	: Specific Gravity
H	: Height
h_m	: Height of model
h_p	: Height of prototype
r	: Radius
r_c	: Curvature radius
R_e	: Effective centrifuge radius
rpm	: Revolutions per minute
s	: seconds
SC	: Clayey sand
SP	: Poorly graded sand
u,v	: Displacement Vector Components
v	: Velocity
W	: Width
γ_d	: Dry unit weight
$\gamma_{d\,max}$, $\gamma_{d\,min}$	: Maximum and Minimum Dry unit weight
ρ	: Density
ρ_{max}, ρ_{min}	: Maximum and Minimum density
σ	: Mean effective stress

σ_v : Vertical stress

σ_{vm} : Vertical stress of model

σ_{vp} : Vertical stress of prototype

τ : Shear stress along the failure surface

τ_f : Soil shear strength

ω : Angular velocity

LIST OF TABLES

Page

Table 1.1 : Summary of characteristics of different slope modelled in a geotechnical centrifuge..... **9**
Table 1.2 : Results obtained from back-calculation of slope failure without rainfall, (Ling et al., 2009)..... **13**
Table 2.1 : Scaling factors for centrifuge modelling,(Schofield, 1981)..... **22**
Table 4.1 : Technical specifications of the geotechnical centrifuge at BOKU. **38**
Table 4.2 : Parameters of Soil 1. ..... **42**
Table 4.3 : Parameters of Soil 2. ..... **43**
Table 5.1 : List of the experiments..... **53**
Table 5.2 : The properties of experiment 1. ..... **54**
Table 5.3 : The properties of experiment 2. ..... **57**
Table 5.4 : The properties of experiment 4. ..... **62**
Table 5.5 : The properties of experiment 6. ..... **66**
Table 5.6 : The properties of experiment 9. ..... **70**
Table 5.7 : The properties of experiment 3. ..... **74**
Table 5.8 : The properties of experiment 5. ..... **78**
Table 5.9 : The properties of experiment 7. ..... **82**
Table 5.10 : The properties of experiment 8. ..... **86**
Table 6.1 : Summary of experiment results. **93**
Table 6.2 : Centrifuge test results in RPM. **94**

LIST OF FIGURES

Page

Figure 1.1 : Geometry used in slip circle analysis,(Abramson et al., 2002). **3**
Figure 1.2 : Forces acting on a slice of slope,(Tsuchida & Athapaththu, 2014)..... **5**
Figure 1.3: Concepts related to slip mass,(Seed et al., 1990). **6**
Figure 1.4 : Types of possible failures in a slope,(Han et al., 2004). **7**
Figure 1.5 : Variation of vertical settlement and lateral displacement,(Viswanadham and Mahajan, 2004)..... **10**
Figure 1.6 : Model embankment set up,(Kitazume and Takeyama, 2013). **11**
Figure 1.7 : Structural view of slope overlying smooth cambered bedrock,(Zhao et al., 2018). **13**
Figure 1.8 : Displacement vector plot of unreinforced slope,(Hayward et al., 2000). **15**
Figure 1.9 : Grading curve of the samples, (Daraei et al., 2018). **16**
Figure 1.10 : Slope model,(Arya et al., 2018)..... **17**
Figure 1.11 : a) weakly; b) moderately cemented sand cliffs in northern California; and c) variably cemented sand cliffs in southern California,(Collins and Sitar, 2011). **18**
Figure 2.1 : Centrifuge modelling concept,(Taylor, 1995). **20**
Figure 2.2 : Object movement in a fixed circular orbit,(Hedayati, 2012)..... **21**
Figure 2.3 : Normal stress distribution in centrifuge model and prototype,(Taylor, 1995). **23**
Figure 2.4 : Comparison of stress variation by depth,(Taylor, 1995). **24**
Figure 2.5: Coriolis acceleration due to particle movement with $\nu *$ velocity beside angular velocity,(Hedayati, 2012). **26**
Figure 2.6 : Radial acceleration field in centrifuge,(Hedayati, 2012)..... **27**
Figure 3.1 : Measurements of particle tracking of 2D unsteady flow around a cylinder by using cinematography,(Nayler and Frazer, 1917)..... **30**
Figure 3.2 : Modelled ground using aluminum rods before and after loading, (Yamamoto and Kusuda, 2001). **31**
Figure 3.3 : Principles of PIV analysis,(White and Take, 2002). **33**
Figure 3.4 : Information conversion from image space into real space,(White et al., 2003). **34**
Figure 4.1 : Schematic presentation of the centrifuge testing facility at BOKU,(Idinger, 2016). **37**
Figure 4.2 : Geotechnical centrifuge at BOKU..... **38**
Figure 4.3 : Model box mounted on swing basket. **39**
Figure 4.4: Sketch of the model box, including the imaging equipment with camera and light panels,(Idinger, 2016). **40**
Figure 4.5: Sketch of PIV-model assembly, top view,(Ertan, 2012). **40**
Figure 4.6 : Grain size distribution of Soil 1. ..... **41**
Figure 4.7 : Grain size distribution of Soil 2,(Barbir and Mathews, 2016). **42**
Figure 4.8 : Slope model in the box. **45**
Figure 4.9 : Black dots surrounded by white rectangular on plexiglass. **46**
Figure 4.10 : The LED panels on both sides of model box. **47**
Figure 4.11 : Assembling the digital camera in front of the model box. **47**
Figure 4.12 : Assembling two cameras on top of the model box for taking video. .. **48**
Figure 4.13 : Centrifuge control room. **49**

Figure 4.14 : Starting the centrifuge system. **50**
Figure 4.15 : PSRemote for taking the images during the test..... **51**
Figure 5.1 : Sketch of the slope models. **54**
Figure 5.2 : Soil model at a) start of the test, and b) maximum acceleration. **54**
Figure 5.3 : Vector field of soil displacement. **55**
Figure 5.4 : Contours of vertical and horizontal displacement. **56**
Figure 5.5 : Contours of shear strains at, a) maximum acceleration, and b) 60s before the maximum acceleration. **57**
Figure 5.6 : Soil model at a) start of the test, and b) maximum acceleration. **58**
Figure 5.7 : Vector filed of soil displacement. **59**
Figure 5.8 : Contours of vertical and horizontal displacement. **60**
Figure 5.9 : Contours of shear strains at, a) maximum acceleration, and b) 60 seconds before the maximum acceleration. **61**
Figure 5.10 : Soil model at a) start of the test, b) 10 seconds before the failure, and c) failure. **62**
Figure 5.11 : Vector field of soil displacement. **63**
Figure 5.12 : Contours of vertical and horizontal displacement. **64**
Figure 5.13 : Contours of shear strains at, a) 10s before the failure, and b) 60s before the failure. **65**
Figure 5.14 : Soil model at a) start of the test, b) 10 seconds before the failure, and c) failure. **66**
Figure 5.15 : Vector field of soil displacement. **67**
Figure 5.16 : Contours of vertical and horizontal displacement. **68**
Figure 5.17 : Contours of shear strains, 10 seconds, 60 seconds, and 240 seconds before the failure. **69**
Figure 5.18 : Soil model at a) start of the test, and b) maximum acceleration. **70**
Figure 5.19 : Vector field of soil displacement. **71**
Figure 5.20 : Contours of vertical and horizontal displacement. **72**
Figure 5.21 : Contours of shear strains at, a) maximum acceleration of 95g, b) 60s before maximum acceleration. **73**
Figure 5.22 : Soil model at a) start of the test, b) 10 seconds before the failure, and c) failure. **74**
Figure 5.23 : Vector field of soil displacement. **75**
Figure 5.24 : Contours of vertical and horizontal displacement. **76**
Figure 5.25 : Contours of shear strains at, a) maximum acceleration of 95g, and b) 60s before maximum acceleration. **77**
Figure 5.26 : Soil model at a) start of the test, b) 10 seconds before the failure, and c) failure. **78**
Figure 5.27 : Magnified vector field of soil displacement. **79**
Figure 5.28 : Contours of vertical and horizontal displacement. **80**
Figure 5.29 : Contours of shear strains at, a) 10s before the failure, and b) 60s before the failure. **81**
Figure 5.30 : Soil model at a) start of the test, b) 10 seconds before the failure, and c) failure. **82**
Figure 5.31 : Magnified vector field of soil displacement. **83**
Figure 5.32 : Contours of vertical and horizontal displacement. **84**
Figure 5.33 : Contours of shear strains, a) 10 seconds before the failure, and b) 60 seconds before the failure. **85**
Figure 5.34 : Soil model at a) start of the test, b) 10 seconds before the failure, and c) failure. **86**

Figure 5.35 : Magnified vector field of soil displacement. **87**
Figure 5.36 : Contours of vertical and horizontal displacement. **88**
Figure 5.37 : Contours of shear strains, a) 10 seconds before the failure, and b) 60s before the failure. **89**
Figure 6.1 : Variation of centrifuge acceleration for the tests 1 to 5. ..... **94**

STABILITY ANALYSIS OF CEMENTED SOIL SLOPES IN A GEOTECHNICAL CENTRIFUGE

SUMMARY

Slope stability is one of the major geotechnical problems. Civil engineers are always trying to increase the stability of soil slopes by different methods. One of the main stabilizers that has always been studied for stabilizing the geotechnical structures is cement.

Geotechnical centrifuge technology is a strong and successful method for physical modeling of slope. It provides the benefit of studying the slopes' failure mechanisms.

In this dissertation, slope models of cemented soils were tested in a geotechnical centrifuge to study the possible failure mechanism. The slope models' tests were conducted by varying slope inclination, soil type, relative density, and height of slope models. All the tests were conducted according to self-weight of the slopes by increasing the acceleration of geotechnical centrifuge. Acceleration was increased until the slope models failed. However, the maximum acceleration of centrifuge was 95g and in some tests, there was no failure. The cement content in all of the tests was 3 % of dry weight of soil. Images of slope models were taken during the tests (during flight) by a digital camera. Analysis of the images in order to evaluate the soil deformation were conducted by Particle Image Velocimetry (PIV) method.

Results of the experiments indicated that cement has a valuable effect on soil slope stabilization. Geotechnical centrifuge acceleration at failure was increased by adding 3% cement in all slope models. In addition, non-cemented slopes have failed catastrophically. It is rational to see that the required acceleration of the centrifuge at slope failure was decreased with increasing slope inclination. Increasing the height of the slope, resulted failure in slope at lower acceleration of geotechnical centrifuge.

According to results of image analysis, soil particle displacement and shear strain was much lower in cemented models than in non-cemented models. By adding 3% cement to soil slope models, amount of soil particle displacements was decreased from 18mm down to 2.5 mm. In slopes with 70º inclination, the location of the slope failures is not changing in cemented and non-cemented slope models. By increasing relative density, soil displacement and shear strain have reduced. In addition, by increasing the slope height and slope inclination, maximum displacements amount has increased. Furthermore, using PIV method along with geotechnical centrifuge tests was found very valuable and useful to study displacement and deformation behavior of the soil slopes.

ÇİMENTOLU ZEMİN ŞEVLERİN GEOTEKNİK SANTRİFÜJ İLE STABİLİTE ANALİZİ

ÖZET

Şev stabilitesi en önemli geoteknik problemlerden biridir. İnşaat mühendisleri her zaman farklı yöntemlerle yamaçların stabilitesini arttırmaya çalışırlar. Geoteknik yapıların stabilize edilmesi için her zaman kullanılan malzemelerden biri çimentodur.

Geoteknik santrifüj teknolojisi, şevin fiziksel modellenmesi için güçlü ve başarılı bir yöntemdir. Yamaçların yenilme mekanizmalarını incelemekte fayda sağlar.

Bu tezde, çimentolu zeminlerin şev modelleri, olası yenilme mekanizmasını incelemek için bir geoteknik santrifüjde test edildi. Şev modellerinin deneyleri, değişen şev eğimi, zemin tipi, rölatif sıkılık ve şev modellerinin yüksekliği ile yapılmıştır. Tüm deneyler, geoteknik santrifüjün ivmesini artırarak yamaçların kendi ağırlıklarının artması ile yapılmıştır. Şev modelleri yıkılana kadar ivme arttırıldı. Bununla birlikte, santrifüjün maksimum ivmesi 95g idi ve bazı testlerde yenilme meydana gelmedi. Tüm deneylerdeki çimento içeriği, zeminin kuru ağırlığının %3'ü idi. Şev modellerinin görüntüleri deneyler sırasında bir dijital kamera tarafından çekildi. Zemin deformasyonunu değerlendirmek için Tane Görüntüsünün Hızının Ölçülmesi (Particle Image Velocimetry (PIV)) yöntemi ile yapılmıştır.

Deneylerin sonuçları, çimentonun şev stabilizasyonu üzerinde değerli bir etkiye sahip olduğunu göstermiştir. Tüm şev modellerinde %3 çimento eklenerek geoteknik santrifüj ivmesi arttırılmıştır. Şev stabilitesi santrifüjün gerekli ivmesinin artan şev eğimi ile azaldığı görülmüştür.

Görüntü analizi sonuçlarına göre, çimentolu stabilize modellerde çimentolu olmayan modellere göre zeminin yer değiştirmesi çok daha azdı. Şev modellerine %3 çimento eklenerek, zemin yer değiştirme miktarı 18 mm'den 2.5 mm'ye düşürülmüştür. Ayrıca, PIV yöntemi ile birlikte geoteknik santrifüj testleri kullanılarak, şevlerin yer değiştirme ve deformasyon davranışını incelemek için çok yararlı bulunmuştur.

1. INTRODUCTION

The soil masses that stand with an angle to horizontal surface are soil slopes. These slopes could be natural or artificial. They could fail because of the factors like soil weight, existence of water, effect of external loads, decrease of strengths factors and etc.

All experiments explained in this thesis was conducted at Geotechnical laboratory of Bodunkultur University, Vienna.

To identify the possible failure mechanisms in this dissertation, cemented soil slopes are tested in a geotechnical centrifuge. The variables of this research are slope inclination, two different type of soils, relative density and height of the slopes. Centrifuge modeling and the PIV analysis is used in this study. The centrifuge modelling is a successful method in geotechnical engineering. The model must be evaluated in a gravity area N times greater than that of a prototype structure, in order to reproduce the gravity induced stresses of a prototype structure in a geometrically 1 / N reduced model.

1.1 Purpose of Thesis

The main purpose of this research work is to study the failure mechanism of cemented-soil slopes. The other objectives are:

- To study the cement effect on soil slope stability.
- To evaluate the PIV application in combination with centrifuge tests for sand and coarse-grained soils.
- To investigate the slope stability according to self-weight of the slopes.
- To calculate the slopes dimensions in critical condition (before the failure) according to acceleration of the geotechnical centrifuge.
- To evaluate the cemented soil in centrifuge scale.

- To compare the failure mechanism of the different slopes according to height, angle and soil type.

1.2 Sections of Thesis

In this research, all the slope models were built in the same strong and rigid box in this research. In the centrifuge, the slope models are placed on a swing-up basket and acceleration of the centrifuge increased until the failure of the models. The model box was rigid enough to provide the plane strain condition. Displacement and deformation of the slope models are examined with GeoPIV software. Images of the slope models are taken during the flight of geotechnical centrifuge. The intervals of images are 10 seconds. The images are used to study the failure mechanism of soil slopes.

This thesis consists of 6 sections.

Chapter 1 describes general information of slope stability analysis and literature review.

Chapter 2 explains geotechnical centrifuge, its usage in geotechnical engineering.

Chapter 3 explains the particle image velocimetry (PIV), that was used for image analysis in this study.

Chapter 4 consists of experimental setup and test procedure.

Chapter 5 explains results of tests and analysis. And;

Chapter 6 includes conclusions and recommendations regarding to results of the study.

1.3 Slope Stability Analysis

Slope stability analysis is one of the basic problems in soil mechanics and has vital importance in geotechnical engineering. Slope stability analysis is a process where safety of natural or artificial slopes (a slope that is created by excavation and embankment) is controlled. Slope stability analysis includes shear stresses calculation along the most critical and possible slip surface and is compared with soil shear strength. Slope stability analysis is difficult because of variables such as stratification and in-situ soil shear strength as well as groundwater condition and the critical slip surface. Factors that affect stability of soil slopes can be divided into two groups:

A. Factors that reduce the resistance

B. Factors that increase the forces

First group (A) includes increased soil water content (naturally like raining or artificially like water leakage from pipeline, duct and tanks) and excavation. Second group (B) includes earthquake or other dynamic forces, tectonic motions and loading.

1.3.1 Factor of safety

Factor of safety is critical in slope stability analysis. Generally, the final aim of slope stability analysis is to determine the factor of safety against slip and failure. According to different analysis methods, there are different definitions for factor of safety. The aim of factor of safety in all methods is same; that is, presenting shear stresses ratio in the most possible slip surface to soil shear strength.

Practically, slope stability analyses are based on Limit Equilibrium Theory (Abramson et al., 2002). Figure 1.1 presents the simplest geometry of slope analysis and factor of safety of this slope is obtained as equation 1.1.

$$F_s = \frac{\tau_f}{\tau} \tag{1.1}$$

F_s: Factor of safety

τ: Shearing stress along the assumed failure surface

τ_f: Soil shear strength

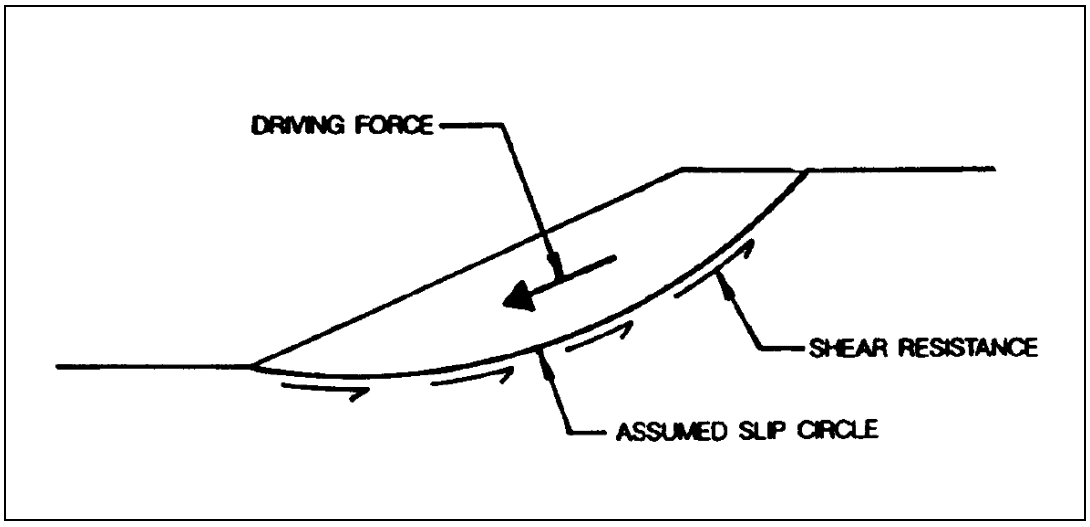

Figure 1.1 : Geometry used in slip circle analysis,(Abramson et al., 2002).

Soil shear strength based on Mohr–Coulomb equation includes cohesion and soil's internal friction angle and is obtained as equation 1.2.

$$\tau_f = c + \sigma \tan \phi \tag{1.2}$$

Where c is cohesion, ϕ is friction angle of soil and σ is mean effective stress on possible failure surface. Therefore, shear stress along possible failure surface is as equation 1.3.

$$\tau_d = c_d + \sigma \tan \phi_d \tag{1.3}$$

Where, c_d and ϕ_d are cohesion and internal friction angle along possible failure surface, respectively.

Replacing equations 1.2 and 1.3 in equation 1.1, equation 1.4 is obtained.

$$F_S = \frac{c + \sigma tan\phi}{c_d + \sigma tan\phi_d} \tag{1.4}$$

Other types of factor of safety are factor of safety relative to cohesion, F_c, and relative to friction angle, F_ϕ, which are defined in equation 1.5.

$$F_c = \frac{c}{c_d} \qquad F_\phi = \frac{tan\phi}{tan\phi_d} \tag{1.5}$$

Limit equilibrium methods currently are most used for slopes stability analysis. These methods consist of dividing the slope into fine slices,(Baba et al., 2012).

For design of the slopes by using limit equilibrium methods following steps are followed:

1. General shape of failure surface (planar, circle, non-circular) assumed.

2. Specific failure surface chosen.

3. Some or all of static equilibrium conditions used to compute equilibrium shear stress on failure surface, τ

I. $\Sigma Fx=0$

II. $\Sigma Fy=0$

III. $\Sigma M=0$

4. Available shear strength, along failure surface computed using Mohr-Coulomb failure criteria.

5. Factor of safety computed.

6. Back to step 2, continue until minimum factor of safety found.

Figure 1.2 presents a slope with height of H. A possible slip line is drawn in order to study slope stability by limit equilibrium; then stability conditions of slope over slip surface can be studied.

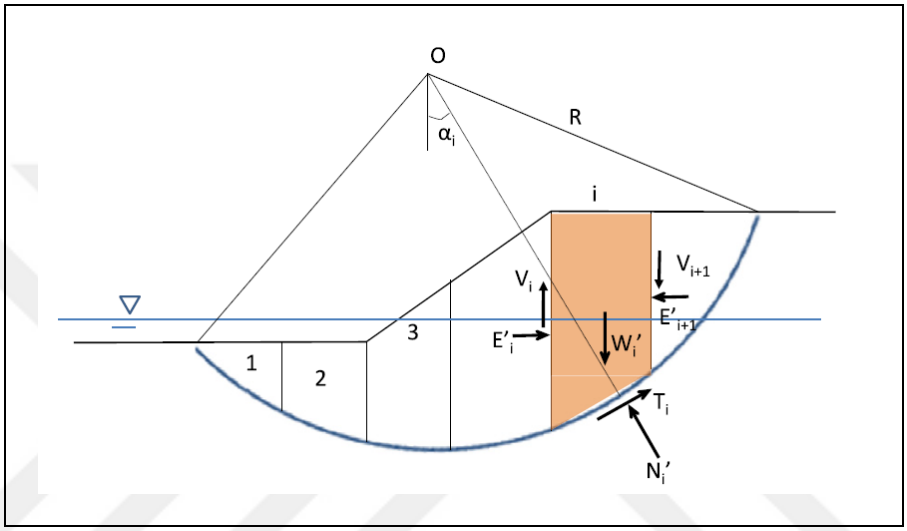

Figure 1.2 : Forces acting on a slice of slope,(Tsuchida & Athapaththu, 2014).

One of the most common methods of estimating factor of safety is to replace soil parameters (c and ϕ) with reduced values of c_d and ϕ_d. With reduced values, the slope reaches to failure. Commonly, factor of safety is considered relative to cohesion and friction angle, and then factor of safety is defined as equation 1.8.

$$F_s = \frac{c}{c_d} = \frac{tan\phi}{tan\phi_d} \tag{1.6}$$

Where F_s is factor of safety, c, ϕ are cohesion and internal friction angle of soil, and c_d, ϕ_d are cohesion and friction angle on critical failure surface.

The minimum factor of safety of different conditions depends on data accuracy and slope failure conditions. In addition, experience plays vital role.

Normally, the factor of safety of a slope, changes with various methods. This difference is due to hypotheses of various methods and difference between critical failure surfaces,(Duncan et al., 2014).

Seed et al. (1990) calculated factor of safety of various cross sections in order to analyze sliding land which occurred on Kettleman Hills in 1990; factor of safety of critical slip surface was between 1.1- 1.35, while factor of safety of small cross sections near the slope was 0.85.

1.3.2 Critical slip surface

One of the most important steps of slope stability analysis is to find a slip surface with the least factor of safety. This cross section is called critical slip surface and is considered circular or spiral for simplicity of calculations. The critical slip surface is obtained through changing radius and center of rotation. It must be mentioned that slope failure is not circular specially when soil mass is heterogeneous. Finding critical slip surface will be difficult, if its cross section is not considered circular.

The notable point is that slip surface does not follow a special rule in limit equilibrium method but follows special principles in limit analysis method. Most of methods that are based on limit equilibrium method, consider slip surfaces with specified shapes such as circular and logarithmic spiral. These hypotheses are for calculation simplicity. Figure 1.3 shows the concepts related to slip surface.

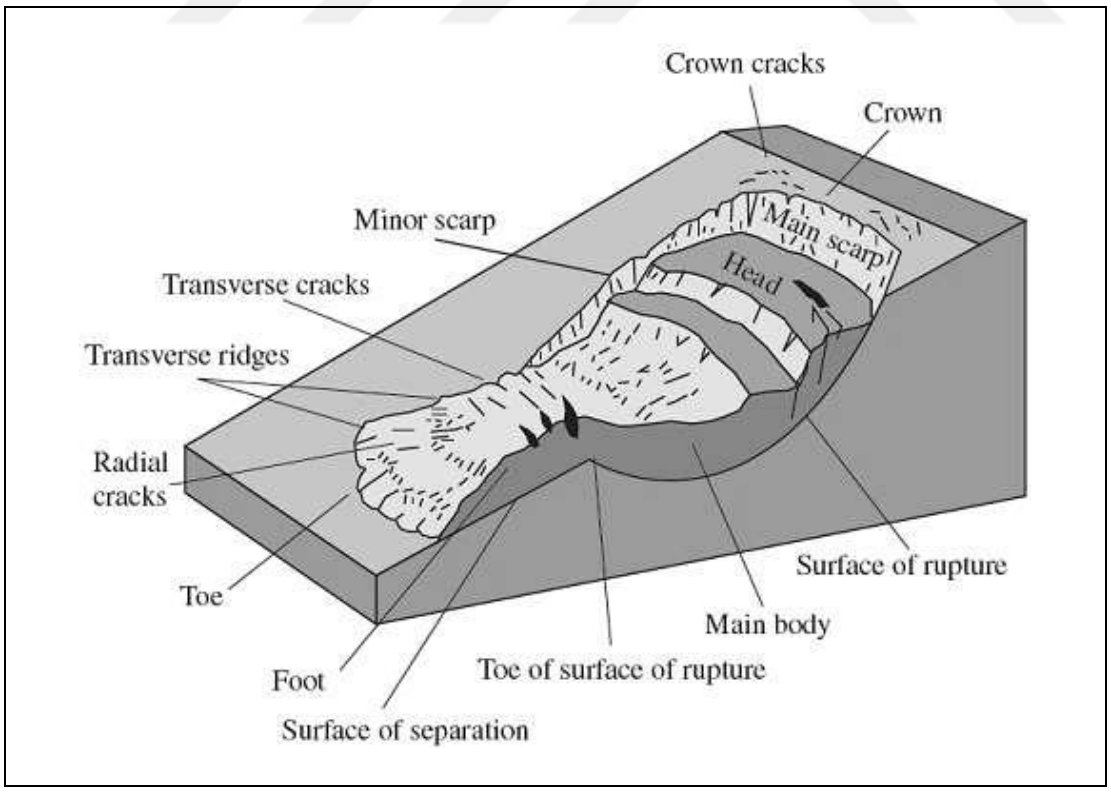

Figure 1.3: Concepts related to slip mass,(Seed et al., 1990).

Predicting slip surface is difficult due to uncertainties especially in three dimensional forms. If a limited slope width is considered, critical slip surface will not be matched and three- dimensional analysis is necessary. 3D slip surfaces can be created by using hypotheses of 2D slip surfaces. Types of failures in a slope are shown in Figure 1.4.

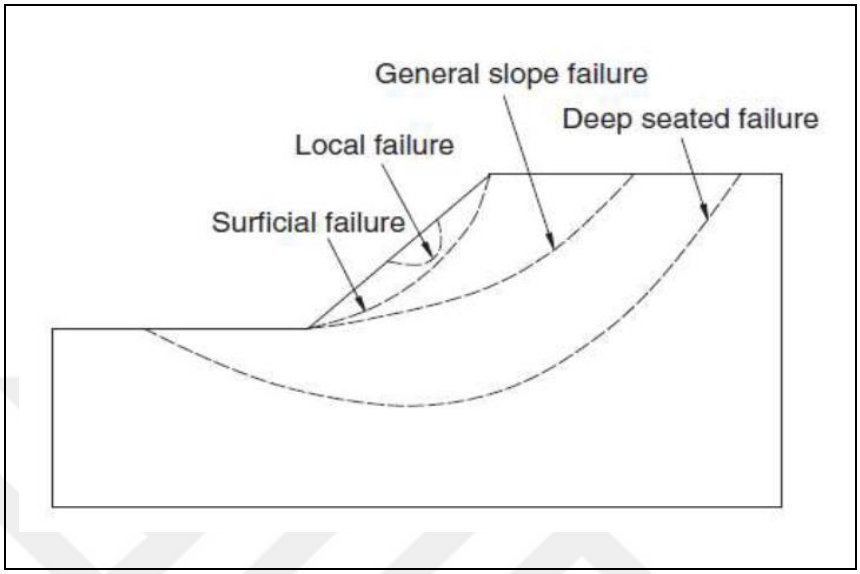

Figure 1.4 : Types of possible failures in a slope,(Han et al., 2004).

1.3.3 2D and 3D analyses

Generally, slope stability analyses are conducted two- dimensionally and plane strain, (Nasiri, 2015). 2D analyses are popular due to following reasons: providing conservative factor of safety, difficulty of working with 3D software, 3D data entry and data output. However, 2D analysis is not feasible for many cases and 3D analysis is necessary.

3D analysis of slope stability is done since 1970. These methods are based on limit equilibrium method.

Most of 3D slope stability analysis methods are proposed through generalizing 2D methods into 3D spaces. Expanding 2D methods into 3D methods will result in expanding restrictions of these methods in 3D spaces, (Hovland, 1978). On the other hand, complexity of expanding Spencer method by Chen and Chameau (1983) resulted in erroneous results; as a result, factor of safety, calculated using 2D methods were more than the one calculated by 3D methods,(Ugai, 1988).

It can be said that slope analysis methods that factor of safety, calculated by 3D methods are more accurate than the ones calculated by 2D methods. According to

Azzouz et al. (1981), factor of safety ratio, calculated by 3D method to 2D method (F_{3D}/F_{2D}) is between 1.07- 1.3 for slopes of undrained cohesive soil. The important point is that such results must not be generalized to other cases because of the limited number of studies.

The restrictions related to 3D analyzes do not diminish their importance and high accuracy, because rational and principal hypotheses of this analysis method are more valid than 2D one. Slope stability analysis must be conducted based on scientific background as well as ability of analyzing results. Practically, different methods provide different factor of safety. Comparing analysis results through field measurements instead of comparing factor of safeties can be acceptable criteria.

Different factor of safety results, achieved from various methods is because of difference between mathematical equations and simplifications used in these methods. Conclusions on difference between 2D and 3D analyses will be based on the fact that 2D analyses are conducted at critical cross section or for another cross section.

1. 4 Literature Review

When looking of previous studies, they can be divided into dynamic and static. Other classifications of slope stabilities are: failure due to self-weight of slope and due to loading, centrifugal and non-centrifugal condition, slopes with and without stabilizers.

The experimental studies of slope stability can be classified in three groups:

a) Physical modelling or 1g condition

b) Modelling by geotechnical centrifuge or Ng condition

c) Big scale modelling or prototype

1.4.1 Centrifugal studies

The centrifugal studies are discussed in this section. Table 1.1 shows the studies that were performed in geotechnical centrifuge on slopes.

Ling and Ling (2012) examined the landslides due to rainfall. For this purpose, they have considered a case study of landslide. The scale used is 1:100 and the slope real height is 27m. The results express the advantages of centrifuge modelling over 1g modelling. The most benefit is the ability to achieve the simulation of stress with field

condition in a prototype model. Generally, local failure has happened at the toe of the slope and cracks are created at the crest. During extreme rainfall events stable gentle slopes may become unstable.

Table 1.1 : Summary of characteristics of different slope modelled in a geotechnical centrifuge.

References	Soil Type	Reinforcement type	Slope inclination	Model Slope Height(cm)	Acceleration at Failure (g)	Specimen Preparation
(Ling & Ling, 2012)	Sand-clay	-	29°	27	100	Tamping (compaction)
(Viswanadham and Mahajan, 2004)	Sand	Geotextile	63.4°	27	15,25,40,45, 45,45	Air pluviation
(Viswanadham and Mahajan, 2007)	SP	Geotextile	63.48°, 79.58°	27	15,25,45,37, 12	Pluviation
(Li et al., 2013)	Sandstone and mudstone	Geosynthetic	1:075	37	20,50,80,100	-
(Kitazume and Takeyama, 2013)	Soft clay		1:1.5	15,9,3	Fixed at 50g	
(Aklik and Wu, 2009)	Standard Sand II (DIN 1164/58)	Geotextile	65°,75°, 85°	27	Increasing until failure	-
(Costa et al., 2013)	dry sand (SP), poor sand	Geotextile	-	-	20,19,21	Air pluviation
(Viswanadham and König, 2009)	Bochum sand	Non-woven geotextile	63.4°	27	fixed at 40g	Pluviation
(Zhao et al., 2018)	Silty clay	_	2:1 1:1	28	32,27,42.5,33,3 8,33,33.5	___
(Ling et al., 2009)	Sand, and sand mixed with fines	_	90°, 75°, 60°	10,15,20	10 to 182	Compaction at the optimum conditions
(Mandal et al., 2005)	Silty sand	Tire chips	D/H = 0.5 ,1, 2		130 to 145	
(Park and Kutter, 2012)	Clay	Cement	55°	-	Max g level:50	
(Luo et al., 2018)	Silty clay (CL-ML)	Geogrid	1:15	20	Fixed at 40g	Compaction
(Hayward et al., 2000)	Uniform clay	Pile/ without pile	1:2	10	Fixed at 60g	One-dimensional consolidation
(Ling et al., 2016)	Nevada Sand (fine sand)	Fiberglass mesh	Retaining Wall	32	Fixed at 50g (scale 1:50)	_
(Zornberg and Arriaga, 2003)	Sand	Geotextile	1H:2V	25.4	76.5 ,60 ,66 ,52.5	_
(White et al., 2003)	Clay	_	36°	9	60	_

SP: poor sand, H= Height (or opposite side) of a right triangle, V= adjacent side of a right triangle, x: y (ratio of height to adjacent side of triangle)

Six tests with the same slope heights of 27cm were performed by Viswanadham and Mahajan (2004). All the slopes were reinforced by 2 types of geotextile. The tests were performed based on self-weight of the slopes. The results demonstrate that there are 2 types of failure mechanism:

A) catastrophic failing due to breakup of reinforcement layers

B) progressive failing arising from heavy strain of wrapped geotextile reinforcement layers

It was found that the highest peak strain occurs at the mid height of geotextile slope. It means that the collapse of the reinforced geosynthetic slope is triggered from the mid height of it. Figure 1.5 presents the variation of vertical settlement and lateral displacement obtained from these experiments.

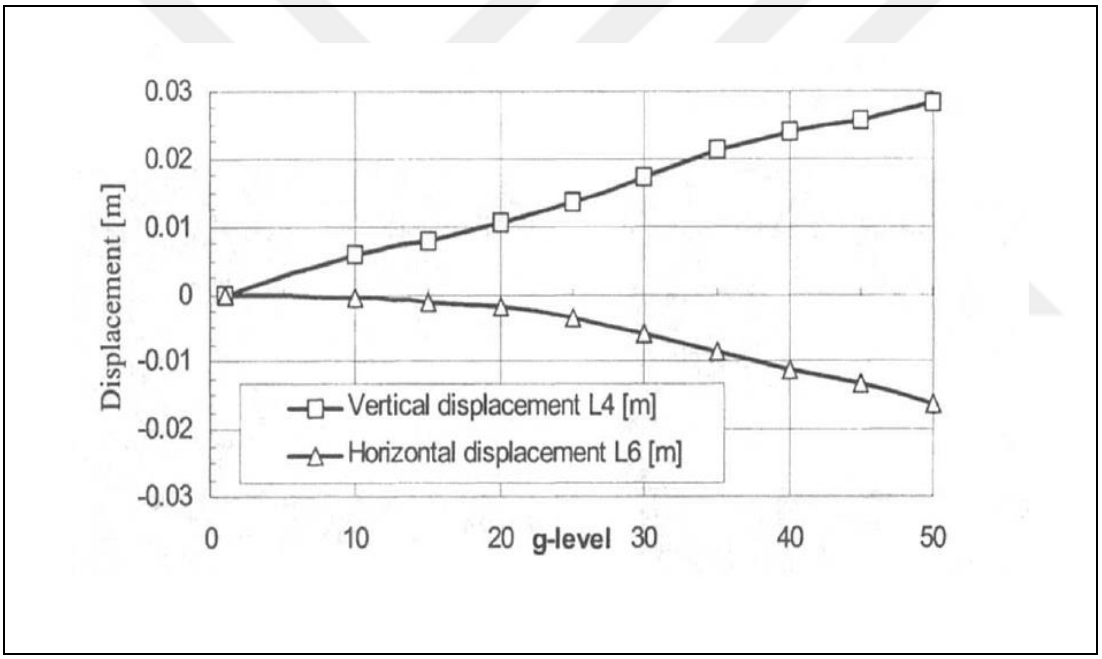

Figure 1.5 : Variation of vertical settlement and lateral displacement,(Viswanadham and Mahajan, 2004).

Viswanadham and Mahajan (2007) discusses the static reaction of geotextile-reinforced slopes over a solid foundation to the self-weight loading in a geotechnical centrifuge. The results prove the result of Viswanadham & Mahajan (2004) study about the maximum peak strain being in mid-height of the geotextile reinforced slopes. In addition, by increasing the slope inclination, maximum peak strain was increased and its position was moved from mid-height to downwards. Stability analysis confirmed the results of the centrifuge tests. Results show that the position of the failure surface and the position of the highest peak strain were not influenced by the

form of reinforcement or inclination of the slope. According to results, using digital image analysis technique is very useful and valuable beside geotechnical centrifuge tests to study displacement and deformation of the slopes.

Two types of test (with/without using geosynthetic) were performed by Li et al. (2013) for analyzing high steep slopes. They have done a 2-dimensional finite element method. On both reinforced and unreinforced slopes major horizontal displacements and mean stresses existed at the slope's toe. Horizontal displacements are comparatively less in reinforced slopes.

Kitazume and Takeyama (2013) studied slope's failure under embankment loading. To investigate the effect of slope's height on slope stability, experimental and numerical methods were done. The acceleration is fixed at 50g. Figure 1.6 shows the model set up of this research.

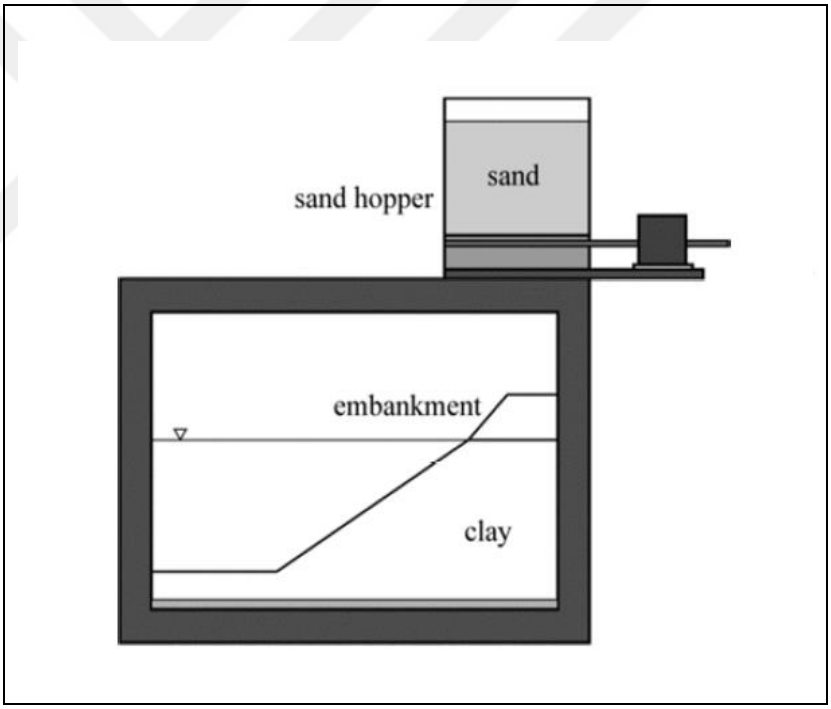

Figure 1.6 : Model embankment set up,(Kitazume and Takeyama, 2013).

The results indicate that deformation of clay slope is affected by the height of slope. By decreasing slope height, the embankment height at the failure was increased. Slope settlement grows slowly as the height of the embankment stays low, but progresses very quickly to collapse.

Aklik and Wu (2009) conducted model tests on foundation on geosynthetic reinforced slope. The tests were performed in IGT Beam Centrifuge of Universität für

Bodenkultur (BOKU) in Vienna. Standard Sand II (DIN 1164/58) was used in this research. Displacement analysis was performed by PIV analysis method. Results of 65º slopes indicate that in unreinforced slopes, failure surface passes through the slope toe, but in reinforced slopes, it is created in lower part of slope. The shear strains of 75º slopes particularly in front of the shear surface are more intense when compared with 65º slopes. In 85º slopes bigger shear strains were created in whole surface of the slope. According to conclusion the PIV is very useful for analyzing the deformation of model slopes in geotechnical centrifuge.

Geotextile-reinforced soil walls under stress were examined by Costa et al. (2013). In this research, dry poor sand was used for construction of the soil wall models. As models approach failure, the peak reinforcement strain distribution with the wall height implies load redistribution across reinforcement layers. This distribution appears to raise the difference between expected and experimental outcomes.

All tests of Viswanadham and König (2009) were performed in fixed acceleration at 40g to investigate influence of deformation of a foundation on the reinforced slope. There was no collapse in reinforced slopes with flexible facing even after the settlement of 1m in prototype. Using digital image analysis and Particle Image Velocimetry along centrifuge model tests was found very useful and practical to study behavior of the slopes.

Seven centrifuge tests were performed by Zhao et al. (2018) to investigate slope behavior on bedrocks. Three types of failure have occurred: a) sliding along the bedrock, b) failure within soil c) combination of a and b. The effect of bedrock was remarkable; because slip surface of pure soil slopes was much shallower in comparison to the slopes on the bedrock. Presenting bedrock influenced slopes deformation that caused change in the form of slip surface and slope's stability level. Figure 1.7 shows structural view of slope overlying smooth cambered bedrock.

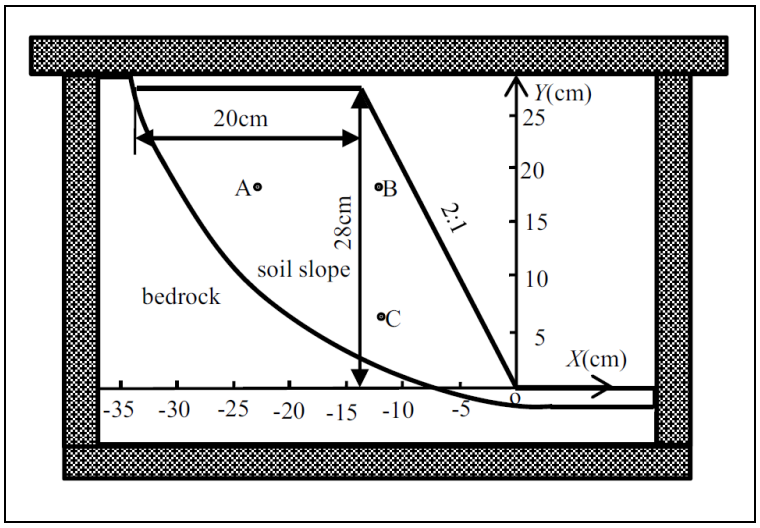

Figure 1.7 : Structural view of slope overlying smooth cambered bedrock,(Zhao et al., 2018).

Slopes with various inclinations, heights and soil types were examined by Ling et al. (2009). Other tests were performed for modelling rainfall with 60° slopes. As the full-scale models are not economic and are hard to perform, centrifuge tests for modelling slopes were found to be very useful and valuable. This modelling method was validated using slopes with various heights, properties and geometries. Table 1.2 shows the summary of the results from Ling et al. (2009).

Table 1.2 : Results obtained from back-calculation of slope failure without rainfall, (Ling et al., 2009).

Soil types	Slope angle i' (°)	Model height, H_m (cm)	Acceleration at failure, n (g)	Prototype height, $H=H_m \cdot n$ (m)	Apparent cohesion at $F_s=1$ c^* (kPa)	Stability number $N^*=c^*/\gamma H$
Pure sand (γ_t=17.56 kN/m^3)	90	10	24.31	2.421	5.95	0.140
		15	19.07	2.854	7	0.140
		20	10.96	2.190	5.4	0.140
	75	10	27.76	2.767	3.5	0.072
		15	21.01	3.146	3.7	0.067
		20	14.28	2.853	3.5	0.070
	60	10	47.15	4.680	2.8	0.034
		15	45.37	6.773	4.1	0.034
		20	33.72	6.736	4.05	0.034
Sand with 15% fines (γ_t=19.4 kN/m^3)	90	10	31.62	3.142	8.1	0.133
		15	24.15	3.611	9.4	0.134
		20	19.29	3.851	9.8	0.131
	75	10	40.14	3.974	5.2	0.067
		15	37.11	5.527	7.2	0.067
		20	26.07	5.196	6.8	0.067
	60	10	108.00	10.684	6.1	0.029
		15	92.73	13.791	8	0.030
		20	48.75	9.699	5.5	0.029
Sand with 30% fines (γ_t=20.67 kN/m^3)	90	10	66.04	6.497	19.7	0.147
		15	56.78	8.457	25.6	0.146
		20	29.34	5.838	17.7	0.147
	75	10	113.51	11.237	18.8	0.081
		15	89.84	13.352	22.3	0.081
		20	81.78	16.319	27.6	0.082
	60	15	181.83	26.923	22	0.040
		20	149.93	29.690	24.2	0.039

Mandal et al. (2005) investigated the slope stability of unreinforced slopes and slopes reinforced by tire chips (that were constructed from waste tire). Different D/H ratios were examined by centrifuge tests; where D is depth of foundation soil and H is height of the slope. According to results by increasing tire chips the factor of safety and shear strength parameters were increased. There was no failure in the slopes, only settlement was observed. The settlement was more in unreinforced slopes in comparison to reinforced slopes.

Park and Kutter (2012) investigated cemented clay slopes by performing seven centrifuge tests. High plasticity clay with cement amount of 3% to 5% and low plasticity clay with cement amount of 0 to 2% was used for construction of the models. Both static and dynamic tests were accomplished in this research. The results indicate that physical modeling of cemented clay slopes can simulate sensitive clay beaviour. There was one slip surface in static tests, however multiple slip surfaces have occurred in dynamic ones.

Slope and superstructure reaction under differential settlement were examined by Luo et al. (2018). Unreinforced and reinforced slopes were studied. The superstructural foundation pressure is fixed at 40 kPa. The slope displacement has occurred only in a small area, near to the vertical path. The differential settlement caused the slope to fail. The bottom ends of every slope's slip surface were exactly positioned at the edges of the subsidence zone.

Hayward et al. (2000) examined use of single row of piles in slope stability by performing four centrifuge tests. The tests were performed in fixed acceleration of 60g for the period of 20 hours. According to the scale which is 60, 20 hours means 3000 days at prototype scale. According to results, installing separate piles can help to stabilization of the slopes. Unreinforced slopes and slopes that were reinforced by 2 piles have failed. There was no failure in slopes which were reinforced by 3 or 4 piles. Three-dimensional finite element analyses and slope stability analysis program Slope/W were carried out to see the behavior of the slopes. The numerical methods were not successful in comparison to experimental results. Figure 1.8 shows displacement vector plot for unreinforced slope.

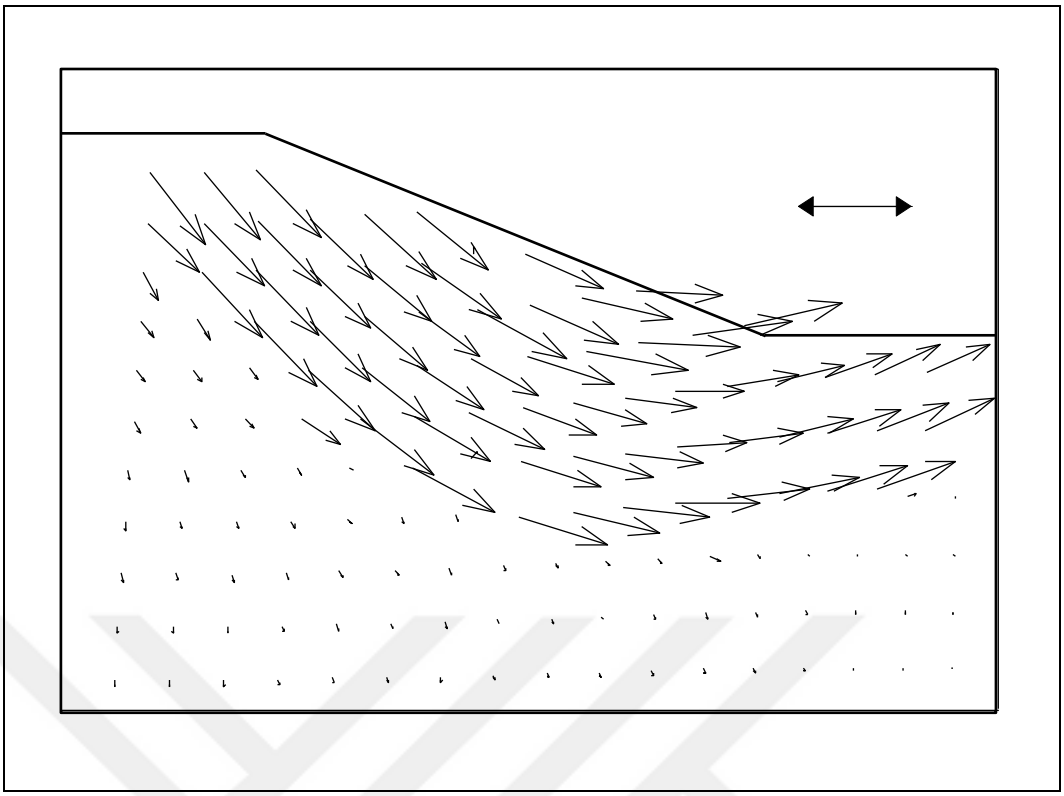

Figure 1.8 : Displacement vector plot of unreinforced slope,(Hayward et al., 2000).

Ling et al. (2016) studied the reinforced soil retaining wall with scale of 1:50 under acceleration of 50g in a geotechnical centrifuge. After reaching full height of prototype none of the models were failed. The cracks in models were shallow and superficial.

According to results of a research that were studied by Zornberg and Arriaga (2003), the maximum peak strain in geotextile reinforced slopes, is not near the slope's toe. It has occurred at mid-height of the reinforced slopes.

1.4.2 Non-centrifugal studies

Evirgen et al. (2017) has done both numerical and experimental study under 1g condition. Numerical study was carried out in PLAXIS software. After physical modelling of clayey sand slope, a static load was placed on the slope until failure. Bearing capacity and settlement of the slopes were examined. All slopes have 20cm height and inclination of 90º with the concrete face. The slope's height was considered 5m in numerical study. The unreinforced slopes and slopes reinforced by geotextile, geogrid, steel strip, were investigated. The model was constructed by compacting the soil. Results indicate that unreinforced slopes have collapsed under the 0.86 kg/cm^2 low stress condition with toe circle form of failure mechanism. By using steel strips

and geogrids, related stress level was raised about 10 times. At failure, the vertical and horizontal unreinforced slope displacements were 6.2 mm and 4.2 mm, respectively.

Daraei et al. (2018) investigated slope stability of expansive soils by using cement grout, which was a case study by performing laboratory tests and numerical analysis. The cement grout with water-cement ratio of 1:1 was prepared with amounts of 2%,4% and 6% of weight of dry soil. The results indicate that by injecting 2% cement grout, compressive strength of the soil has raised from 0.16 to 0.67 MPa; and with injection of 6% cement, soil swelling was reduced by 90%. Uniaxial compressive strength of the soil has increased by 2.2 times after adding cement grout. Figure 1.9 shows the grading curves of the samples.

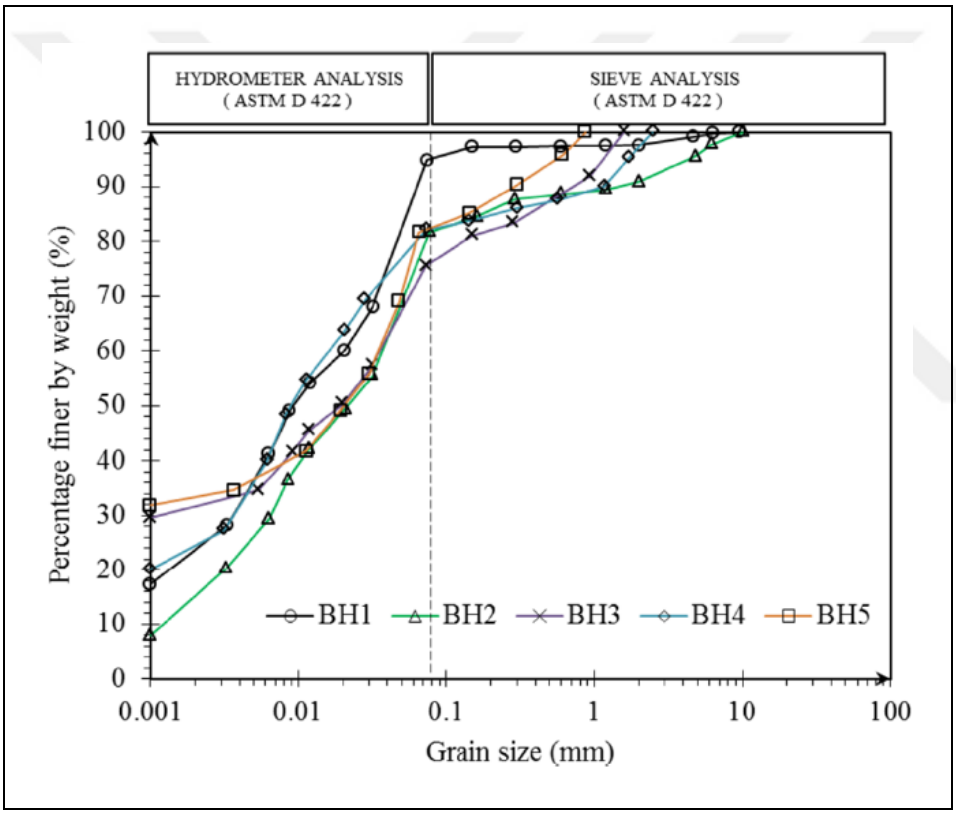

Figure 1.9 : Grading curve of the samples, (Daraei et al., 2018).

Arya et al. (2018) has done an experimental study in 1g condition that investigates the sandy soil slope stability by injecting cement with various interval distance of injection points. The load was applied on the model up to failure. According to results, shear strength of the soil was increased after injecting the cement. Furthermore, factor of safety was increased from 078 up to 1.17 for the cement-injected soils. Figure 1.10 shows the slope model used in the study.

Figure 1.10 : Slope model,(Arya et al., 2018).

Collins and Sitar (2011) have done an analytical research that investigates how cementation ratio influence the development of steep sandy slopes. The results clarify that for identifying the failure mode characteristics, knowledge about slope geometry is significant. According to analysis using standard Culmann method for modelling the steep cemented sand slopes is not appropriate; because this method overestimates the crest reaction and underestimates angle of failure plane. A simplistic analysis utilizing infinite slope principles when extended to a slope with finite dimensions subject to altering geometric circumstances, is recommended for study of steep cemented sand slopes. Because of their high cementation power, moderately cemented sands can create steeper slopes and cliffs in comparison to weakly cemented ones, where the possible mode of collapse is a result of tensile stress instead of shear stress. Figure 1.11 is the example of weakly, moderately and variably cemented sand cliffs.

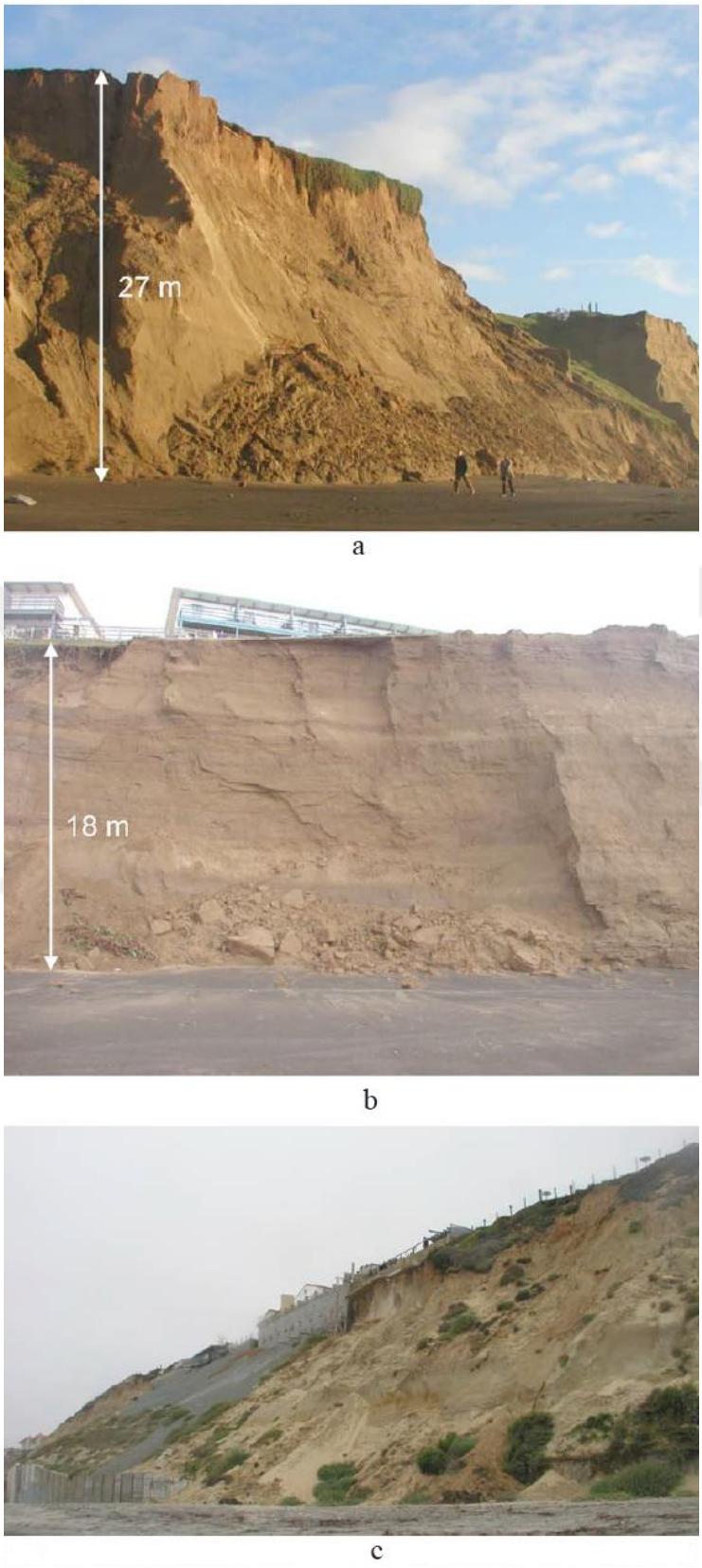

Figure 1.11 : a) weakly; b) moderately cemented sand cliffs in northern California; and c) variably cemented sand cliffs in southern California,(Collins and Sitar, 2011).

2. GEOTECHNICAL CENTRIFUGE

2.1 Introduction

Designing the engineering structures is not possible without recognition of behavior of them. The purpose of modelling is guessing the behavior of the structure before (or during) the construction of it. The modelling can be analytical, numerical and physical.

Since physical modelling is used in this thesis, in beginning of this chapter the concept of centrifuge modelling has been described. In addition, the errors of this method have been explained.

2.2 Concept of Centrifuge Modelling

One of the significant research tools in geotechnical engineering is physical modelling. The model has to be scaled and sometimes the model response can be totally different than prototype response. For this reason, it is necessary to examine the effect of scaling in all of the modelling studies.

Since geotechnical structures often have big dimensions, errors of modelling (scaling effect) are remarkable. On the other hand, nature of geotechnical structures is added to this problem which depends on stress; they behave differently based on stress level. If the stress conditions of corresponding points of model and prototype are aligned, scale effect errors will be minimized. Geotechnical centrifuge is a device that satisfies reduced stress of small prototype through increasing gravitational acceleration. The linear dimensions (l/N) of a model are reduced based on the ratio of gravitational acceleration to earth's gravitational acceleration (N).

Centrifuges create high acceleration field. If a model rotates within radius, r and angular velocity of ω, in rad/sec, its radial acceleration will be $r\omega^2$ and $N= r\omega^2/g$, where g is earth's gravitational acceleration. The idea was proposed for the first time by Bucky (1931) in Colombia and Pokrovsky (1932) in Russia and then was used in different research centers. Model testing by centrifuge is a powerful tool for geotechnical engineering, since it makes possible analysis using geotechnical materials and provides special loading environment where soil samples are tested. Centrifuge is able to create a behavior of model’s materials where stress distribution in model and prototype are equal. Both model and prototype must behave similarly,

and this similarity is based on scaling rules. If the prototype or similar soil is used in the model and the sample is prepared accordingly, then the model experiences the same history of prototype. The model soil is chosen considering the particle size effect. Then centrifugal acceleration of N equal to earth's gravitational acceleration is applied and, vertical stress at model depth of (h_m) will be $h_p=N.h_m$, where $h_{p\ is}$ depth of prototype. This is the main rule of centrifugal modeling.

Two main problems of centrifuge modeling are scaling rules and scaling errors. Scaling rules can be obtained using dimensional analysis or differential equations.

Sometimes, centrifuge modeling is criticized for scaling errors and difficulty of modelling with all the details. It is clear that restrictions of any modeling methods need to be accepted and considered. Figure 2.1 illustrates concept of centrifuge modelling.

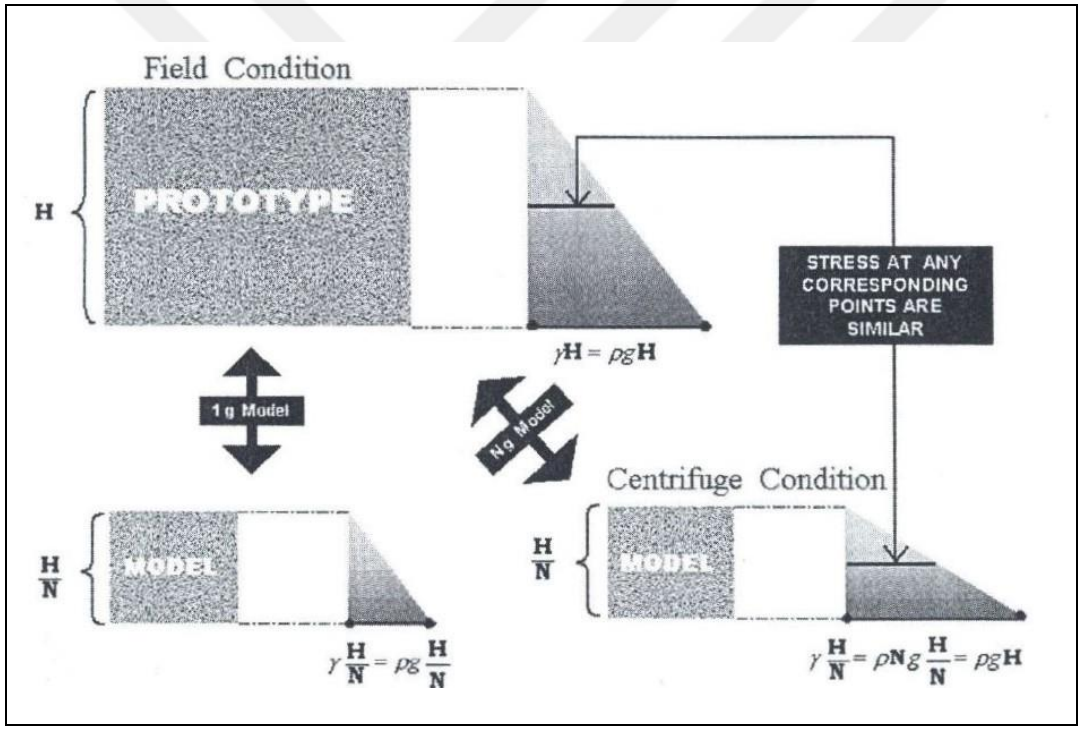

Figure 2.1 : Centrifuge modelling concept,(Taylor, 1995).

2.3. Scaling Rules of Centrifuge Modelling

The mechanical theory of centrifuge modelling is simple. If a body circulates with mass of m in a fixed radius of r around an axis, with velocity of v (Figure 2.2), to fix it in a circular axis, radial acceleration of v^2/r or $r\omega^2$ (ω is angular velocity), which tries to throw body out of axis, has to be overcome. In other words, a radial force of $r\omega^2$ must be applied to center of the body.

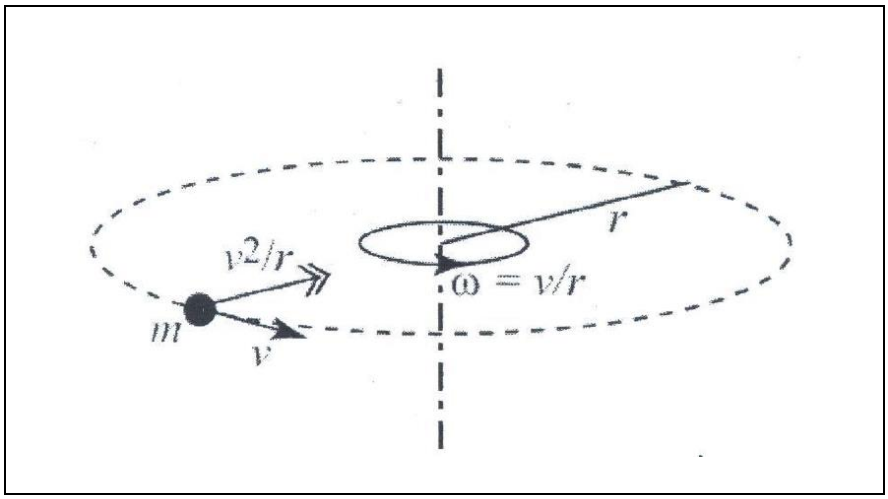

Figure 2.2 : Object movement in a fixed circular orbit,(Hedayati, 2012).

Physical model tests in centrifuge provide powerful tools for geotechnical engineers in order to study, analyze and design geotechnical structures. In fact, modeling is simulation of prototype through downsizing with certain ratio in order to study real response of the prototype.

It is essential to examine scale effect on models in order to solve the problems. Scaling rules of model include: 1. dimensional analysis method, like fluid mechanics 2. studying differential equation of problem. Some of modeling scale rules in centrifuge will be explained. It must be mentioned that two scale errors are significant in centrifuge modeling: a. Non-uniform acceleration field error (or function of radius) in centrifuge b. errors of inability to model in full detail and very small scale in centrifuge.

The main scaling rule is obtained when the stresses are similar between model and prototype. If an acceleration of N that is equal to earth's gravitational acceleration is applied to a material with density of ρ, at depth of h_m in model (subscript m is for the model), then vertical stress σ_v will obtained by equation 2.1.

$$\sigma_{vm}=\rho N g h_m \tag{2.1}$$

And in prototype, it will be obtained by equation 2.2. subscript p is for the prototype.

$$\sigma_{vp}=\rho g h_p \tag{2.2}$$

Therefore, to satisfy $\sigma_{vm}= \sigma_{vp}$, $h_m=h_p N^{-1}$ must be applied. As a result, scaling factor of $\left(\frac{model}{prototype}\right)$ will be $\frac{1}{N}$ for linear dimensions. Since, model is linear scaled of

prototype, then displacement will have scaling factor of $\frac{1}{N}$ and scaling factor of 1:1 will be obtained for strains. Table 2.1 shows scaling factors used in centrifuge modelling.

Table 2.1 : Scaling factors for centrifuge modelling,(Schofield, 1981).

Physical Value or Event	Dimension in Prototype	Dimension in Centrifuge Model at (N*g)
Gravity	1	N
Length	1	1/N
Displacement	1	1/N
Area	1	$1/N^2$
Volume	1	$1/N^3$
Stress	1	1
Strain	1	1
Force	1	$1/N^2$
Velocity	1	N
Acceleration	1	N^2
Mass	1	$1/N^3$
Energy	1	$1/N^3$
Density	1	1
Time (consolidation)	1	$1/N^2$
Frequency	1	N

2.4 Centrifuge Errors and Studying Scale Effect

Any modeling has advantages and disadvantages which lead to errors and reduced accuracy. Therefore, error sources must be determined and resolved in order to increase accuracy of results. In this section the most important error sources will be

introduced and their effects will be studied on model; in some cases, required actions will be provided in order to reduce their negative effects.

2.4.1 Acceleration change error due to radius change

In nature the Earth's radius is big compared to structure dimensions and soil layers depth. Therefore, earth's gravitational acceleration is considered constant for all soil layers and depths. In centrifuge modelling the applied centrifugal acceleration to different layers of model will change due to change of distance from rotational center (rotational radius). The reason is downsizing the dimensions and limited gyration radius in centrifuge modelling,(Hedayati, 2012). Applied acceleration in any point equals to $r\omega^2$, where r is rotational radius. Figure 2.3 shows vertical stress distribution (normal) of prototype and model.

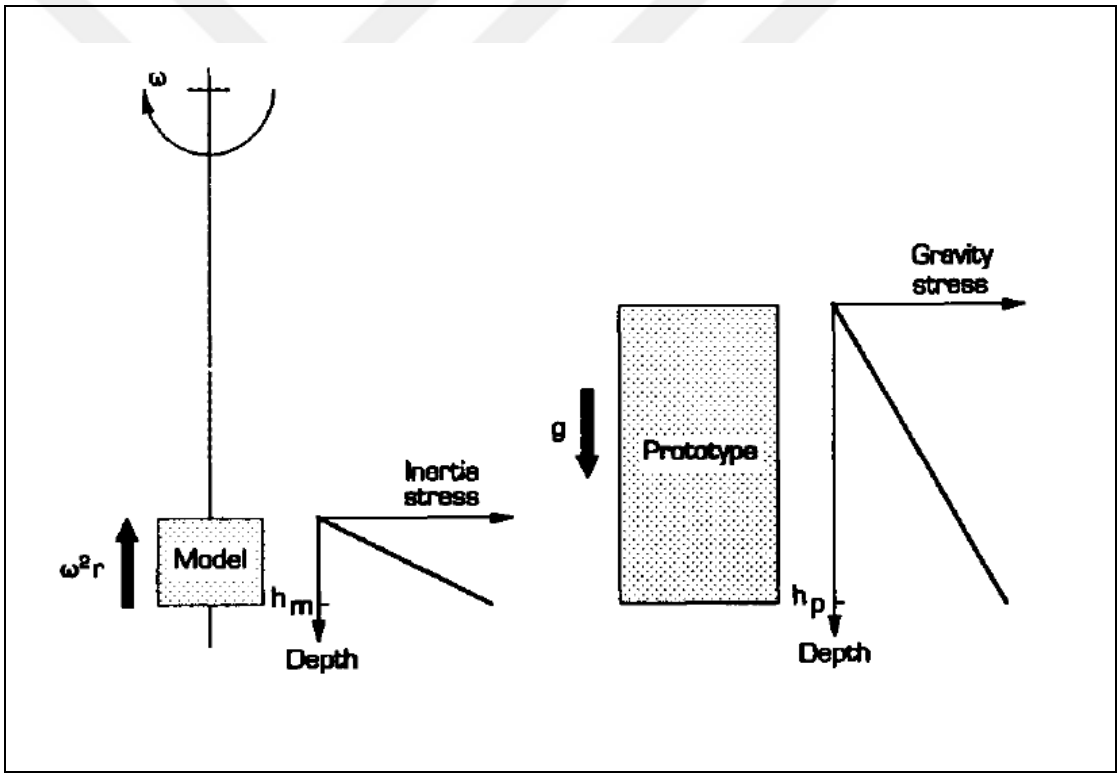

Figure 2.3 : Normal stress distribution in centrifuge model and prototype,(Taylor, 1995).

Stress diagrams of model and prototype are drawn in Figure 2.4. It can be seen that real linear stress distribution is curved in centrifuge model that is due to radius change effect. According to Figure 2.4, model and prototype stresses are matched only in one point. Effective vertical stress of prototype at depth of h_p (h_p =N. h_m) will be obtained by equation 2.3.

$$\delta\sigma_v = \rho.g.h_p = \rho.g.N.h_m \tag{2.3}$$

According to equation 2.4, N scale factor is calculated at effective radius rotation Re:

$$g = \omega^2.R_e \tag{2.4}$$

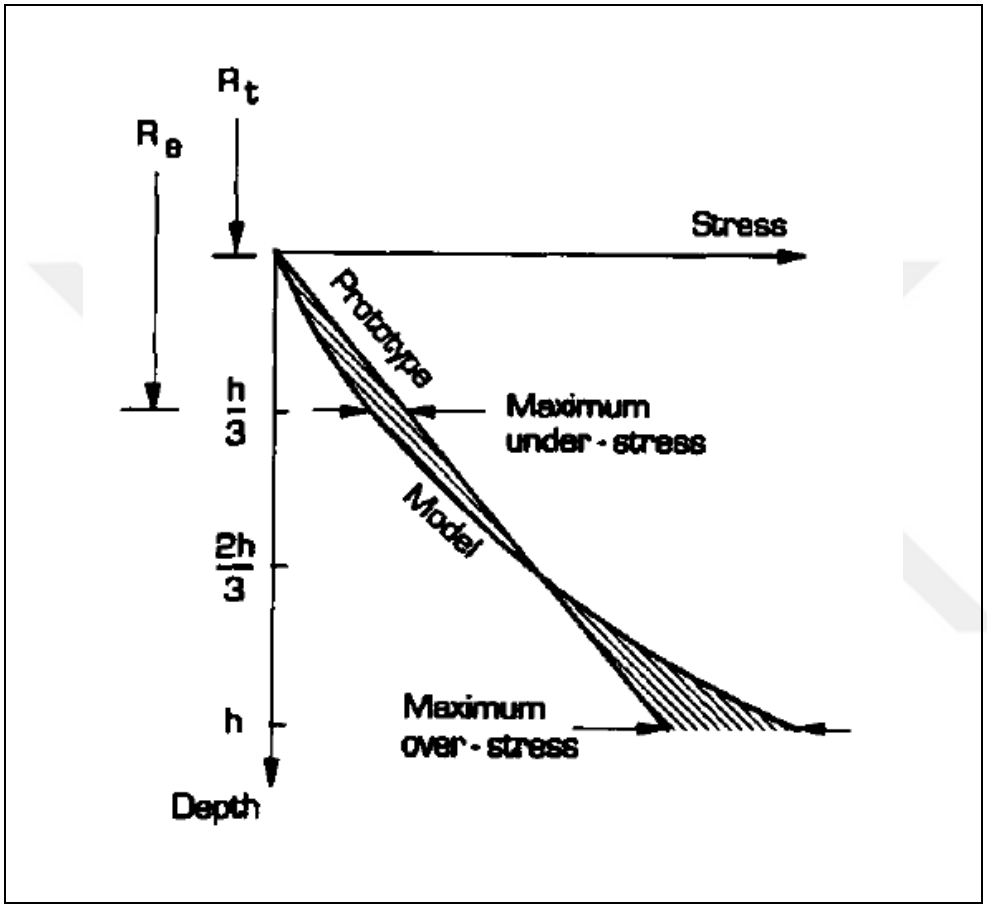

Figure 2.4 : Comparison of stress variation by depth,(Taylor, 1995).

According to Figure 2.4, the correspondence between model and prototype stress at $\frac{2}{3}$ depth of model will be possible. It is possible to calculate maximum error through measuring effective radius from rotation center to $\frac{1}{3}$ depth of model. According to Taylor (1995) if the ratio of model height and effective centrifuge radius (h_m/R_e) will be less than 0.2, the maximum error $h_m/6R_e$ in the stress profile is less than 3% of the prototype stress, it means error is minimum in this case. (h_m/R_e) ratio of most geotechnical centrifuges is less than 0.2. As a result, the maximum error of model stress profile is less than 3% in prototype stress. For example, stress nonlinear

distribution error is only 3.3% in a small centrifuge with effective radius of 1.5m and a great model with 300 mm depth.

2.4.2 Soil particle size

Simulating soil and its particles size change is very important in centrifuge modelling. If it is based on relevant scale factor, real soil particles size will be downsized by N, which is impossible. Because in this conversion, sand particles will be in size of silica or clay and gravel particles will be in size of sand that changes materials behavior and stress- strain curve. Some studies conducted in order to prevent such a problem. The results of these studies define critical ratio between maximum model dimension and mean soil particle diameter. By observing these rules, soil particle size effect will be reduced or eliminated. For example, according to Ovesen (1979-1985), who investigated the performance of circular foundations on sand, in order to reduce the soil particle size effect in centrifuge modelling, the ratio of the foundation diameter of model to soil average particle size should be more than about 15,(as cited in Taylor, 1995).

2.4.3 Error of earth's 1g acceleration

Another error of centrifuge modelling is Earth's gravitational acceleration that is perpendicular to main field acceleration of centrifuge model. Since, gravitational acceleration direction of model (Ng) is along rotation radius; while, Earth's 1g acceleration, perpendicular to rotation radius still exists. It will make errors which effects are not completely clear. The error will be significant when model height is more along Earth's gravity acceleration and centrifuge effective radius is small. Putting the main structure in central range of model can be a good idea to minimize this error.

2.4.4 Coriolis acceleration error

This type of error occurs in movements like earthquakes in dynamic models where soil element moves with velocity, v^* in addition to centrifuge angular velocity, ω, (Figure 2.5). In this case, soil element will experience Coriolis acceleration $a_c = 2.\omega.v^*$. The acceleration will apply force and will create stress in soil element.

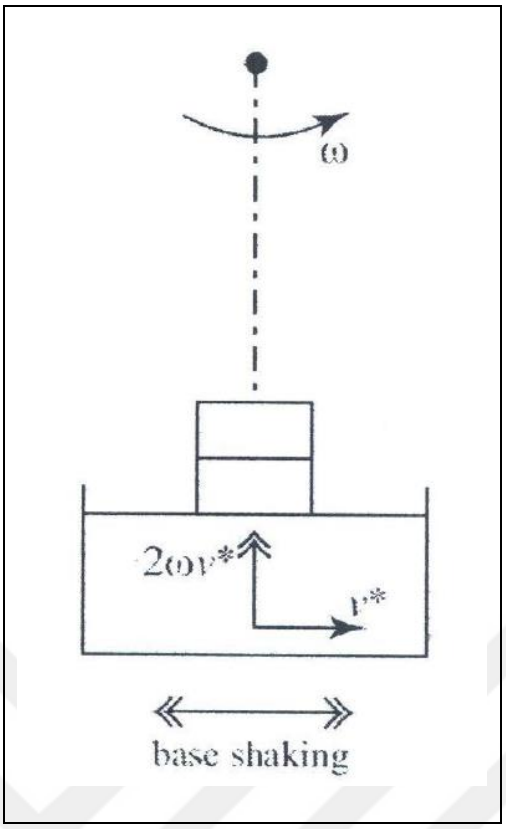

Figure 2.5: Coriolis acceleration due to particle movement with v^* velocity beside angular velocity,(Hedayati, 2012).

Ratio of Coriolis acceleration to centripetal acceleration, is defined as equation 2.5.

$$\frac{ac}{a} = \frac{2v^*}{r.\omega} = \frac{2.v^*}{\sqrt{r.N.g}} \tag{2.5}$$

If above ratio is less than 10%, Coriolis effect will be ignored. In this regard,$v^* \langle 0.05.\omega.R_e$. In other words, v^* upper limit will be $0.05.\omega.R_e$ in order to ignore Coriolis Effect. v^* lower limit will be expressed as equation 2.6 through defining r_c curvature radius:

$$a_c = 2.\omega.v^* = \frac{v^{*2}}{r_c} \Rightarrow \frac{v^*}{2\omega} \tag{2.6}$$

The path of moving object (r_c) must not be less than centrifuge effective radius ($r_c > R_e$), when ignoring Coriolis effect. According to V=ω. R_e, we will have $v^* \rangle 2V$. Therefore, if velocity range of Coriolis effect is within the range shown in equation 2.7, Coriolis effect will be ignored:

$$0.05.\omega.R_e > v^* > 2.\omega.R_e \quad (2.7)$$

2.4.5 Error of gravitational acceleration direction unevenness

According to type 1 error definition, Earth gravitational acceleration will be parallel at all points due to radius of Earth being relatively larger than the structures dimensions. Acceleration field is radial and non- parallel in modeling centrifuge due to small dimensions and limited rotational radius. In other words, if water is in a box, it will be in cylinder form during rotation. Centrifuge models with parallel edges will be made in order to solve this problem (Figure 2.6). Also, if B/r<0.1, this effect is ignorable, where B is width of model box and r is radius of centrifuge. In addition, if model box width is 20% of centrifuge radius, side acceleration of 10% centrifuge acceleration will be applied to soil layers edges. This effect will be reduced through placing important parts of the model on the centerline.

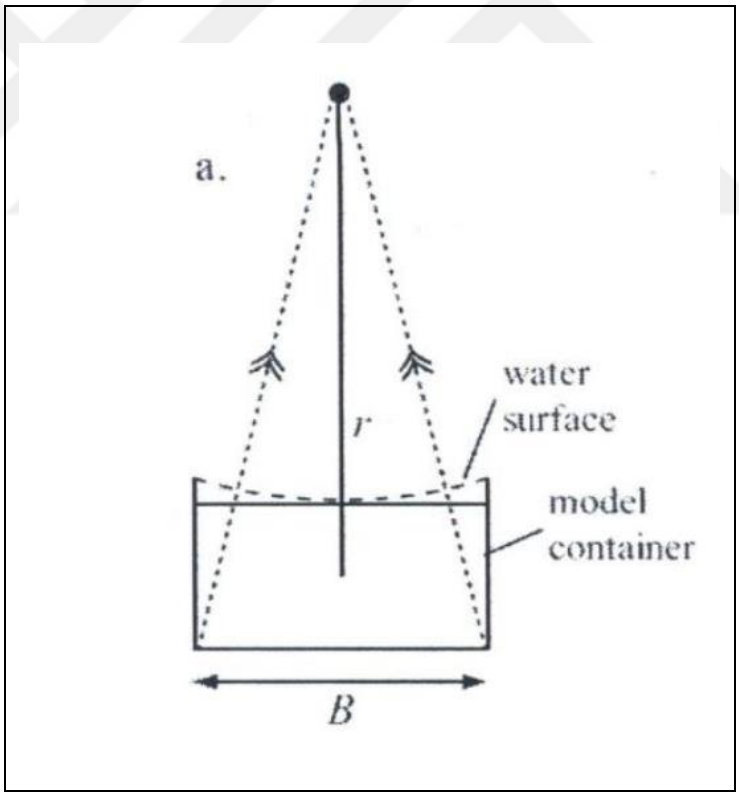

Figure 2.6 : Radial acceleration field in centrifuge,(Hedayati, 2012).

3. PARTICLE IMAGE VELOCIMETRY (PIV)

3.1 PIV History

Motion and deformations within vision interval attracts human. Flight of a bird, fish swimming and etc. attract human attention. Human follows certain body within his vision range. If we consider these phenomena scientifically, their features will be important, such as size, interval, velocity and etc. Understanding flow features in fluid mechanics is very important. If we observe water of a river, it can be said that: wood chip in water has flow features.

Ludwig Prandtl is one of outstanding scientists in fluid mechanics. He took a step in early 20^{th} century using accurate test in order to examine the flow by illustration. He designed techniques in a water tunnel in order to study different aspects of unstable flows. He created the flow through rotating a blade wheel. The tunnel included upper and lower parts that were separated by horizontal plane and created a closed cycle for water. 2D models such as cylinder, prism and fin were installed vertically on upper channel. The flow was observable by Mica particles over water.

Prandtl studied steady and unsteady flow. Variability of some test parameters (slope angle, flow velocity, steady and unsteady flow) directed Prandtl on unsteady flow main features. In that time, qualitative description of flow was possible and there wasn't quantitative information on flow rate.

The first quantitative measurements of particles by cinematography imaging conducted by Nayler and Frazer (1917) to investigate a stormy flow with tracking a model immersed in water. They recorded particle images sequentially on filmstrips. They marked particle points on a piece of paper under film using a pin in order to examine the film. They determined streaks by using multi-frame photos. They applied this process on 80 frames of filmstrips. The first work on Particle Tracing Velocimetry (PTV) was conducted manually that has dynamic range of 80:1. Figure 3.1 provides an image of this study that is similar to modern articles results qualitatively and in detail. It shows that most of advances in PTV are due to computerized tracking process.

Many studies are conducted on measuring particles velocity in order to estimate fluid flow field or multi-phase flow. Particle Streak Velocity (PSV), Laser Speckle

Velocimetry (LSV), Particle Image Velocimetry (PIV), and Particle Tracing Velocimetry are specified names of this technique.

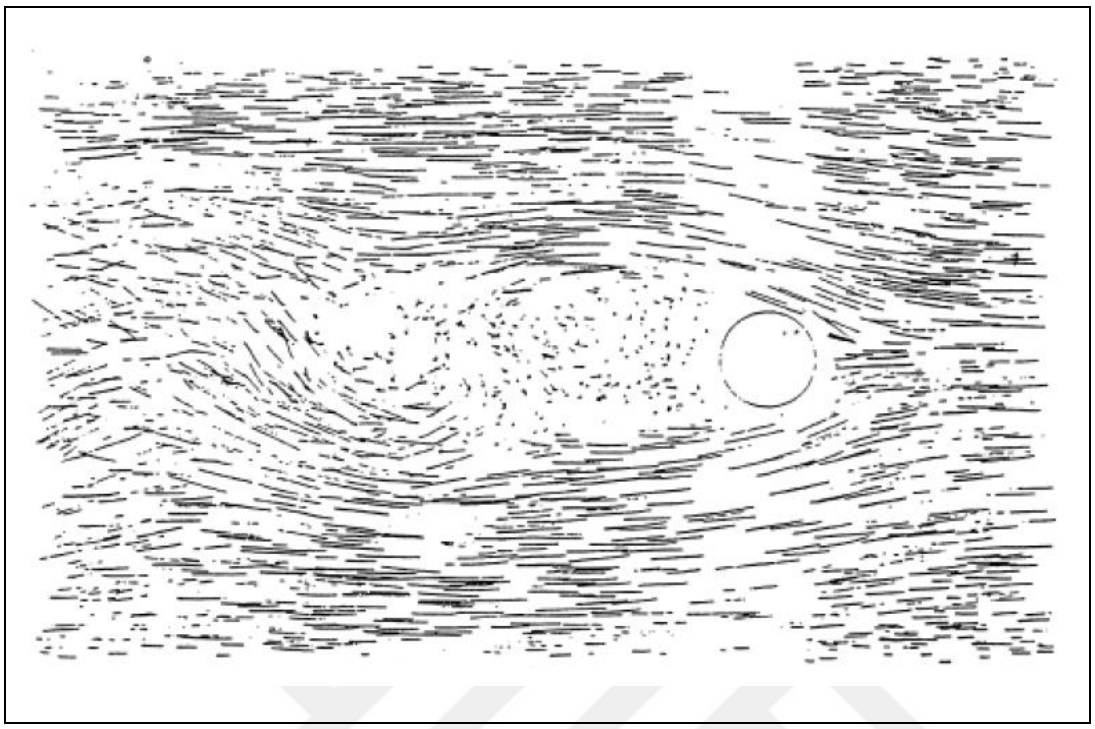

Figure 3.1 : Measurements of particle tracking of 2D unsteady flow around a cylinder by using cinematography,(Nayler and Frazer, 1917).

Other names such as Pulsed Light Velocimetry (PLV), Particle Image Displacement Velocimetry (PIDV), Particle Displacement Velocimetry (PDV) and Digital Particle Image Velocimetry (DPIV) refer to similar content with minimal changes. Holographic Particle Image Velocimetry (HPIV) and Photogrammetric Particle Tracking Velocimetry (PPTV) are 3D methods that can be used with LSV, PIV and PTV,(Ansaripour, 2014). Particle Image Velocimetry was applied for the first time by Adrian in 1991 on fluid mechanics in order to measure velocity fields of 2D and 3D flows, (Ansaripour, 2014). Adrian states that PIV is used in measuring displacement of instantaneous fields of gas and fluid flows in laboratory scale with high quality and precision. Also, he states that this technique is used in millimeters domains per seconds to a few hundred meters per seconds.

3.2 History of PIV Usage in Geotechnics

Yamamoto & Kusuda (2001), conducted a study on failure mechanism and bearing capacity of a reinforced foundation. Firstly, a series of loading laboratory models were performed by using ground modelling by aluminum rods. In these experiments, not

only bearing capacity, but also failure mechanism was studied by image processing analysis. The reasons of using aluminum rods in this study are:

A) Rigid motions such as displacement and rotation are visible

B) Modeled ground using aluminum rods is placed in plain strain conditions.

c) The probability of changing ground model through adding aluminum rods with various diameters

According to Figure 3.2, aluminum colored rods are placed (target points) at certain intervals in order to observe motion. Deformations are photographed at certain intervals. Figure 3.2 represents aluminum rods displacement before and after loading.

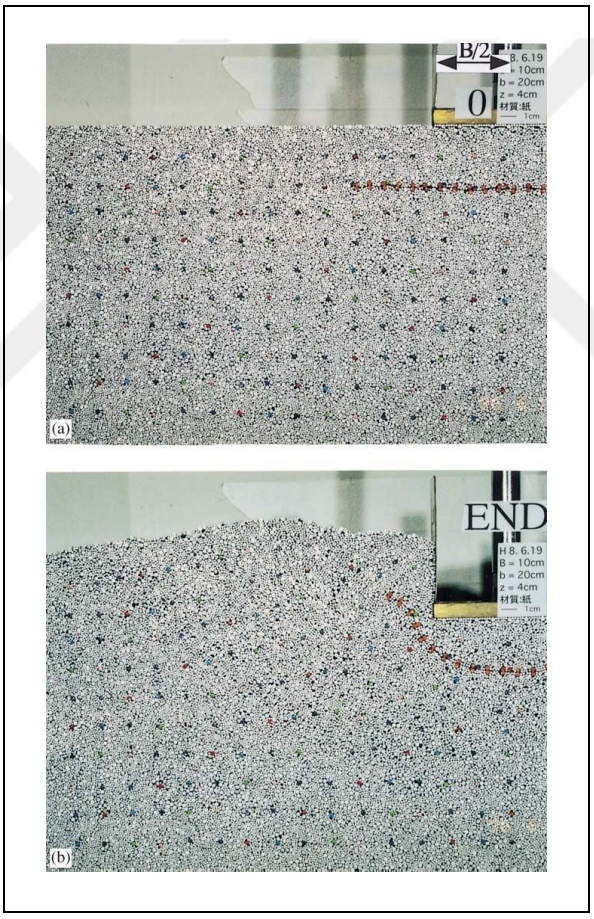

Figure 3.2 : Modelled ground using aluminum rods before and after loading, (Yamamoto and Kusuda, 2001).

They observed that: a) deformed areas are similar to proposed area by Terzaghi (1943) and Prandtl (1920). Therefore, image processing analysis function was observed. b) Points displacement is more in horizontal than vertical direction, when length of aluminum rods increased.

White et al. (2001- 2003) performed tests on PIV method in geotechnics and proposed a modified approach in order to use PIV in geotechnical tests where soil deformation is expressed as flow with low speed. They measured method accuracy in order to displace a plane of soil as well as they wrote GeoPIV codes in MATLAB software in order to calculate displacement in geotechnical tests,(White and Take, 2002).

A study by Knappett et al. (2006) was done on shallow foundations failure mechanism under seismic loading of 1g. Failure mechanism was done using PIV and video with high speed camera. The study was performed through placing the model on soil and then putting both of them on a shaking table and applying various accelerations and imaging from this system. Finally, the failure mechanism of the test was observed.

3.3 PIV Technique in Modelled Geotechnical Structures

White et al. (2001) provided a modified approach for PIV use in geotechnical tests where soil deformation is assumed as a flow with low speed. Using PIV technique in geotechnics is easier than fluid mechanics. Since soil has image texture and there is no need to shining suspended particles in fluid. In addition, there is no need to laser light source for texture detection. Measuring displacement is possible through tracking plane soil patches that are prone to deformity.

3.3.1 Image texture

Image texture describes intensity variations within patch. A patch with fewer changes in pixel intensities seems smooth, while a patch including major changes in pixel intensities seems uneven. A patch with proper texture includes wide range of intensity values, while a patch with weak texture includes too low major features and all pixel intensities are grouped based on background colors. Image texture is determined by patch size, shape, distribution size and differentiation of soil particles color in body space,(White et al., 2001).

In process of image analysis by PIV, images are taken using digital camera from soil during deformation, then soil deformation is determined using particle images velocimetry between a pair of consecutive images.

3.3.2 Particle Image Velocimetry

Image processing that is done during PIV for measuring displacement between a pair of digital images is shown in Figure 3.3. First image is divided into a network of test patches and each test patch ($I_{test}(U)$) includes an image matrix of L*L pixel (I(U)). A search patch is selected in second image (I_{search} (U+S) in order to find test patch displacement between images 1, 2; the search patch defines an area that test patch searches through expanding test patch up to S_{max} in u, v directions (test patch (first rectangular with L size) plus margin that is equal to maximum vertical and horizontal displacement vector). Then it searches test patch location in next image using a function that is defined as fitness function and selects a patch of second image as second location of first image test patch per which fitness function is maximized; also, introduces motion vector between two patch centers as displacement vector. Image processing will be done using MatPIV and GeoPIV software based on MATLAB.

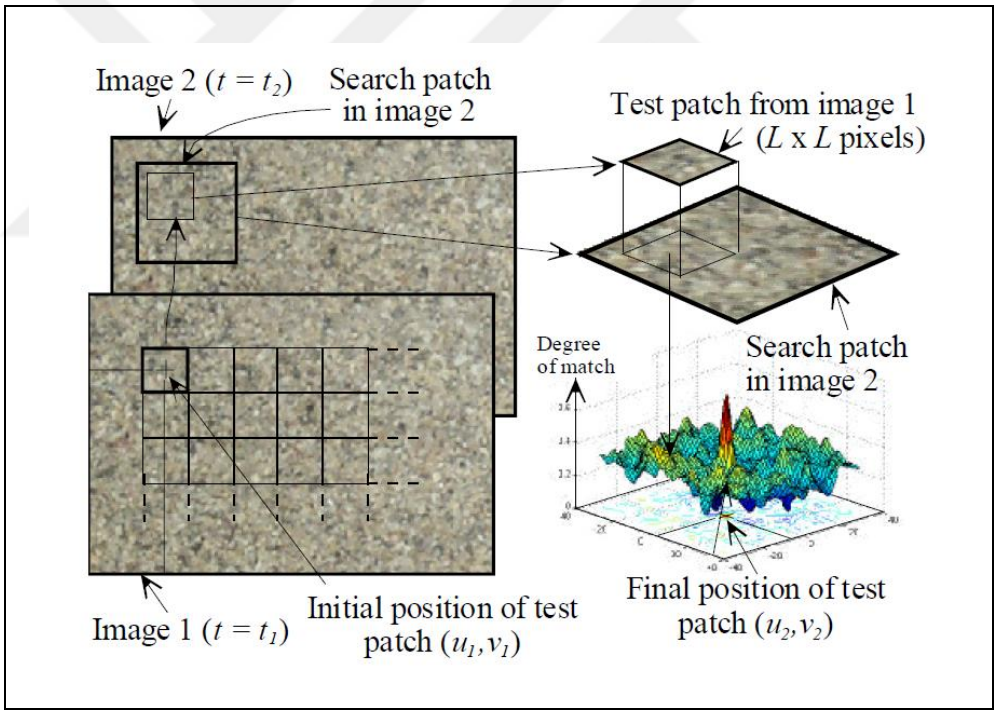

Figure 3.3 : Principles of PIV analysis,(White and Take, 2002).

The software outputs are a 2D matrices of u, v; first one presents horizontal component and second one presents vertical component of each patch displacement vector.

System accuracy is based on PIV method and is a function of PIV patch size and texture. The more image lights, the more accurate measurement will be. Using smaller patches lead to increased measurement points and reduced accuracy.

3.3.3 Centroiding

Centroiding is one of image processing steps and determines special location of reference points. Corresponding pixels and reference point are specified through selecting threshold intensity level and target location is determined as selected pixels center surface at both directions. Determining reference points' location on real space and the points' location on image, image pixel size is determined for each test and measurements on image space in pixel are converted into length in point units,(Stanier et al., 2016).

3.3.4 Close range photogrammetry

All of basic image measurement methods need final conversion of image spatial location vectors into real special displacement in order to get useful measurement. The simplest transformation model is linear scaling (using constant ratio throughout the image) that is used in displacement measurement of physical models. Geometric calibration of camera is aimed to determine camera parameters that explains the relationship between 3D reference coordinates and digital image (2D features of CCD camera).

Figure 3.4 illustrates conversion of information from image space into real space.

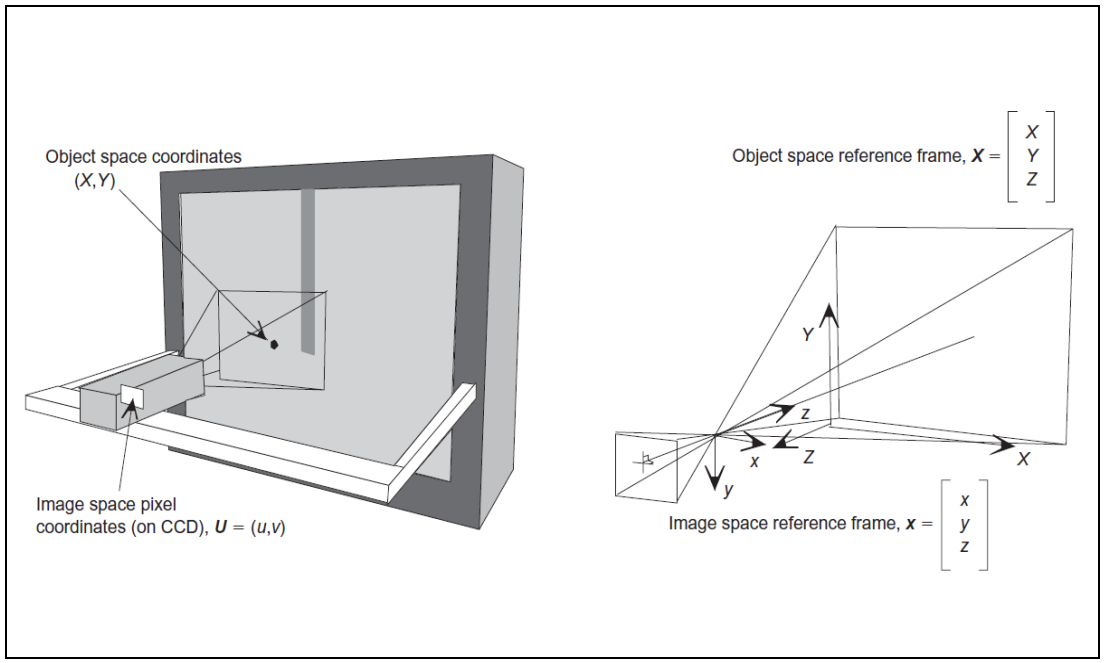

Figure 3.4 : Information conversion from image space into real space,(White et al., 2003).

Parameters of such a transformation must explain direction and 3D location of camera relative to body space coordination system and internal geometry and camera's light features. Effective factors on failure during transformation process were studied by calibration and all factors effects were applied on values using 14 parameters. These parameters are determined through locating image space of reference aims whose body geometry features are known,(Heikkila & Silven, 1997).

4. EXPERIMENTAL SETUP

4.1 Description of IGT Beam Centrifuge

All the tests of this dissertation were performed in the IGT Beam Centrifuge at Universität für Bodenkultur (BOKU) in Vienna. The geotechnical centrifuge was constructed by Trio-Tech, USA and was placed into service with partial financial help of Austrian Science Foundation in 1990 (Trio-Tech, 1988). The components of the centrifuge are: swinging basket, balancing counterweight, DC motor and aerodynamic enclosure. It has 56 electric slip rings for monitoring of processes and collection of data. Two models can be experimented concurrently by using the dual platforms. Nevertheless, it is common to have only one swinging basket bearing a model while loading a balance weight on the other platform. Figures 4.1 and 4.2 shows the geotechnical centrifuge at BOKU. Properties of the centrifuge is described in Table 4.1.

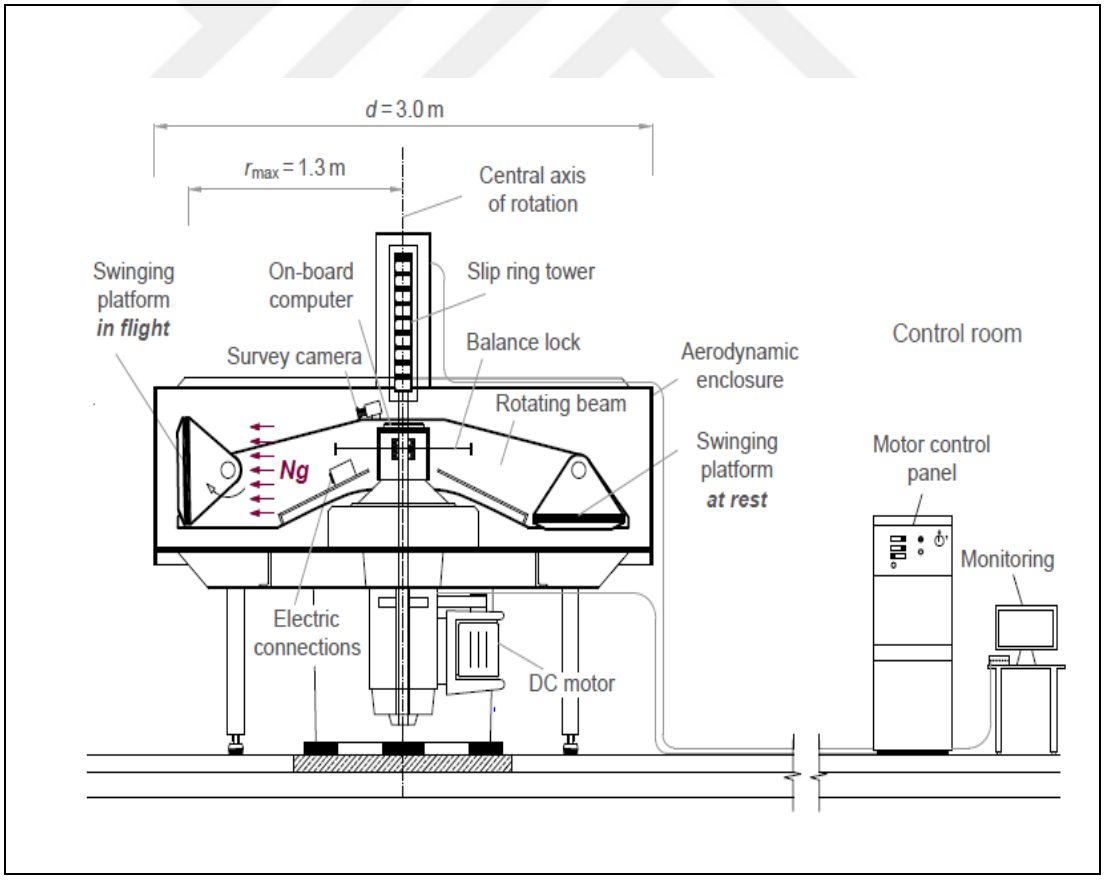

Figure 4.1 : Schematic presentation of the centrifuge testing facility at BOKU,(Idinger, 2016).

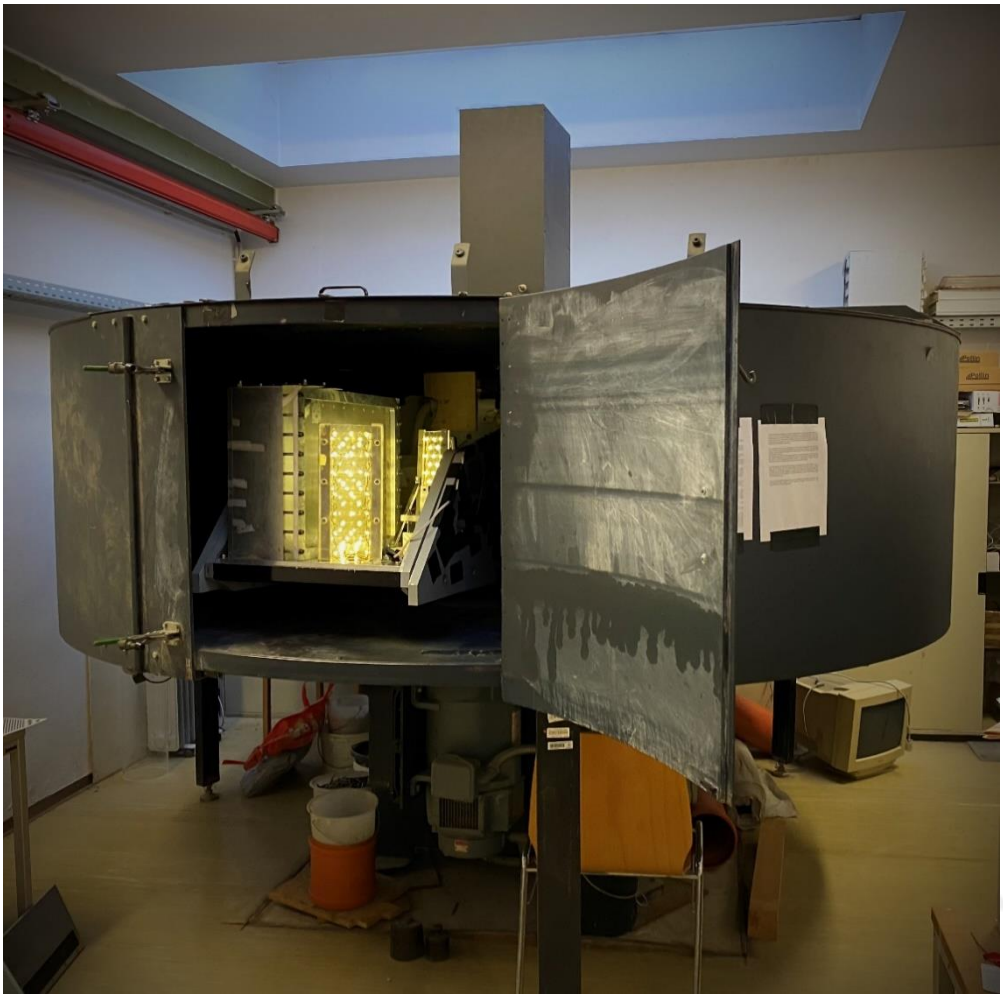

Figure 4.2 : Geotechnical centrifuge at BOKU.

Table 4.1 : Technical specifications of the geotechnical centrifuge at BOKU.

Diameter of the centrifuge [m]	3
Radius of the swinging basket [m]	1.3
Maximum angular velocity [1/min]	400
Maximum radial acceleration [g]	200
Maximum model weight [kg]	90
Maximum Load Capacity(t)	10
Maximum model Dimensions W*D*H [cm]	54*56*56

4.2 Model Box

The model box was designed for Dipl. Eng. Gregor Idinger's thesis. The mechanism with all details totally was designed by him, for the purpose of making a sufficient test set-up for using the PIV technology,(Ertan, 2012).

The model box was rectangular with dimension of 48cm in length, 15.5cm in width and 45cm in height. In order to take digital images during the tests, a transparent plexiglass plate was used on one side of the model box with thickness of 3 cm, (Figure 4.3). The other sides (walls) of the model box are aluminum plates with thickness of 1.5 cm. The model box was rigid enough to keep plane strain condition in the model. The box can be opened using bolts. The main items used beside the box include a digital camera for taking images in order to do analysis by PIV, two panels of LED lights for supplying sufficient lighting and two cameras on top of the box for taking the video during the test. Sketch of model box are illustrated in Figures 4.4 and 4.5.

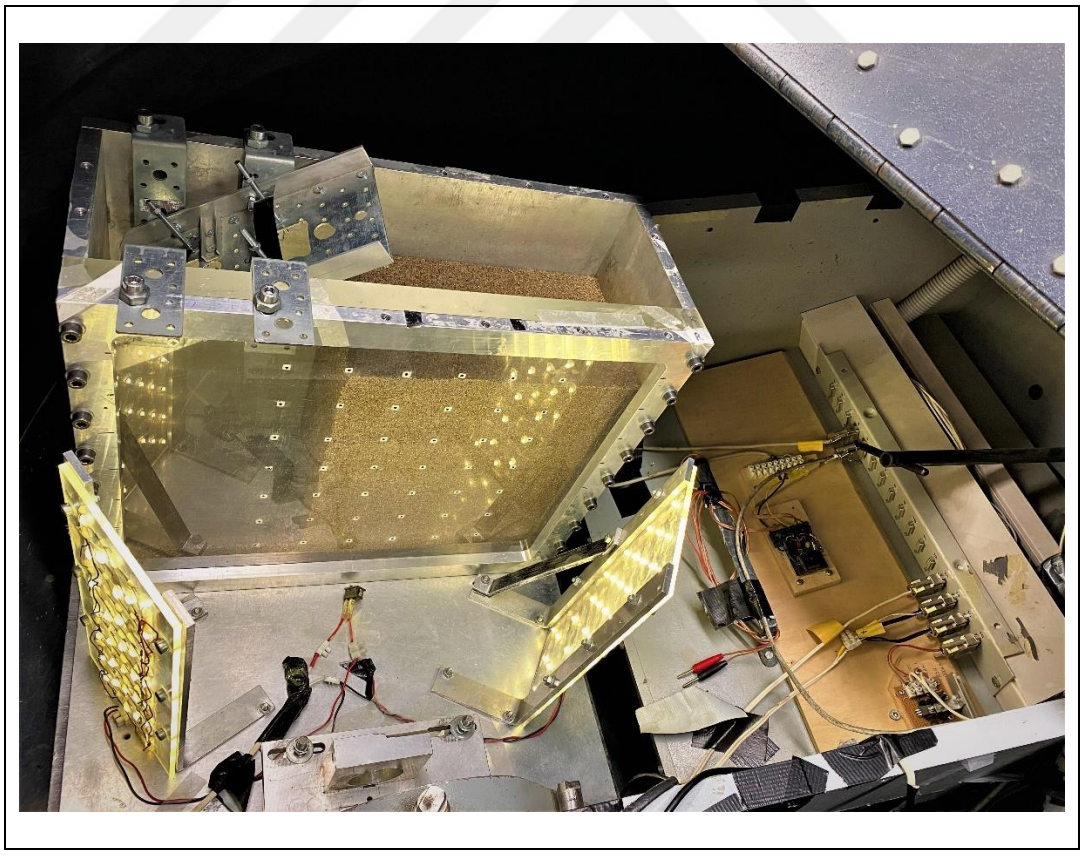

Figure 4.3 : Model box mounted on swing basket.

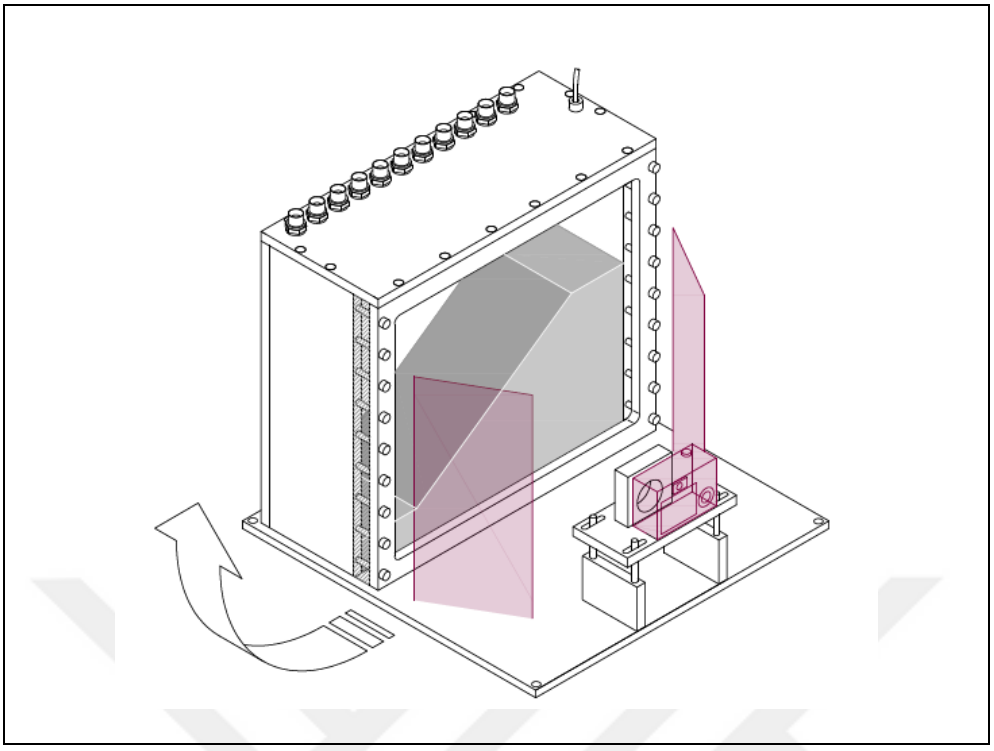

Figure 4.4: Sketch of the model box, including the imaging equipment with camera and light panels,(Idinger, 2016).

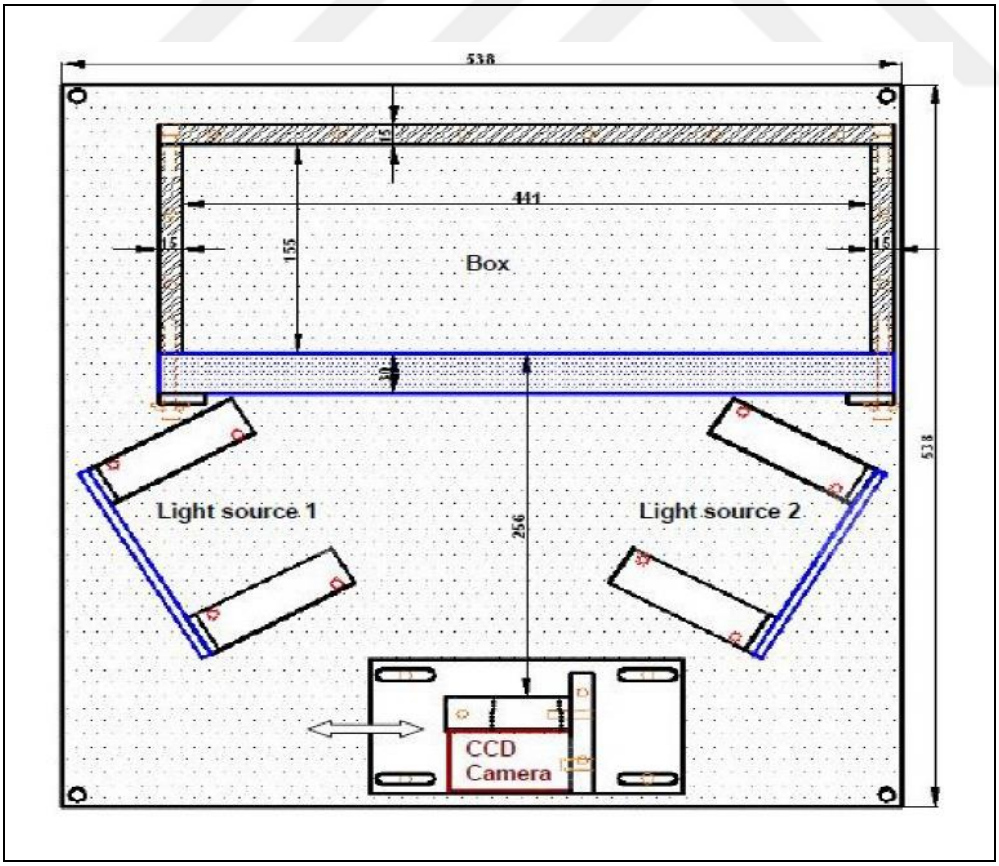

Figure 4.5: Sketch of PIV-model assembly, top view,(Ertan, 2012).

4.3 Designing the Model

Slope models have a slope inclination of about 70 and 90 degrees. The heights of the slopes are 25 ,30 and 35 centimeters. The cement content in all of reinforced slopes was 3% of weight of oven-dried soil. Optimum water content was used in construction of all soil slope models. Two kinds of soils were used in the experiments and named as S1 for soil 1 and S2 for soil 2. The relative density of S1 was chosen about 72% and relative density of S2 was 40%.

4.4 Soil

For performing the tests, two different types of soil were used. The tests were accomplished under wet condition by adding optimum moisture content of the soils.

4.4.1 Soil 1 (S1)

The first soil type that was used in the tests is SP-SC according to USCS and includes 73% sand, 21% gravel and 6% fine content. The other properties of this soil are shown in the Table 4.2. Figure 4.6 shows the particle size distribution curve of Soil 1.

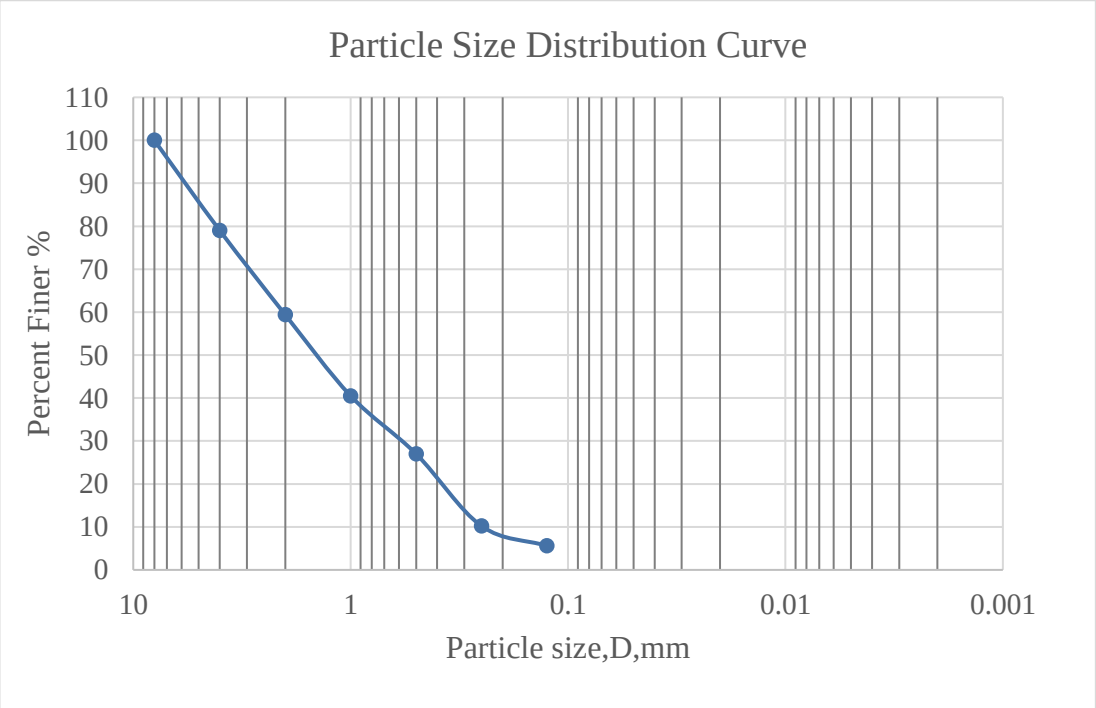

Figure 4.6 : Grain size distribution of Soil 1.

Table 4.2 : Parameters of Soil 1.

D 60	mm	2.061
D 50	mm	1.503
D 30	mm	0.611
D 10	mm	0.245
Fine Content	%	6
Sand Content	%	73
Gravel Content	%	21
PL	%	24
LL	%	31
$\gamma_{d\ min}$	gr/cm^3	1.6
$\gamma_{d\ max}$	gr/cm^3	1.8

4.4.2 Soil 2 (S2)

The second soil type that was used in the tests is uniform, poor graded, coarse sand, Standard Sand II (DIN 1164/58), which is named as Norman Sand. This soil is used under wet condition with relative density of 40%. Table 4.3 shows the properties of the soil2. The particle size distribution curve of Soil 2 is shown in Figure 4.7.

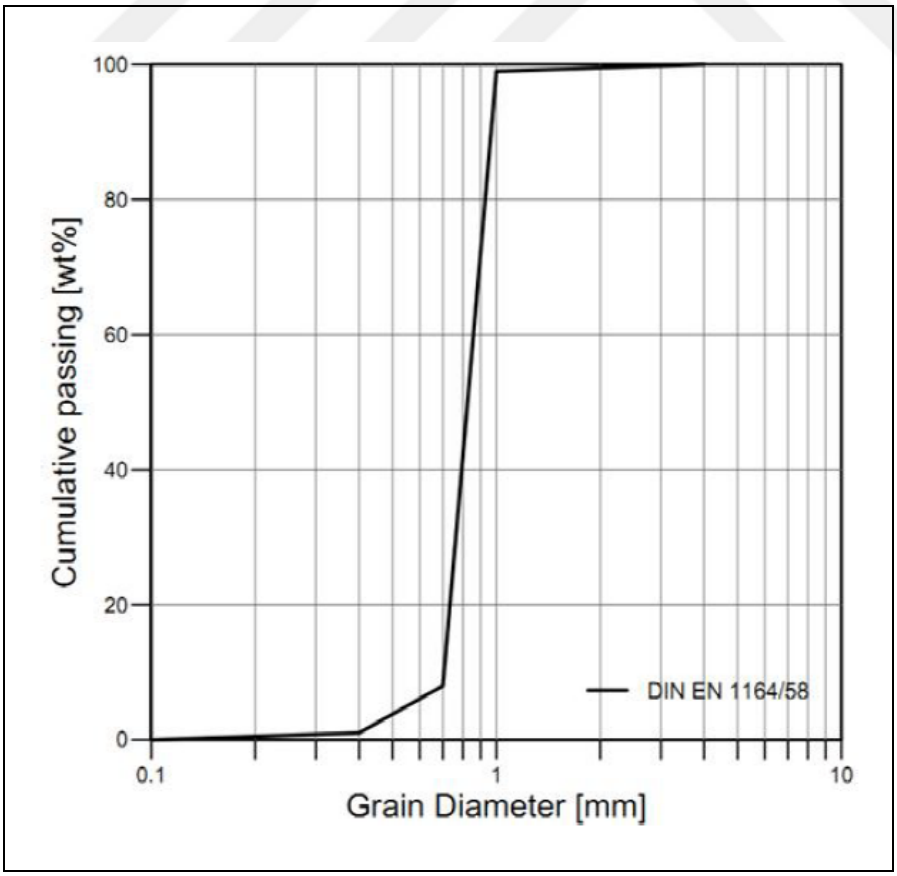

Figure 4.7 : Grain size distribution of Soil 2,(Barbir and Mathews, 2016).

Table 4.3 : Parameters of Soil 2.

Specific Gravity	Gs [gr/cm^3]	2.644
Density range	ρ_{min}, ρ_{max} [gr/cm^3]	1.44-1.65
Void ratio	e_{min}, e_{max}	0.607-0.844
Coefficient of uniformity	C_u	1.4
Coefficient of Curvature	C_c	1.03
Friction angle	φ [°]	34
Cohesion	c [KN/ m^2]	0

4.5 Sample Preparation

Generally performing the centrifuge tests is possible on two kinds of soil sample.

1. Undisturbed samples, which is taken from site with special methods. In these methods and technics, the disturbance and change in the soil is minimum.

2. Remodeled samples, which is made by using soil materials in laboratory condition. For example, in granular soils, methods like “Tamping” or “Pluviation” is being used.

In this research because of the facility and availability of necessary laboratory equipment, tamping method was conducted for soil preparation.

4.5.1 S1 sample preparation

For preparing the sample, cement and oven-dried soil was used. The sample was prepared at optimum water content and relative density of 72%.

At first according to maximum unit weight of 1.8 gr/cm^3 and relative density of 72% the unit weight of soil was calculated. For the reason of compaction, the volume of soil box was calculated for height of 5 cm. Then the weight of soil with relative density of 72% (in one test 77%) for the height of 5 cm was calculated. With an accurate balance the calculated weight of dry soil was weighed. The soil and cement (3 % of weight of dry soil) were mixed. After that water (6.7 % of weight of dry soil) was added to the mixture and it was mixed sufficiently until reaching a uniform mixture.

For the tests that were conducted without cement, in the step of mixing the dry soil was just mixed with water.

4.5.2 S2 sample preparation

At first according to maximum and minimum void ratio and relative density of 40%, the void ratio and unit weight of soil were calculated. The volume of soil box was calculated with the height of 5 cm. Then the weight of soil with density of 40% for height of 5 cm was calculated. With an accurate balance the calculated weight of dry soil was weighed. The soil and cement (3 % of weight of dry soil) were mixed. After that water (5 % of weight of dry soil) was added to the mixture and it was mixed sufficiently until reaching a uniform mixture.

4.6 Slope Modelling

Before preparing the sample, internal walls of the soil box were cleaned sufficiently. For reducing the friction effect the internal walls of box were lubricated by grease. The prepared soil (as described in 4.5 section) was poured uniformly inside of the soil box by hand and was compacted in 5cm layers. For compacting the soil inside the box, a standard proctor hammer and an aluminum plate were used. For this reason, after pouring the soil inside the box and flattening the surface, the aluminum plate was placed on the soil and by slamming the standard proctor hammer on the plate, the soil layer was compacted until reaching to height of 5 cm. This action was continued until reaching the intended height. After construction of all soil layers in the box, it was waited for 3 days. Then, the box was opened and according to intended angle, the soil sample was carved by tools. Finally, the model box was closed and was placed into the centrifuge to perform the test.

For the samples without cement the waiting time for carving and testing was 2 days.

Figure 4.8 shows a slope model of the study with soil type S2, which was prepared for performing the test.

Figure 4.8 : Slope model in the box.

4.7 Instrumentation

The PIV was used for measuring the displacement of slope models. A 14.7 MP digital camera (Canon G10) was used for this purpose. By using this camera high resolution pictures were obtained from soil grains behind the plexiglass wall of the model box. For specifying the reference points for using in PIV, black dots surrounded by white rectangular were drawn by marker on the plexiglass (Figure 4.9). These points were used as references for analyzing the images by using PIV.

A good lighting is required to take suitable pictures for PIV analysis. For this reason, on left and right side of the plexiglass two panels of light containing 33 LED lights on each panel were used for preparing a good Illumination condition. All the test data and taken images during the test were observable from a PC in the control room. For this reason, near the rotating axis of the centrifuge a laptop was placed and was connected to the PC in control room by USB cables. The GeoPIV8 codes, developed by White & Take (2002), was used for analyzing the images in MATLAB software.

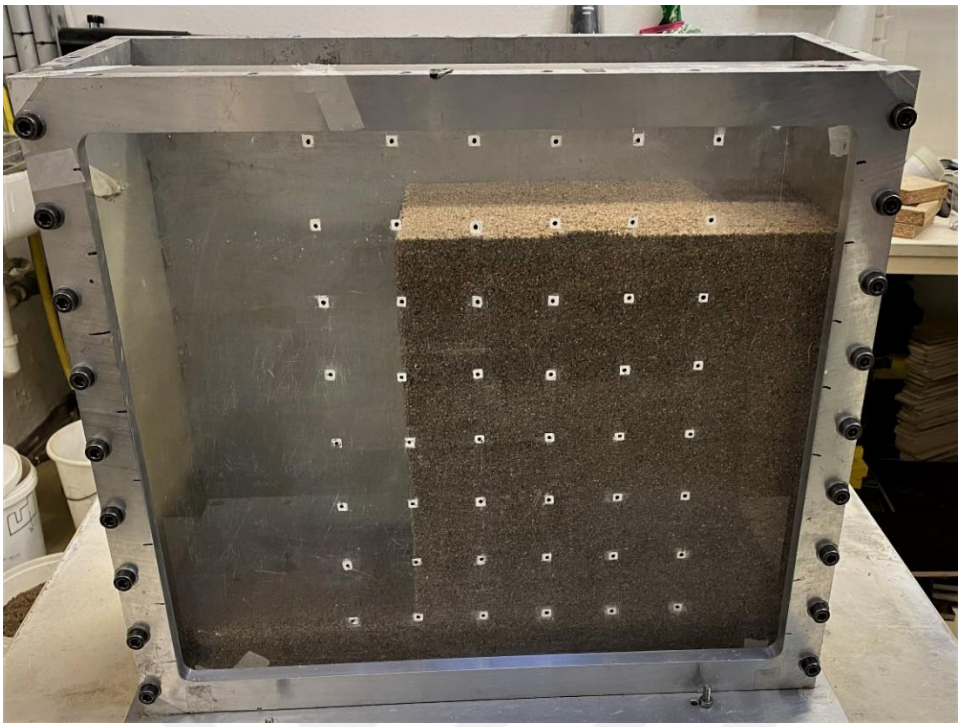

Figure 4.9 : Black dots surrounded by white rectangular on plexiglass.

4.8 Typical Test Procedure

The performed steps of centrifuge tests are listed and explained in this section. This can be a guidance for future researchers that want to perform centrifuge tests, especially if the PIV model box will be used in the research.

1. Preparing the slope model in the model box. (section 4.6)

2. Placing the model box into the centrifuge swinging basket and fixing it.

3. Mounting the LED panels on both sides of model box, (Figure 4.10).

These panels are plugged to channel 3 in centrifuge and in the control room the cable of it is plugged to a power socket.

4. Assembling the digital camera in front of the model box for taking digital images, (Figure 4.11).

5. Assembling two cameras on top of the model box for taking video during the test, (Figure 4.12).

6. Placing the laptop computer inside the geotechnical centrifuge, on a platform near the centrifuge axis.

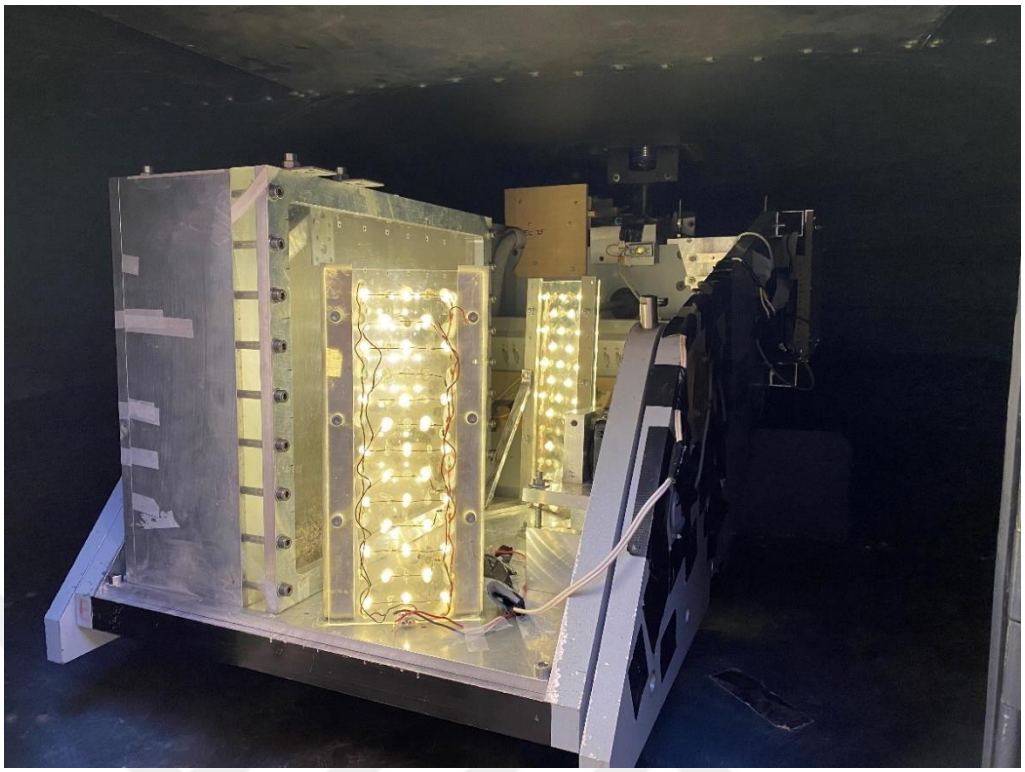

Figure 4.10 : The LED panels on both sides of model box.

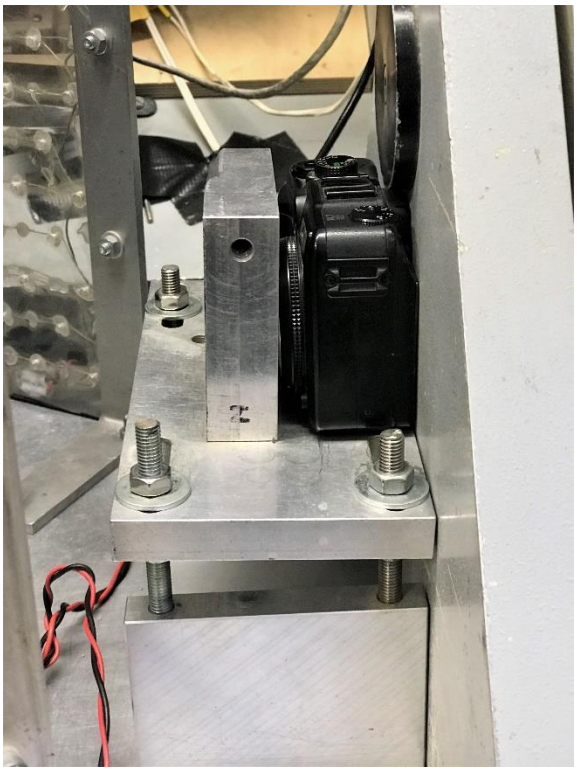

Figure 4.11 : Assembling the digital camera in front of the model box.

Figure 4.12 : Assembling two cameras on top of the model box for taking video.

7. Plugging the cable of Canon G10 digital camera to the laptop and turning on the camera.

The camera is paired with PSRemote Software in the laptop. After turning on the camera and starting the PSRemote software, the slope model is visible on the laptop.

8. Plugging internet cable to laptop for the purpose of connecting it to the PC in the control room.

The laptop computer launches the WinVNC software. This software is a connector between the computers in centrifuge and control room.

9. Untightening the valve (rotation arm) of balancing counterweight of centrifuge in order to balance by adding or removing weight (steel rods) on the balancing counterweight, which is on the opposite side of model box. For balancing, the distance between bottom of the swinging basket and floor of centrifuge should be equal on both sides. This action takes place by try and error.

10. Tightening the rotation arm

11. Starting the video cameras on top of the model box and at the same time starting the stopwatch.

12. Closing the shield of the geotechnical centrifuge.

13. Turning on the power of geotechnical centrifuge.

14. Evacuating the centrifuge room (until end of the test), closing the room door, and going to control room. Figure 4.13 shows centrifuge control room.

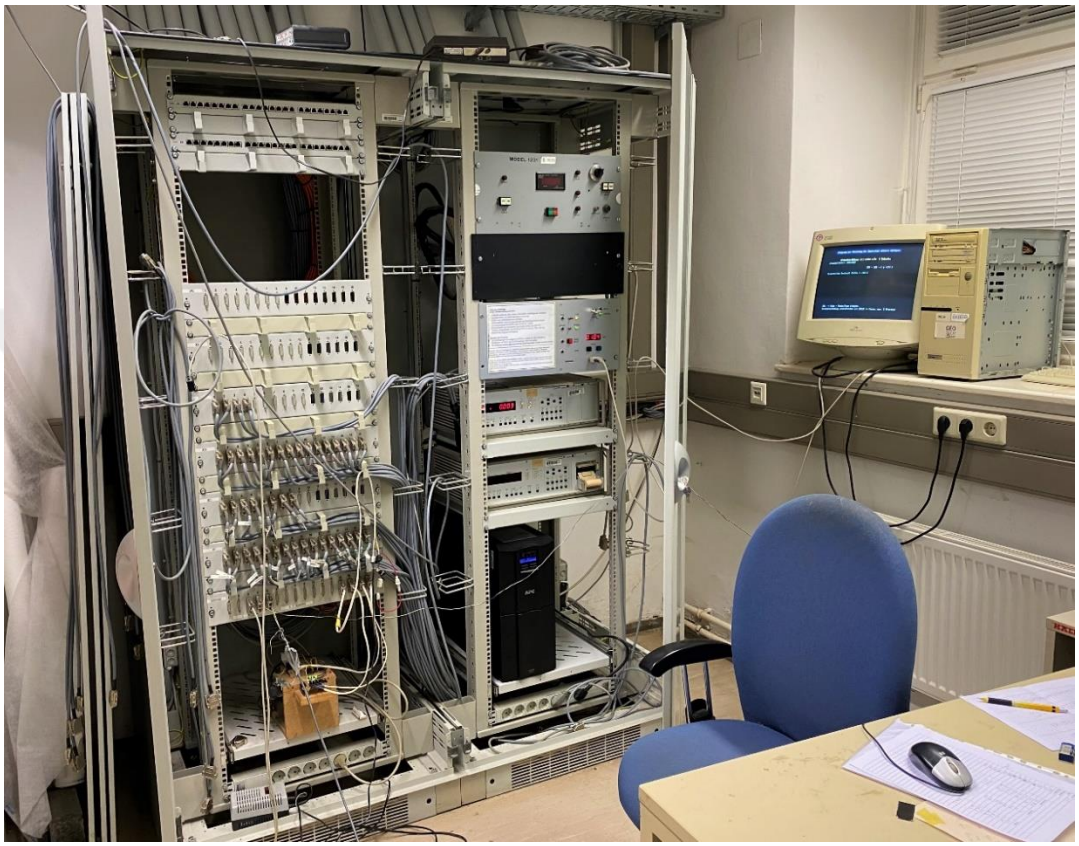

Figure 4.13 : Centrifuge control room.

15. Turning on two computer systems in control room.

One of the computers (PC1) is connected to the laptop inside the centrifuge room. PC1 is used to observing the images during the test. The other computer system (PC2) is used for observing the acceleration (as G and rpm) during the test.

16. Turning on LED light panels on the model box by switching the key in control room.

17. Turning on the system of centrifuge by switching the key from stop mode to the run mode, then switching the other key to remote mode.

Remote mode is used for tests, where the aim is to increase the acceleration gradually and automatically. In this research all the tests were performed in this mode from acceleration amount of 0 g up to 95g, (Figure 4.14).

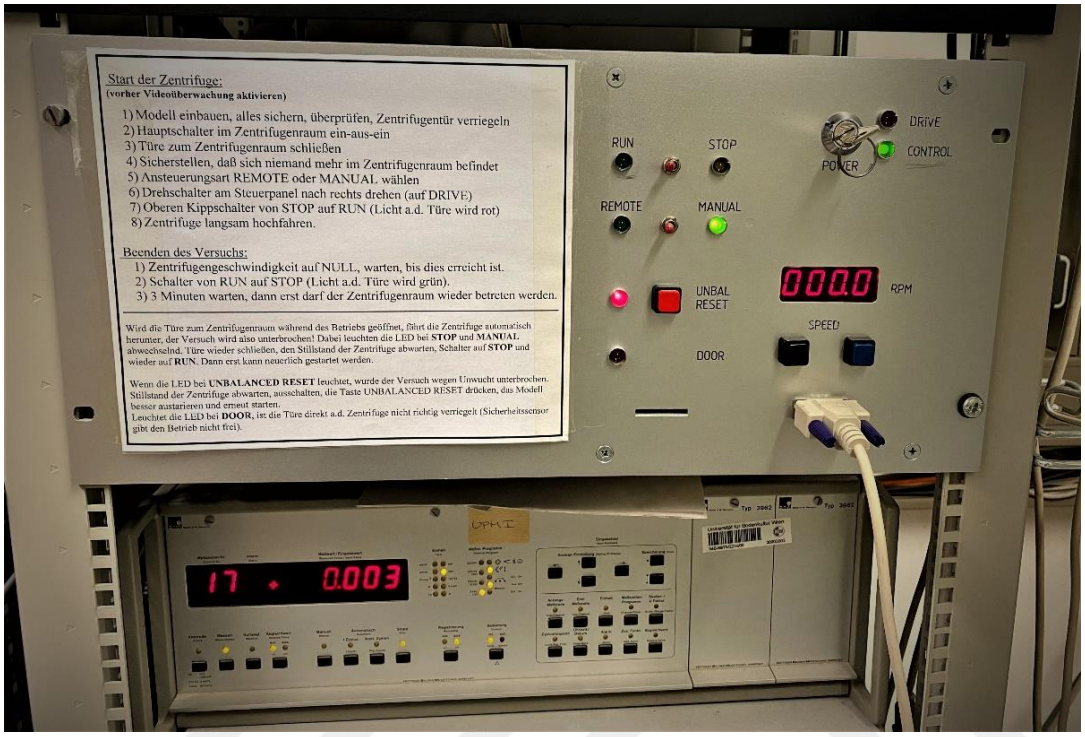

Figure 4.14 : Starting the centrifuge system.

18. Opening the VNC viewer software in PC 1, entering IP address of laptop computer in order to connect and observe the laptop.

19. Starting the PSRemote software in order to take photo in PC 1, hitting the Enter key in PC 2, noting the time of stopwatch.

20. Observing the images from PC1 and acceleration increment in PC2 and writing on the data sheet.

The digital camera was adjusted by PSRemote to take images every 10 seconds, as illustrated in Figure 4.15. The number of the images was defined in the PSRemote Software and was observable during the test in order to correspond with acceleration data and noting in the data sheet for analyzing by PIV.

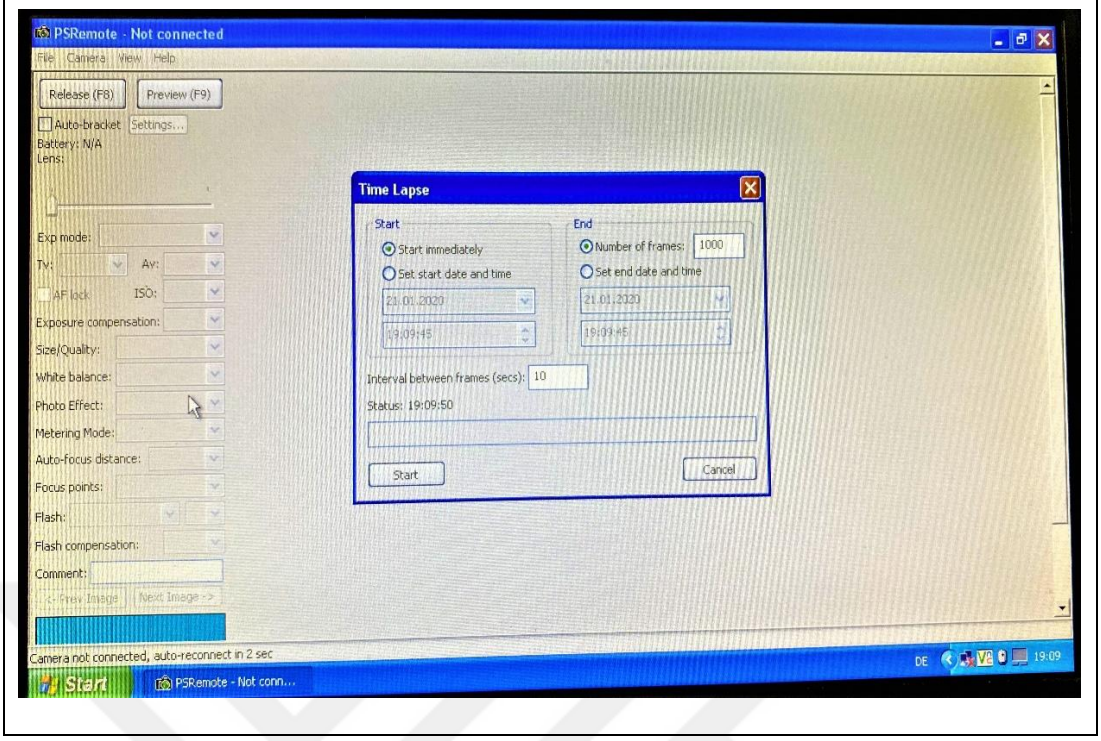

Figure 4.15 : PSRemote for taking the images during the test.

5. RESULTS

5.1 Introduction

The results of the centrifuge model tests of soil slopes are presented in this chapter. To identify the possible failure mechanisms of cemented soil slopes, the slope models are tested in a geotechnical centrifuge. The variables of this research are slope inclination, soil types, relative density and height of the slopes. In addition, non-cemented slope model tests were done to compare the cement effect on stability of the slopes. Image analysis were performed by using GeoPIV8 codes in MATLAB software. The images are analyzed just before the failure. The time interval between each of the images is 10 seconds. It means, the images of slope models are evaluated 10 seconds before the failure. However, there wasn't any failure in some models. These slope models are evaluated until the maximum acceleration (95G) that the model experienced.

5.2 Experimental Results

Totally, 9 tests were performed in this study. List of the experiments and the condition of each experiment are shown in Table 5.1.

The results of experiments were classified according to slope inclination and discussed in this section. Figure 5.1 illustrates sketch of all the slope models. All the slope models have a base layer with a height of 5cm and length of 48cm. The distance of toe of the slope from the head of base layer is fixed amount of 20.4 cm in all the slope models. The length of the upper side of the slope models are changed according to height and inclination of the slope models.

Table 5.1 : List of the experiments.

Test No.	Soil Type	Cement content (%)	Water content (%)	Slope model height (cm)	Relative Density (%)	slope inclination	Acceleration at Failure (g)
1	S1	3	6.7	25	72	70°	-
2	S1	3	6.7	35	77	70°	-
3	S1	3	6.7	35	72	90°	48.2
4	S1	3	6.7	35	72	70°	85.9
5	S1	3	6.7	30	72	90°	59.5
6	S1	0	6.7	25	72	70°	35
7	S1	0	6.7	25	72	90°	12.8
8	S2	3	5	30	40	90°	57.2
9	S2	3	5	30	40	70°	-

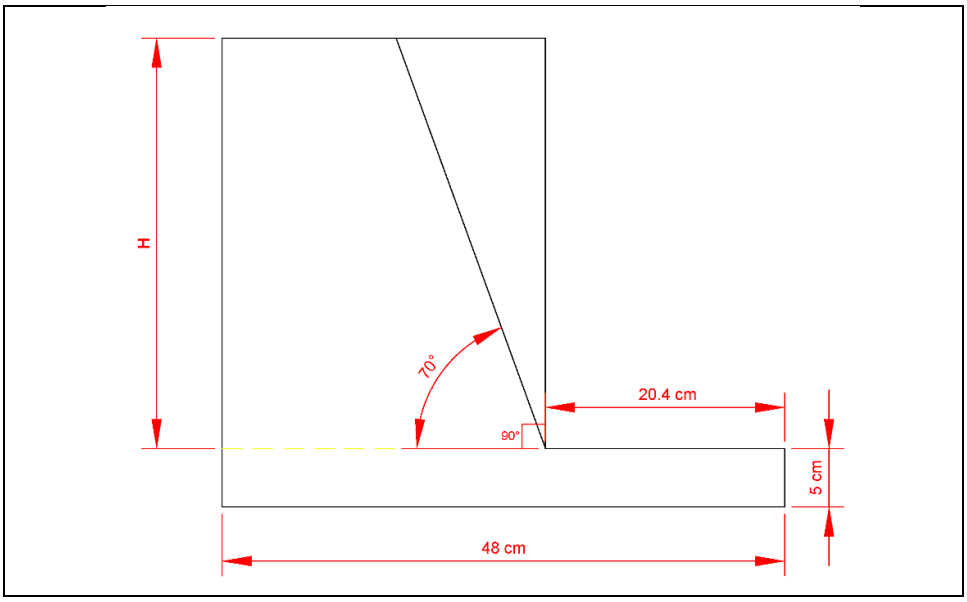

Figure 5.1 : Sketch of the slope models.

5.2.1 Slopes with 70° inclination

The results of experiment 1, 2, 4, 6 and 9 are discussed in this section.

5.2.1.1 Experiment 1

The properties of experiment 1 is shown in Table 5.2.

Table 5.2 : The properties of experiment 1.

Test No.	Soil Type	Cement content (%)	Water content (%)	Slope model height (cm)	Relative Density (Dr) (%)	slope inclination	Acceleration at Failure (g)
1	S1	3	6.7	25	72	70°	-

The first frame (when the experiment was started) and the last frame of this test are shown in Figure 5.2. The acceleration is 95g in last frame.

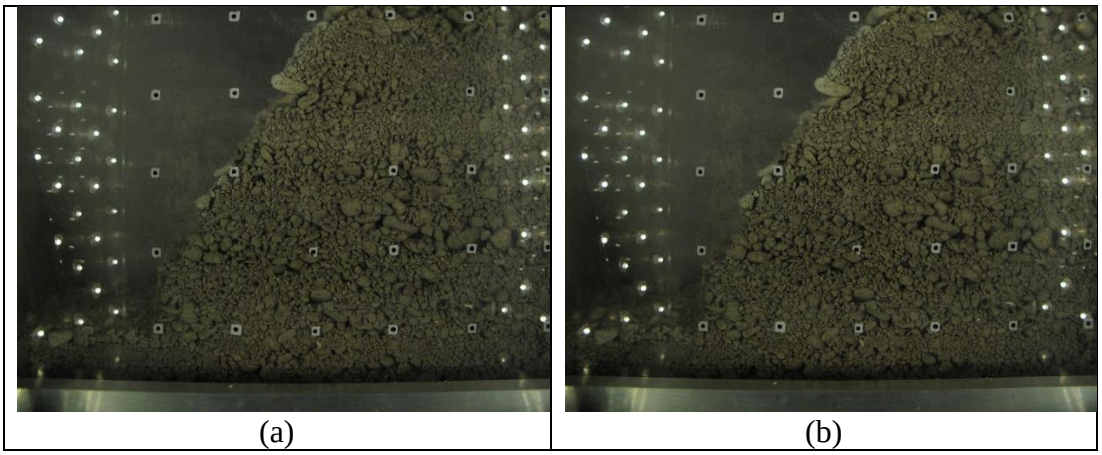

Figure 5.2 : Soil model at a) start of the test, and b) maximum acceleration.

In order to understand the eventual failure mechanism of a geotechnical structure, measuring the plane ground deformations is essential. Figure 5.3 shows the vector field of resultant displacements at maximum acceleration of 95g and 60 seconds before maximum acceleration. Figure 5.4 shows contours of vertical and horizontal displacement at maximum acceleration. According to Figure 5.3 soil displacement is mostly vertical and downward. Figure 5.4, also confirms it. There is little horizontal displacement with maximum quantity of 0.3 mm at toe of the slope and near to slope surface, this shows that by increasing the load of the upper layers, slope tries to move towards the free field.

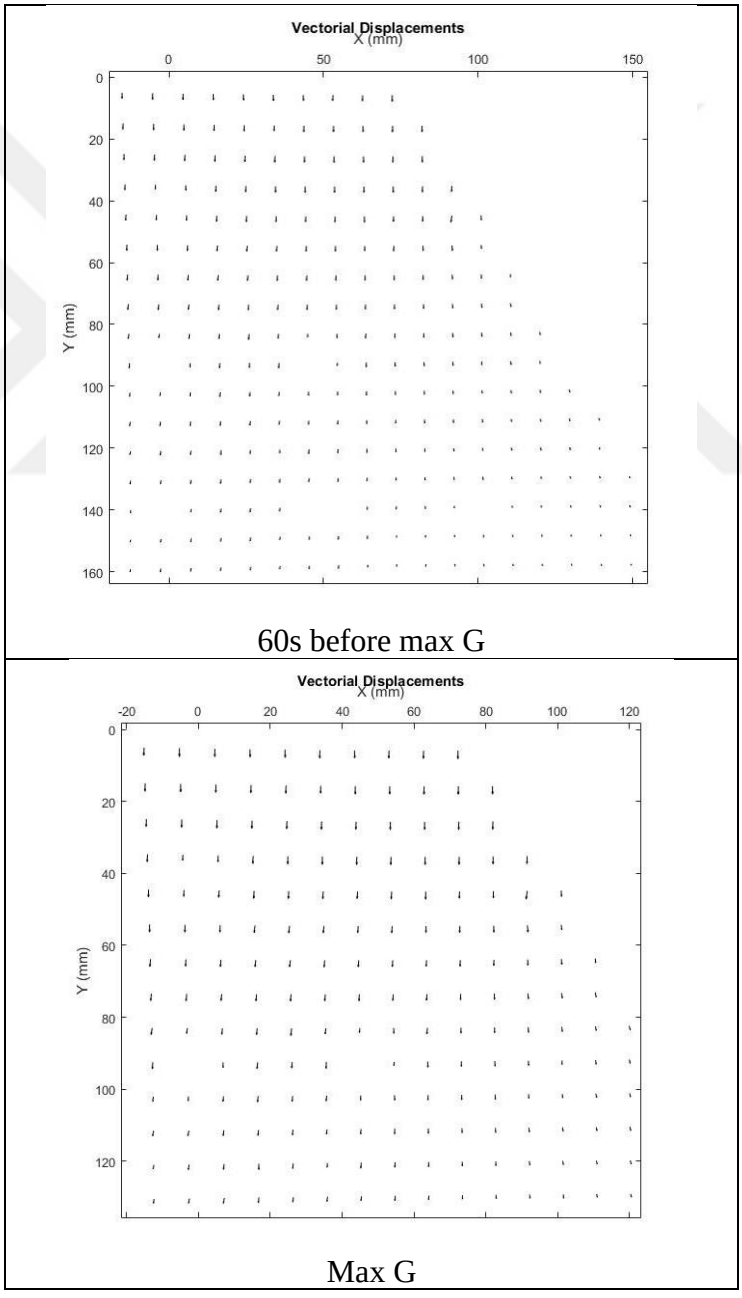

Figure 5.3 : Vector field of soil displacement.

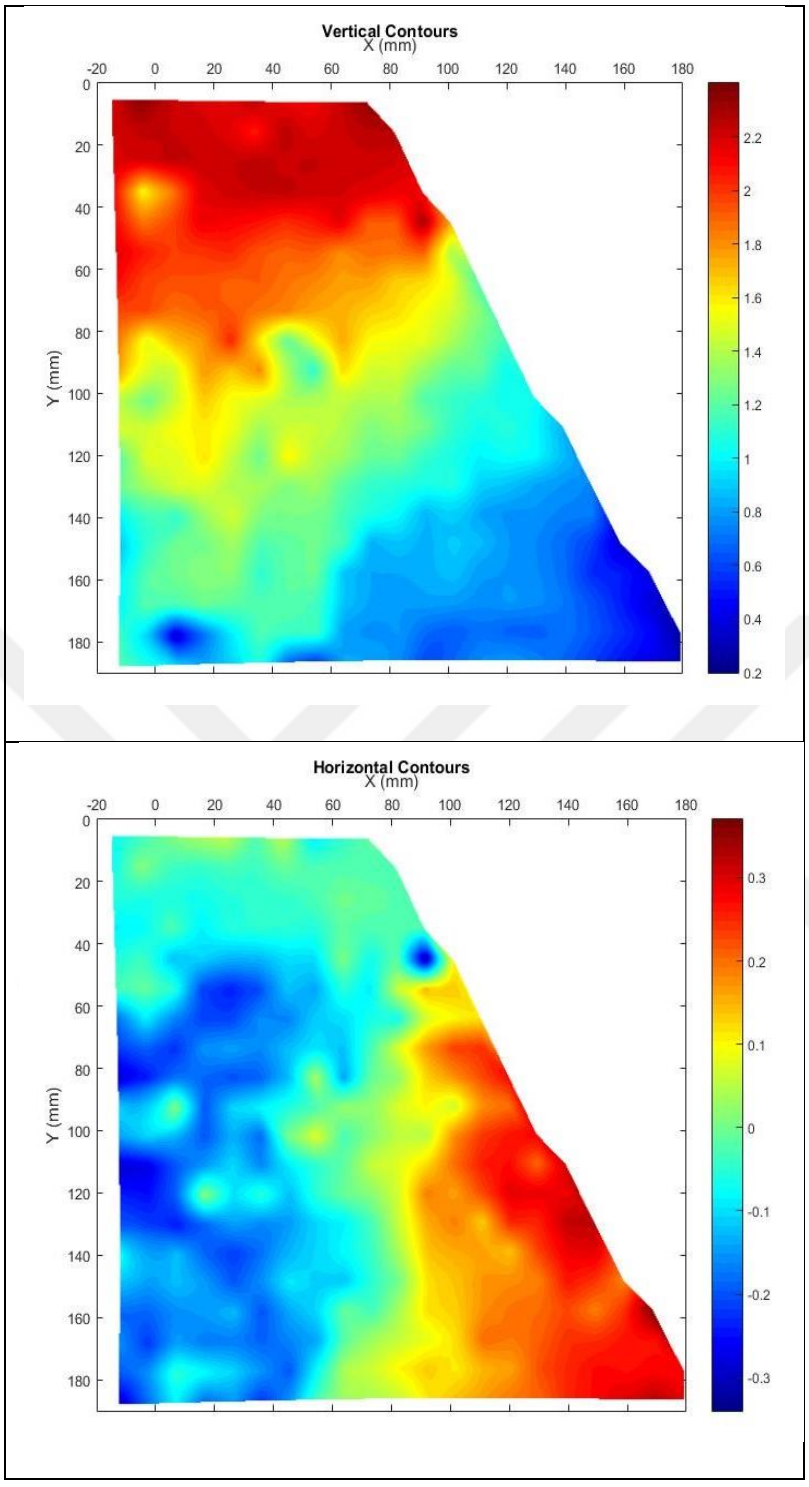

Figure 5.4 : Contours of vertical and horizontal displacement.

Figure 5.5 shows the contours of shear strains at maximum acceleration of 95g and 60 seconds before it. According to Figure 5.5, the soil failures are close to the slope crest. The failure was started from upper side of the slope and tends to expand to lower part.

Strain concentration is at upper part of slope, between -20-100 mms in X direction and between 0-60 mms in Y direction.

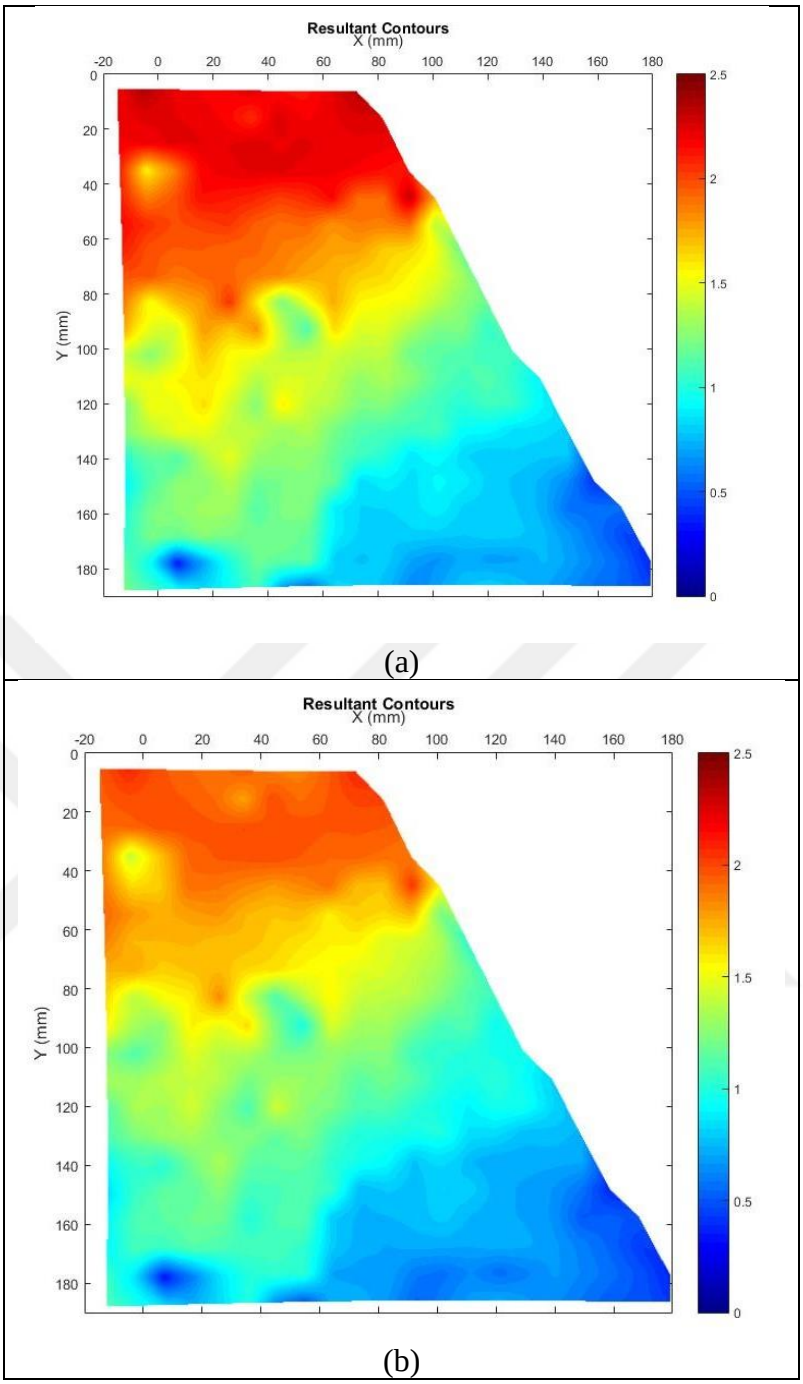

Figure 5.5 : Contours of shear strains at, a) maximum acceleration, and b) 60s before the maximum acceleration.

5.2.1.2 Experiment 2

The properties of experiment 2 is shown in Table 5.3.

Table 5.3 : The properties of experiment 2.

Test No.	Soil Type	Cement content (%)	Water content (%)	Slope model height (cm)	Relative Density (Dr) (%)	slope inclination	Acceleration at Failure (g)
2	S1	3	6.7	35	77	70°	-

The first frame (when the experiment was started) and the last frame of this test are shown in Figure 5.6. The acceleration is 95g in last frame.

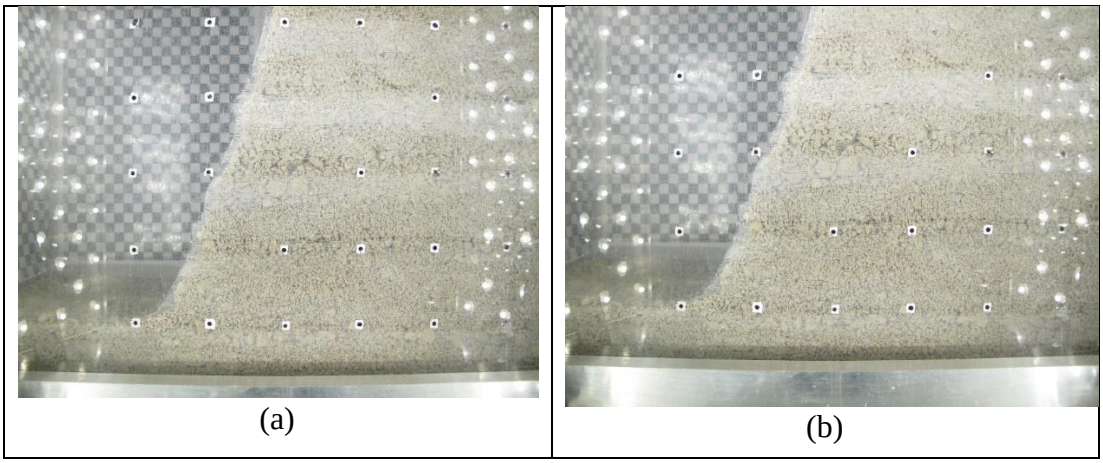

(a) (b)

Figure 5.6 : Soil model at a) start of the test, and b) maximum acceleration.

Since the displacement amount is very little in this test, vectorial displacements are not clear, (Figure 5.7).

Horizontal and vertical contours of displacements at maximum acceleration are shown in Figure 5.8. The displacements are mostly horizontal at upper side of the slope. However, there is little vertical movement in the slope. The displacements of this slope are less when compared with experiment 1, even though the slope height is bigger. The reason is that the relative density of this slope model is more than relative density of previous slope model.

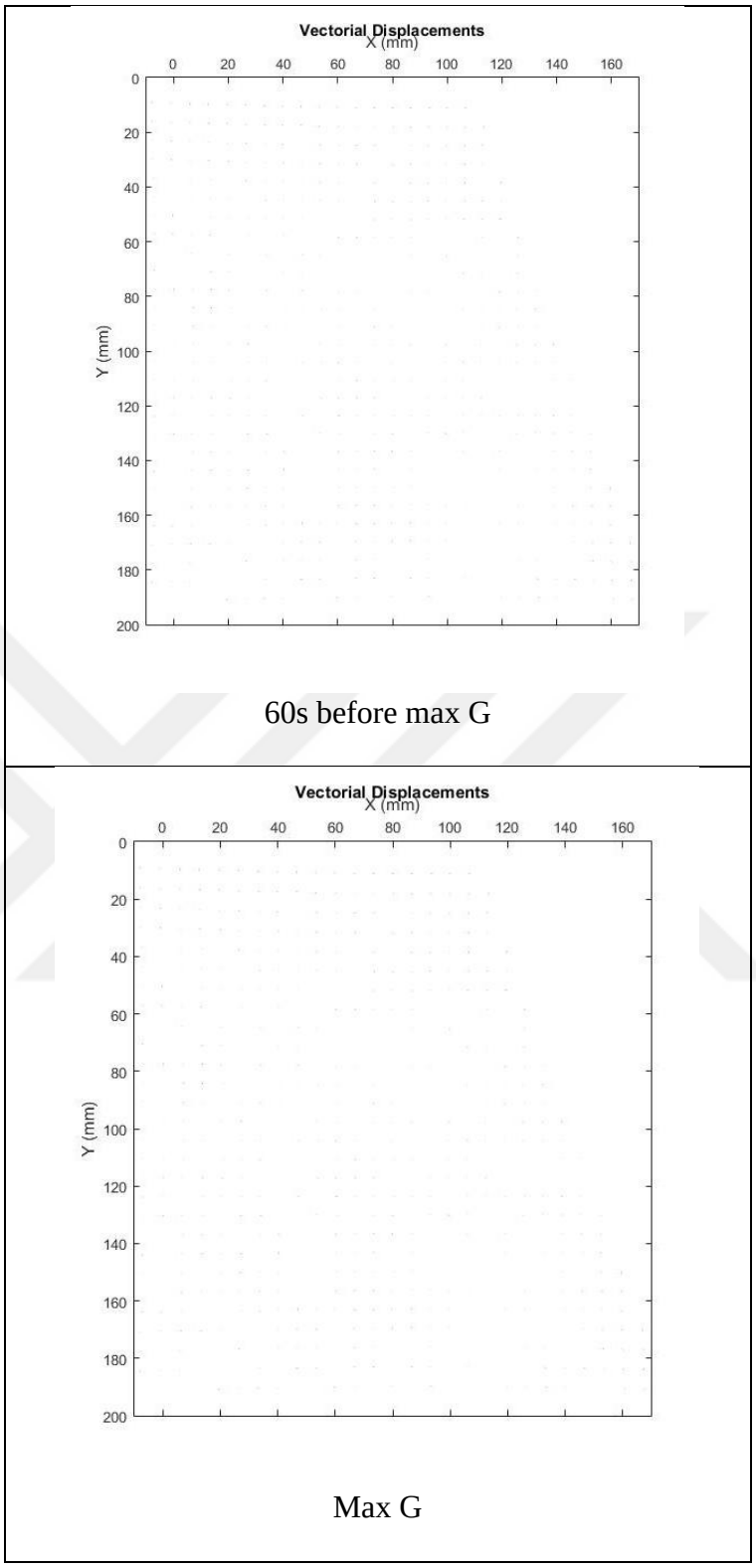

Figure 5.7 : Vector filed of soil displacement.

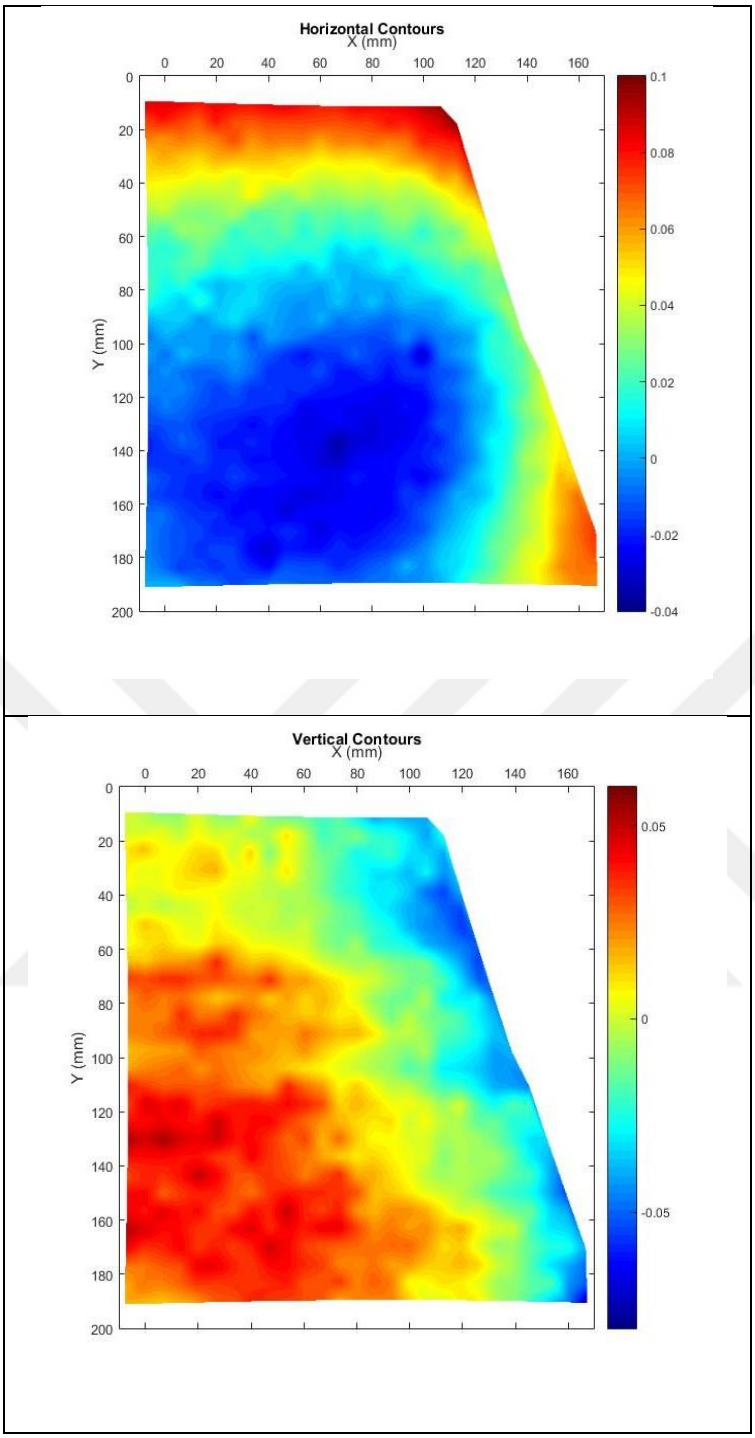

Figure 5.8 : Contours of vertical and horizontal displacement.

Figure 5.9 shows the contours of shear strain of the slope at acceleration of 95g and 60 seconds before it. The maximum displacements are at upper side of the slope. In addition, there are noticeable displacements at slope surface. Generally, the soil failures are close to the slope crest in this slope. Strain concentration are at crest of slope and slope toe.

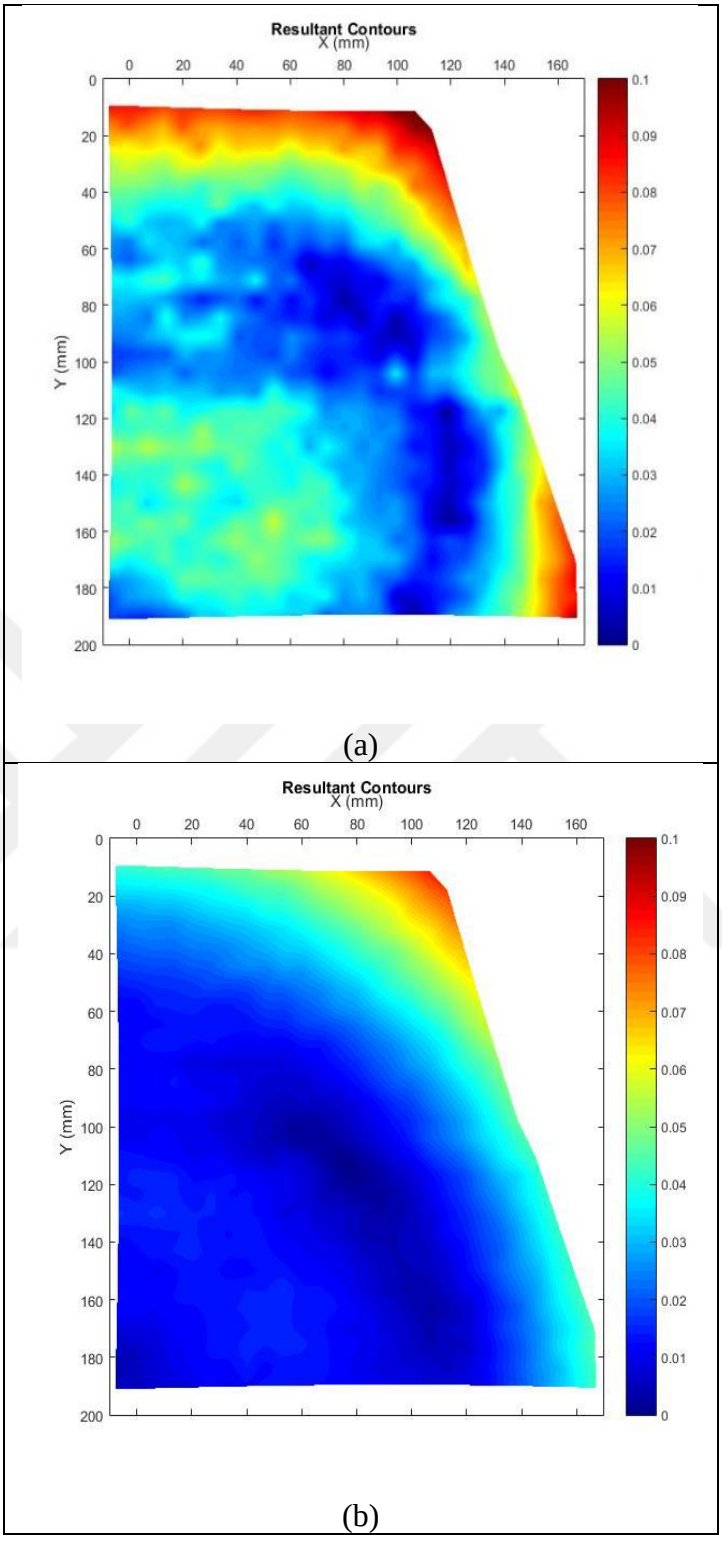

Figure 5.9 : Contours of shear strains at, a) maximum acceleration, and b) 60 seconds before the maximum acceleration.

5.2.1.3 Experiment 4

The properties of experiment 4 is shown in Table 5.4.

Table 5.4 : The properties of experiment 4.

Test No.	Soil Type	Cement content (%)	Water content (%)	Slope model height (cm)	Relative Density (%)	slope inclination	Acceleration at Failure (g)
4	S1	3	6.7	35	72	70°	85.9

The first frame, the last frame (10 seconds before the failure.), and frame of failure are shown in Figure 5.10.

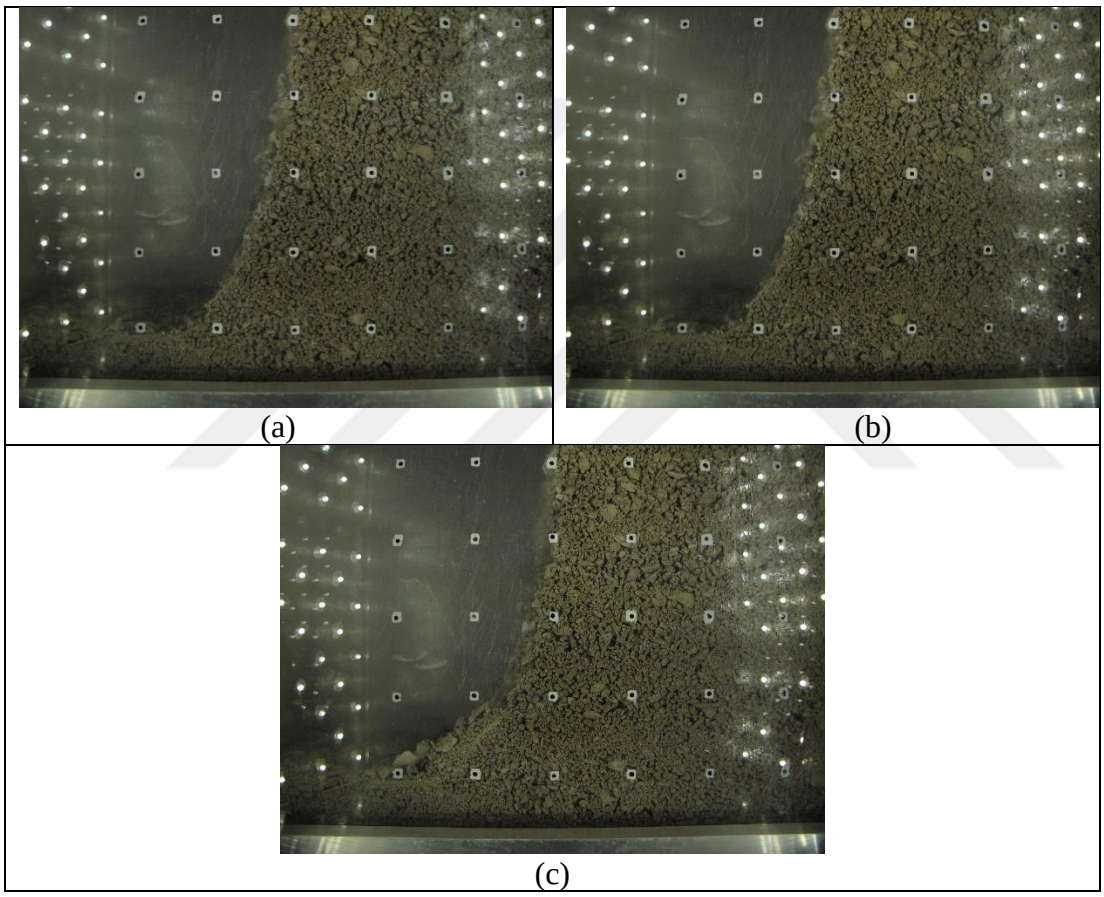

Figure 5.10 : Soil model at a) start of the test, b) 10 seconds before the failure, and c) failure.

In order to observe the displacements, the vectors of displacement at slope crest were magnified and was shown in Figure 5.11. Horizontal and vertical contours of displacements at maximum acceleration are shown in Figure 5.12. The displacements are mostly vertical at upper side of the slope expanding to whole of the slope. However, horizontal displacements with maximum amount of 0.15 mm are at slope surface and slope crest.

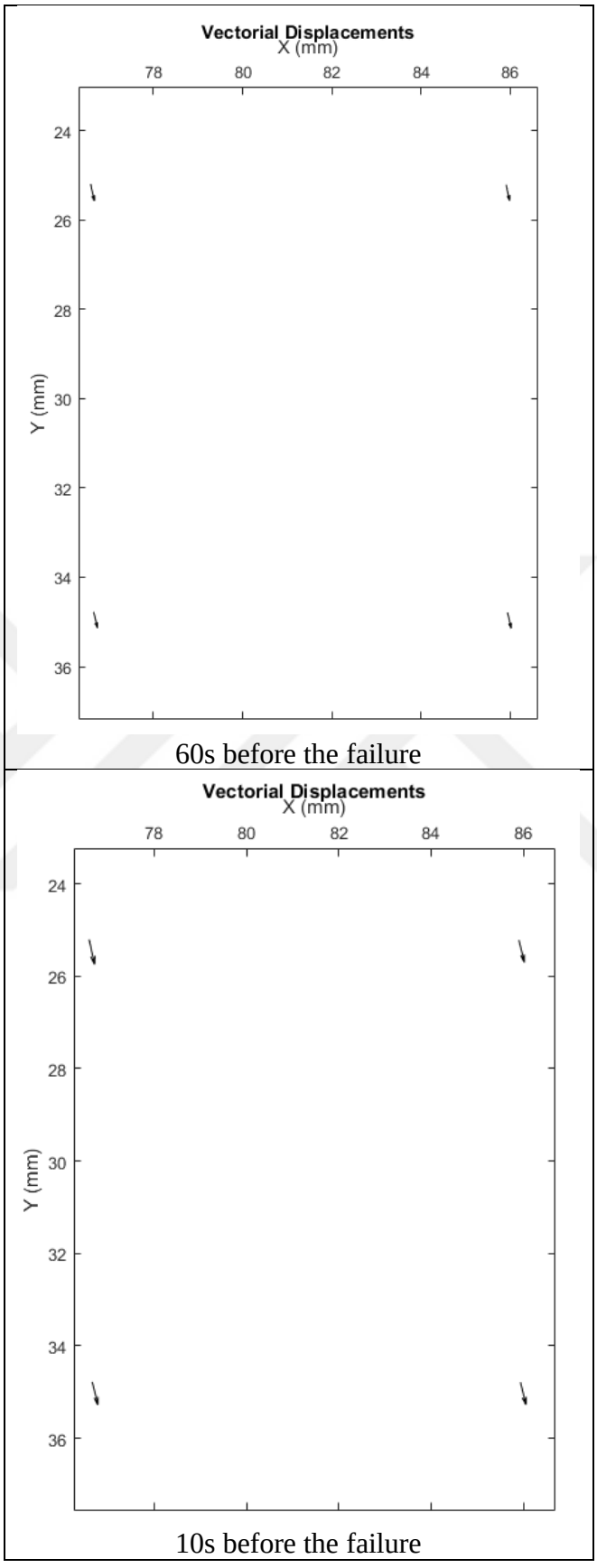

Figure 5.11 : Vector field of soil displacement.

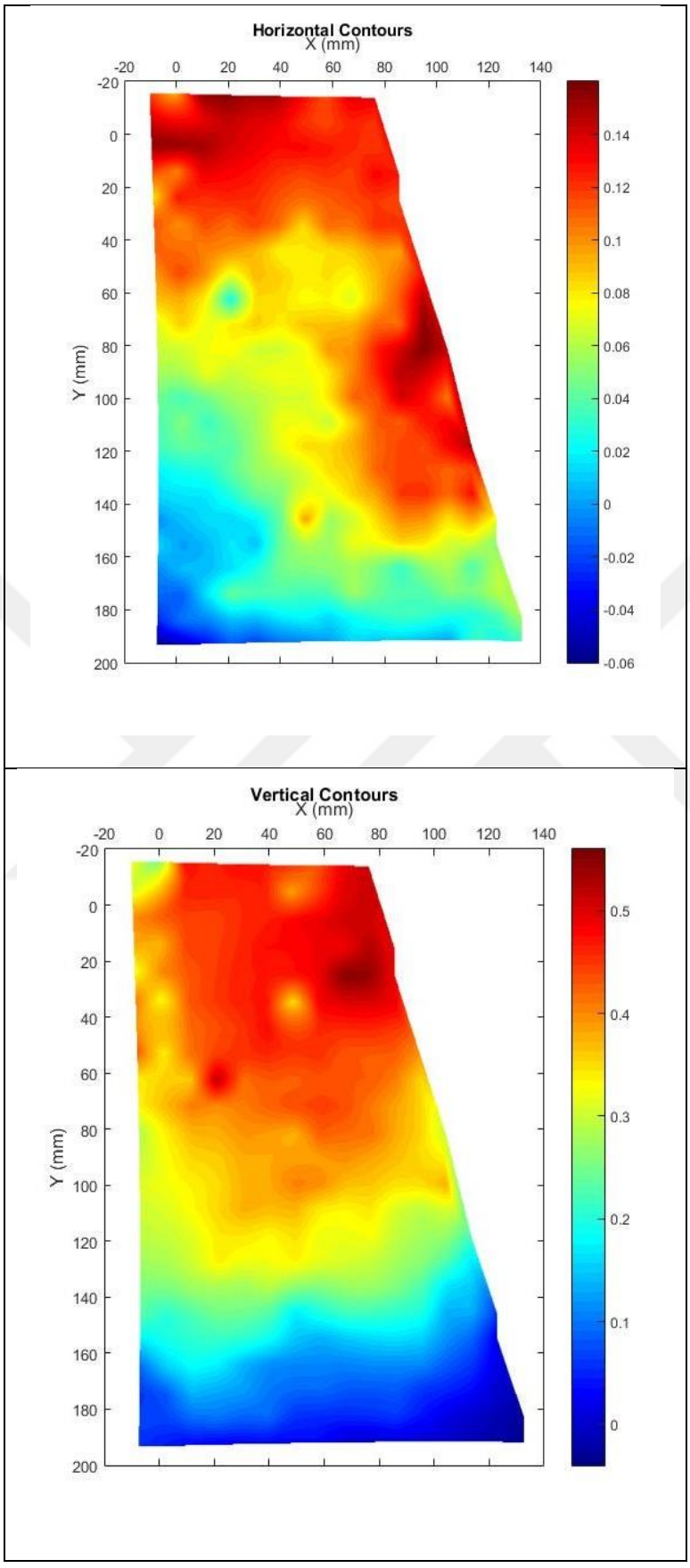

Figure 5.12 : Contours of vertical and horizontal displacement.

Figure 5.13 shows the contours of shear strain of the slope, 10 seconds and 60 seconds before the failure. The soil failures are close to the slope crest. The failure was started from upper side of the slope and tends to expand to lower part.

Strain concentration is at upper part of slope, between 10-90 mms in X direction and between -10-40 mms in Y direction.

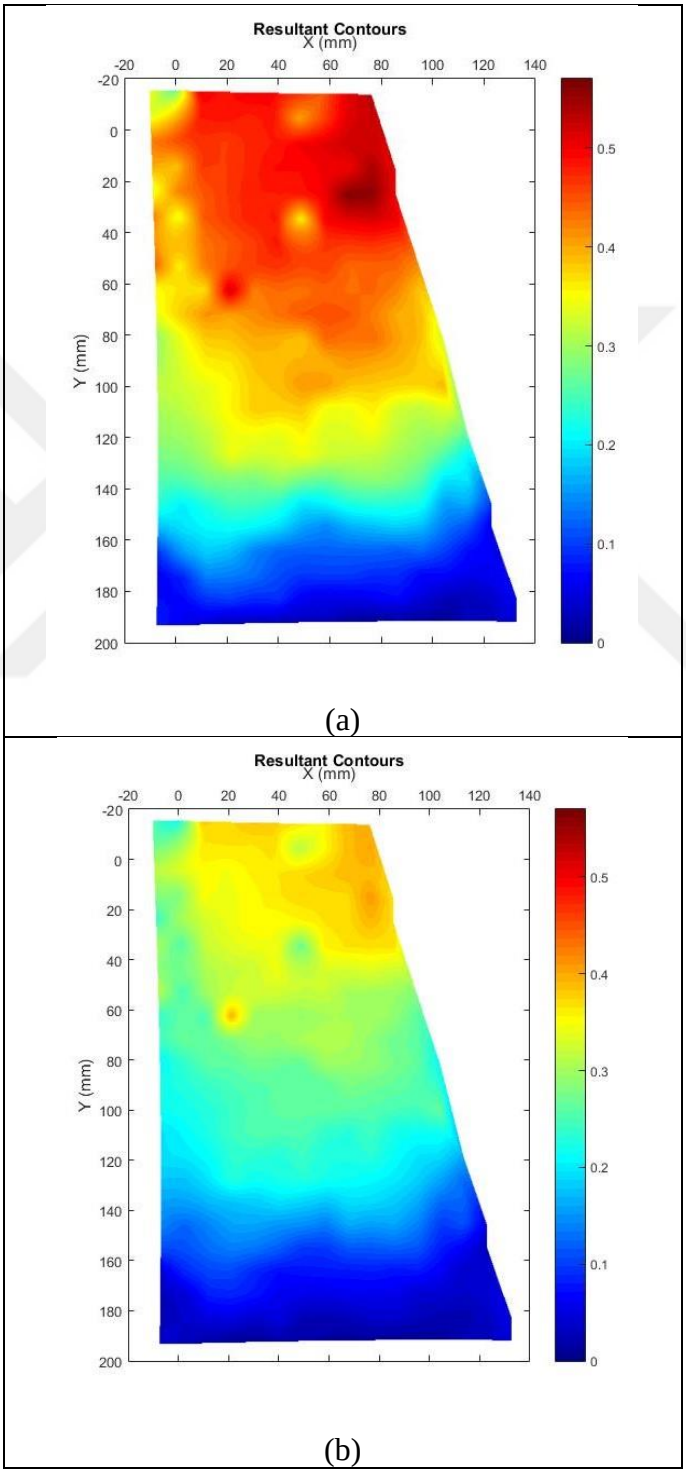

Figure 5.13 : Contours of shear strains at, a) 10s before the failure, and b) 60s before the failure.

5.2.1.4 Experiment 6

The properties of experiment 6 is shown in Table 5.5.

Table 5.5 : The properties of experiment 6.

Test No.	Soil Type	Cement content (%)	Water content (%)	Slope model height (cm)	Relative Density (%)	slope inclination	Acceleration at Failure (g)
6	S1	0	6.7	25	72	70°	35

The first frame, the last frame (10 seconds before the failure.), and frame of failure are shown in Figure 5.14.

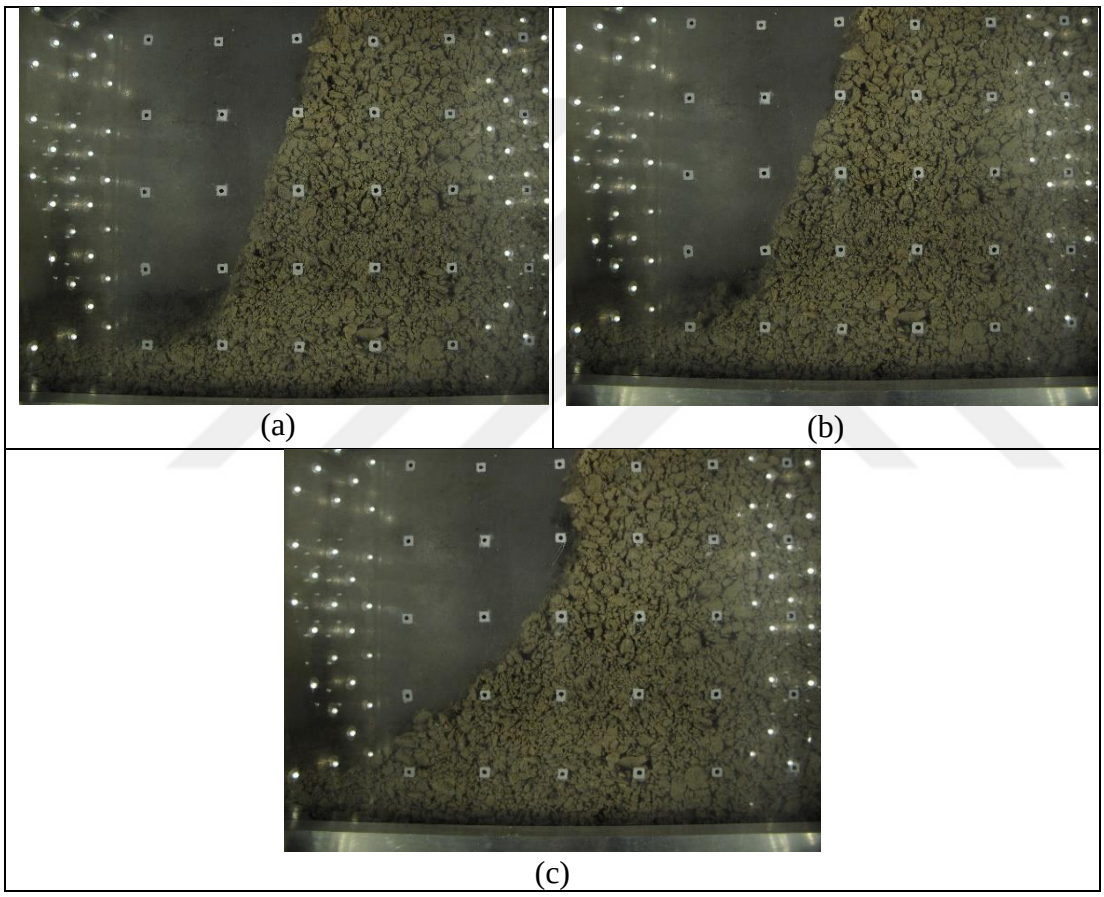

Figure 5.14 : Soil model at a) start of the test, b) 10 seconds before the failure, and c) failure.

The vectorial displacements are shown in Figure 5.15. Since the soil is non-cemented in this model, the displacement vectors are more obvious. The maximum displacement has occurred at upper side of the slope and near the slope surface. Horizontal and vertical contours of displacements at maximum acceleration are shown in Figure 5.16. According to Figure 5.16, The horizontal displacements are significant at slope surface and the maximum vertical displacement has occurred at slope crest.

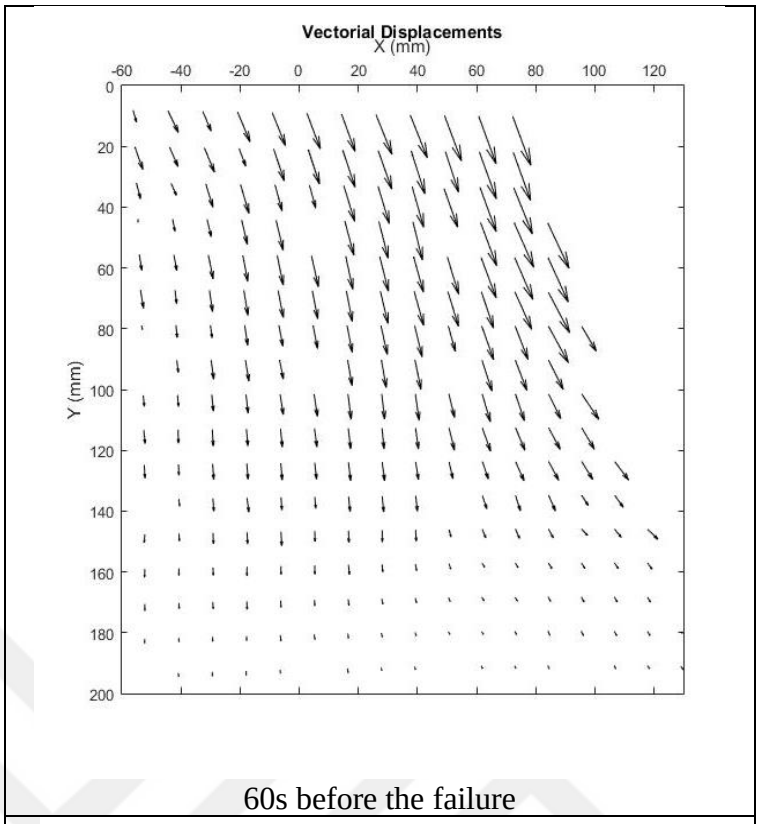

60s before the failure

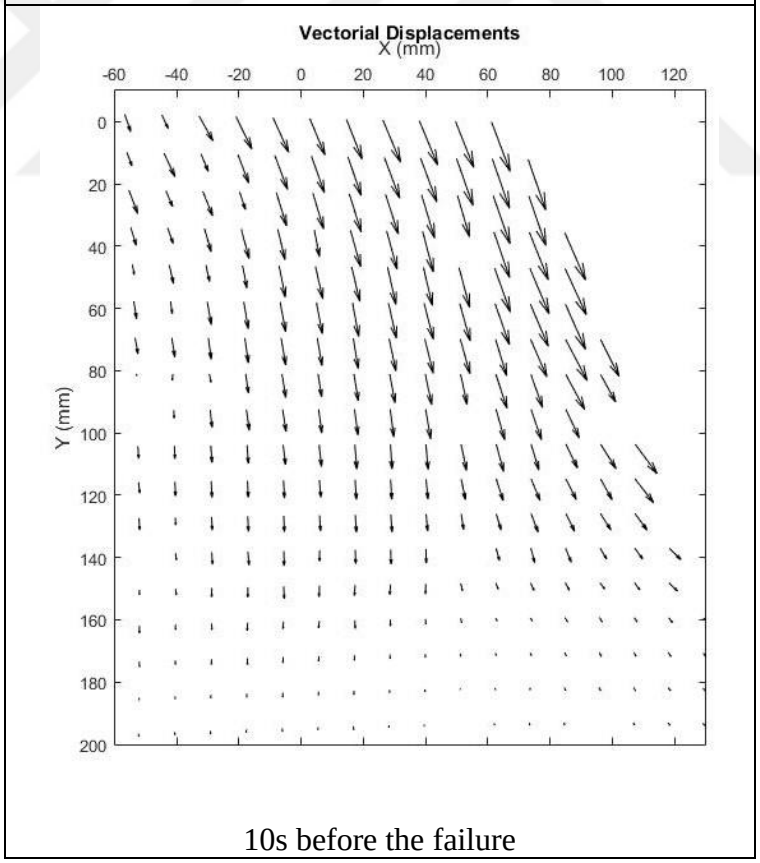

10s before the failure

Figure 5.15 : Vector field of soil displacement.

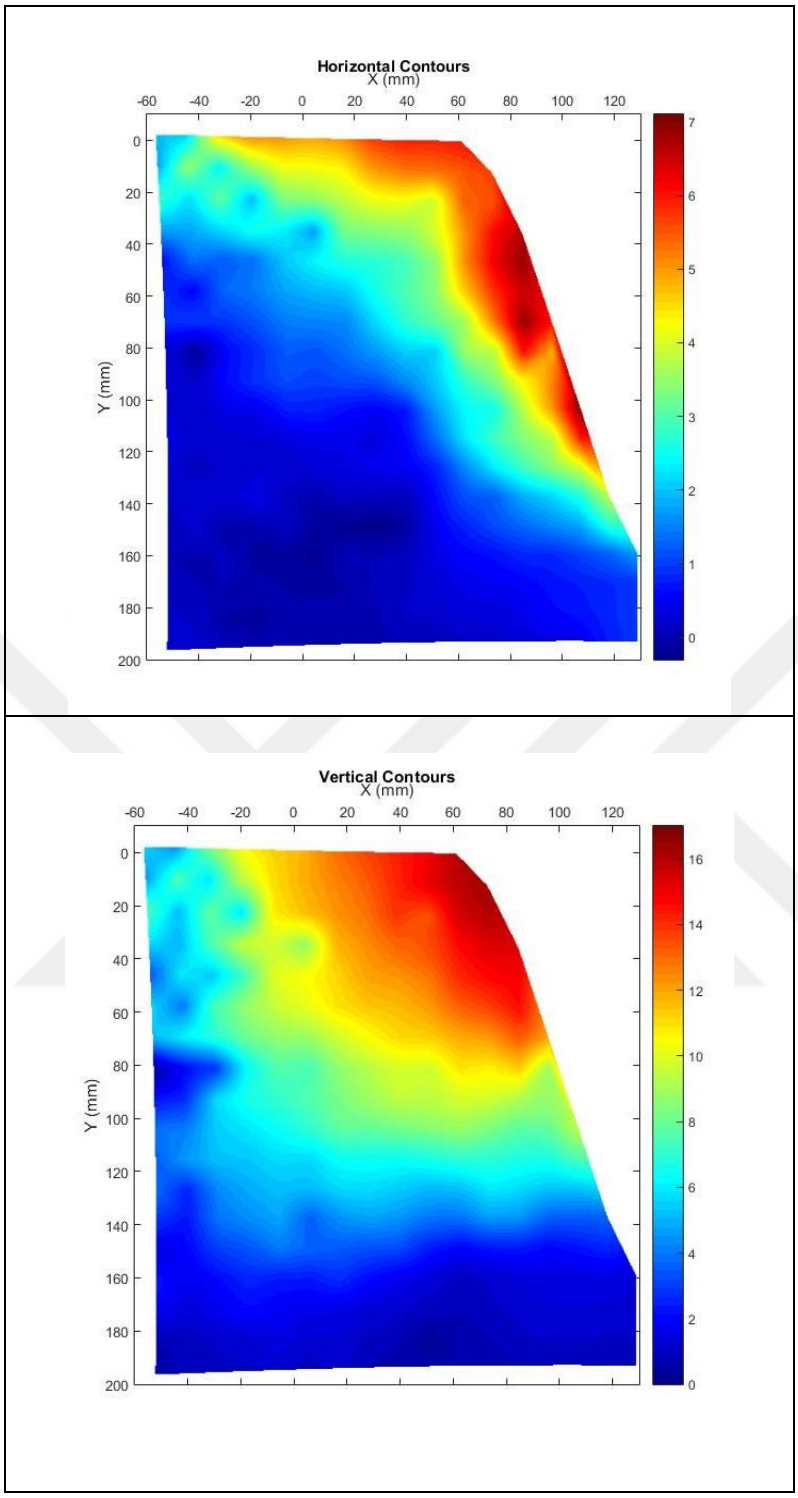

Figure 5.16 : Contours of vertical and horizontal displacement.

Figure 5.17 shows the contours of shear strain of the slope, 10 seconds and 60 seconds, and 240 seconds before the failure. According to results of shear strains, the soil failures are close to the slope crest. The failure has started from upper side of the slope and tends to expand to lower part and slope surface.

Strain concentration is at crest of slope, between 40-90 mms in X direction and between 0-60 mms in Y direction.

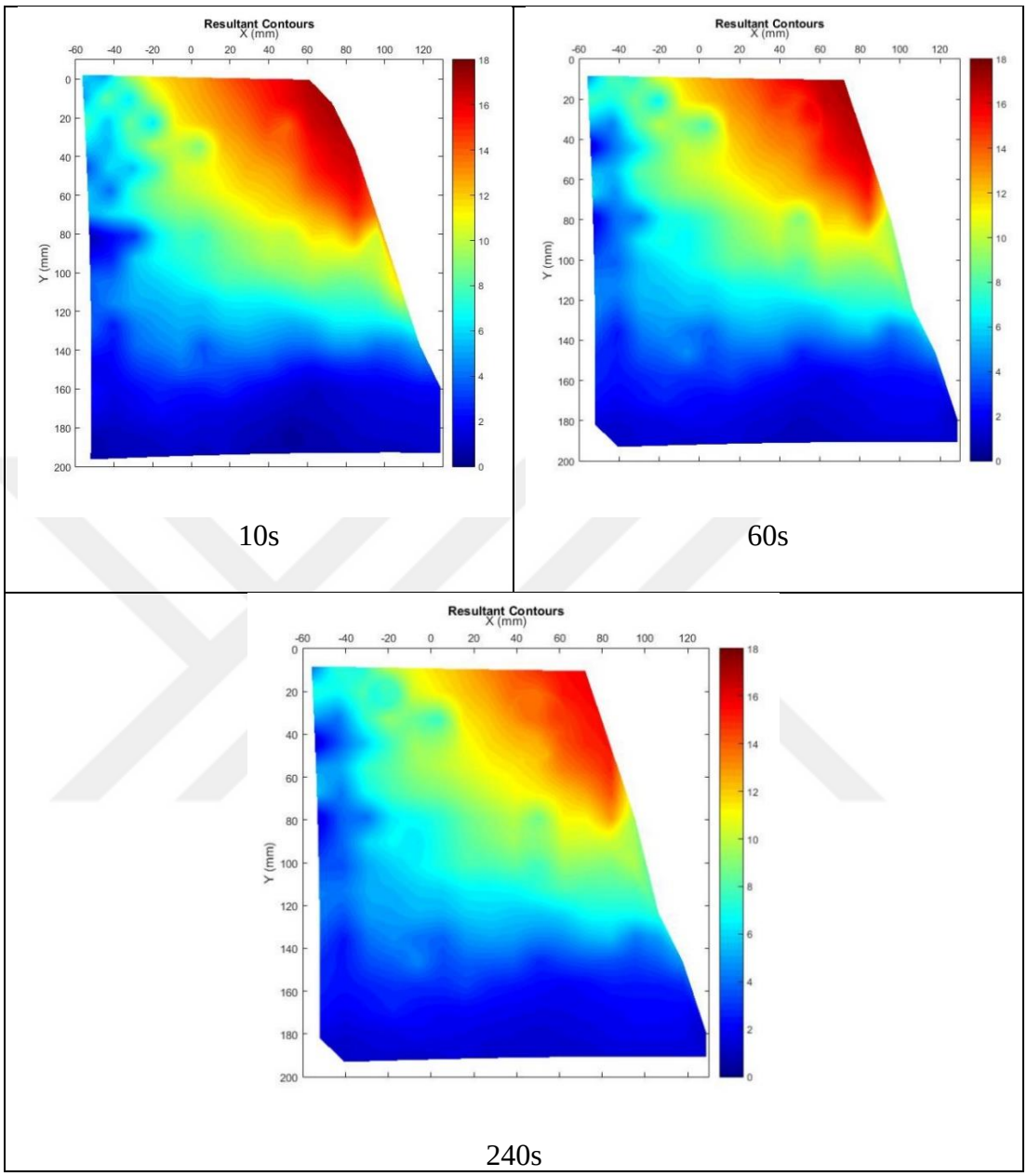

Figure 5.17 : Contours of shear strains, 10 seconds, 60 seconds, and 240 seconds before the failure.

5.2.1.5 Experiment 9

The properties of experiment 9 is shown in Table 5.6.

Table 5.6 : The properties of experiment 9.

Test No.	Soil Type	Cement content (%)	Water content (%)	Slope model height (cm)	Relative Density (%)	slope inclination	Acceleration at Failure (g)
9	S2	3	5	30	40	70°	-

The first frame, the last frame (slope at maximum acceleration of 95 g), and frame of failure are shown in Figure 5.18.

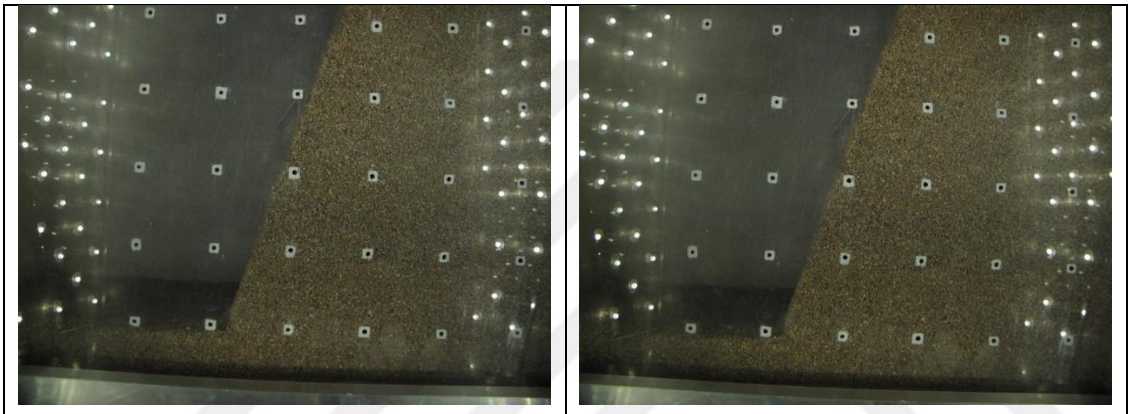

(a) (b)

Figure 5.18 : Soil model at a) start of the test, and b) maximum acceleration.

Since the displacement amount is very little in this test, vectorial displacements are not clear, (Figure 5.19).

Horizontal and vertical contours of displacements at maximum acceleration are shown in Figure 5.20. Both horizontal and vertical displacement have occurred at slope mid-height and near the slope surface. Horizontal displacements developed along the whole surface between 60-120mm in X direction and between 40-140mm in Y direction.

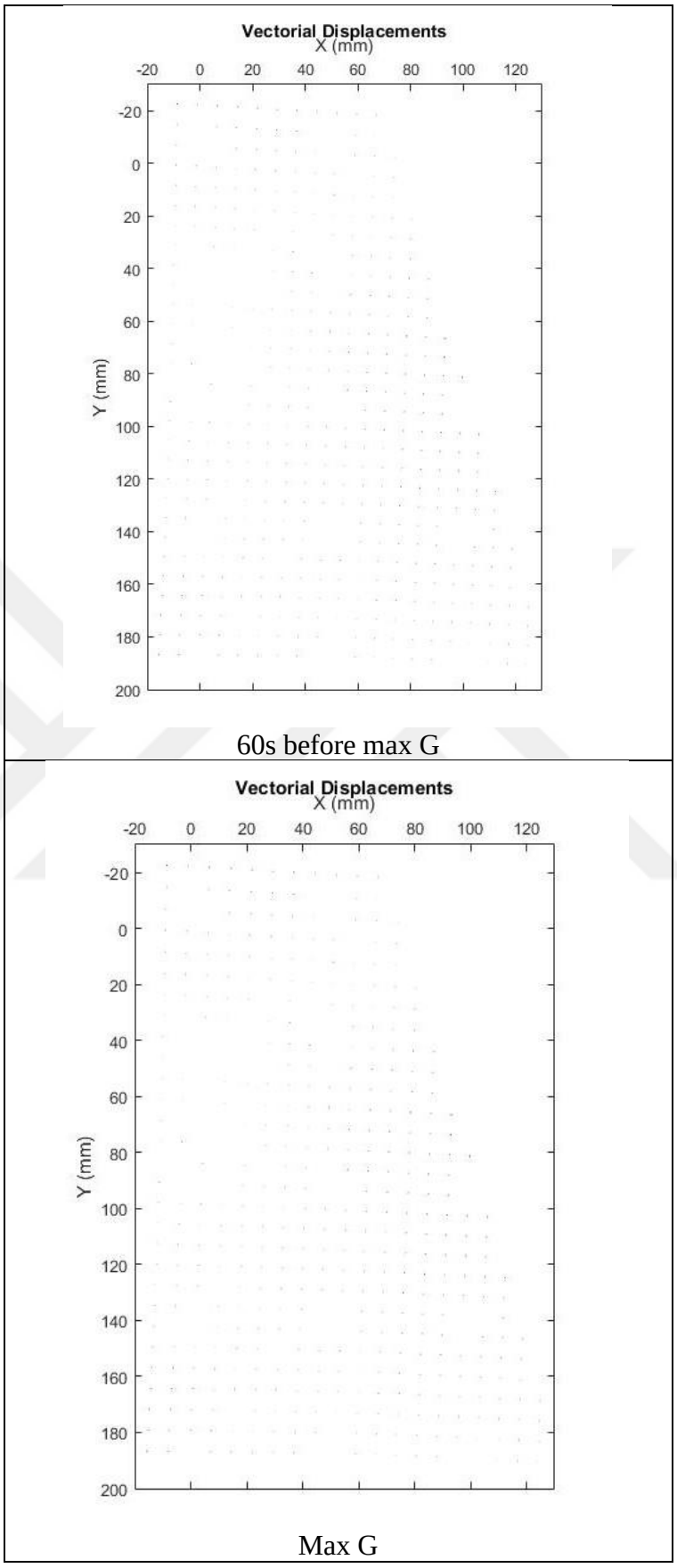

Figure 5.19 : Vector field of soil displacement.

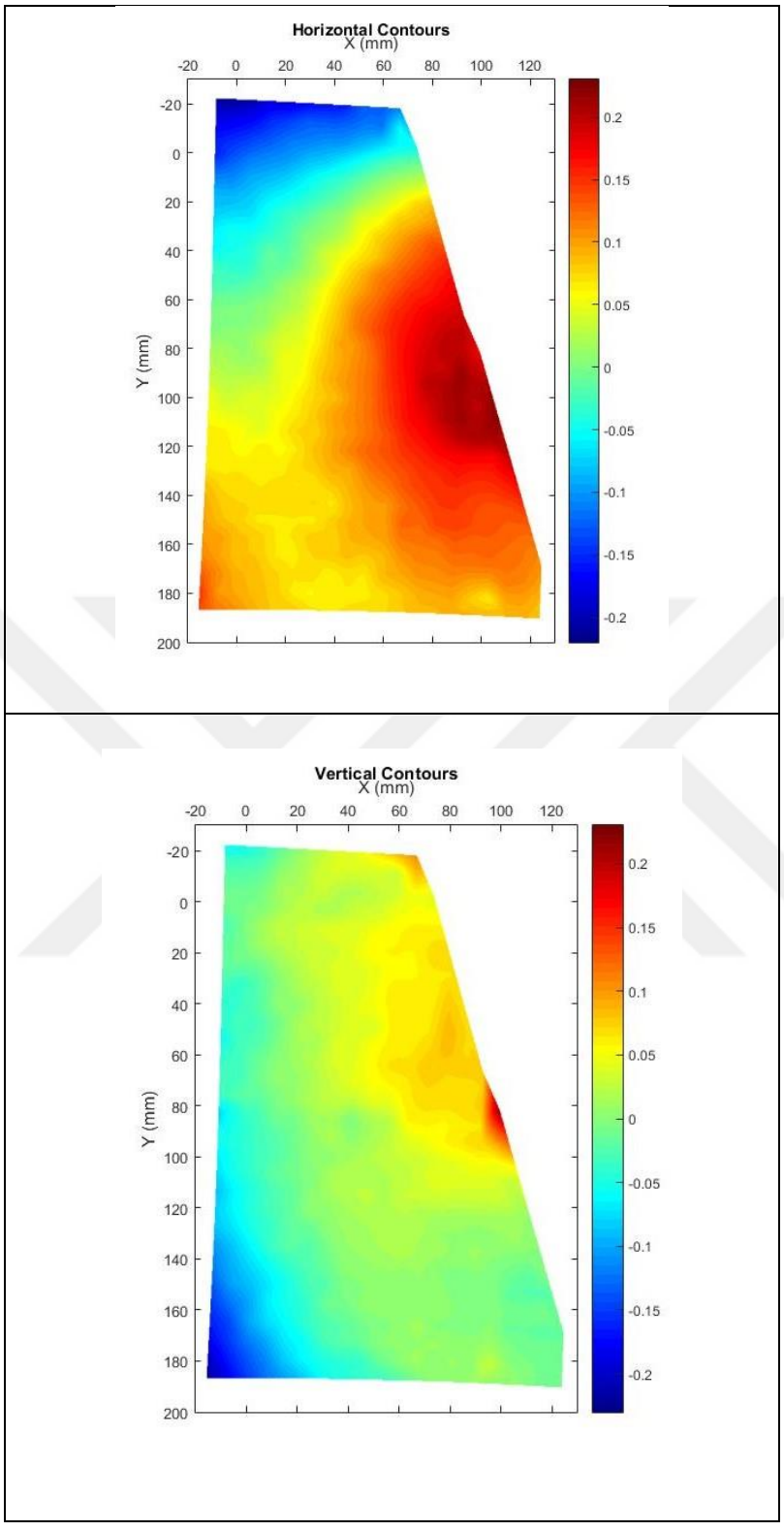

Figure 5.20 : Contours of vertical and horizontal displacement.

Figure 5.21 shows the contours of shear strain of the slope at acceleration of 95g and 60 seconds before the maximum acceleration. The soil failures initiate at mid-height of the slope near the slope surface. However, some displacements are observed at upper side and lower side of the slope in opposite side of the slope surface.

Strain concentration is at middle height of slope, near the surface, and opposite side of slope face at upper and lower part of slope.

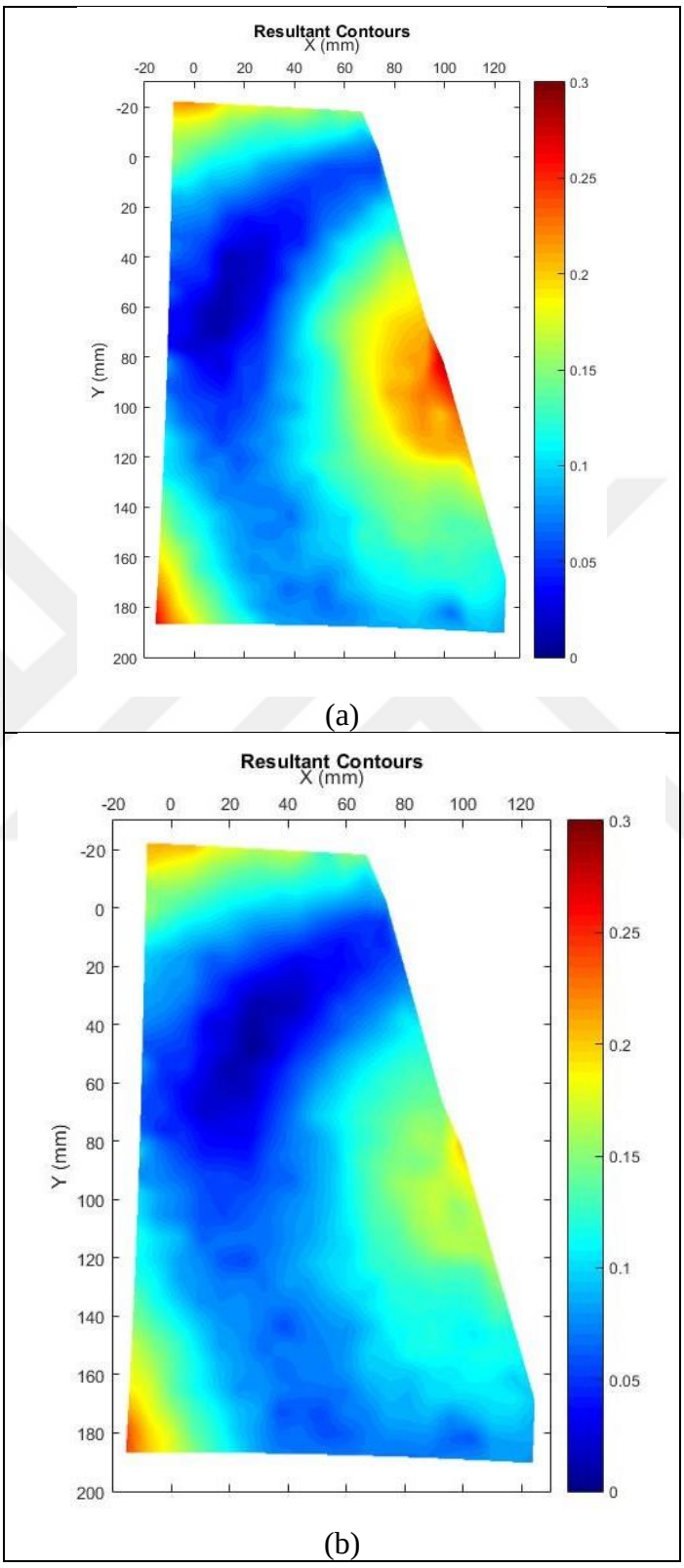

Figure 5.21 : Contours of shear strains at, a) maximum acceleration of 95g, b) 60s before maximum acceleration.

5.2.2 Slopes with 90° inclination

5.2.2.1 Experiment 3

The properties of experiment 3 is shown in Table 5.7.

Table 5.7 : The properties of experiment 3.

Test No.	Soil Type	Cement content (%)	Water content (%)	Slope model height (cm)	Relative Density (%)	slope inclination	Acceleration at Failure (g)
3	S1	3	6.7	35	72	90°	48.2

The first frame, the last frame (10 seconds before the failure.), and frame of failure are shown in Figure 5.22.

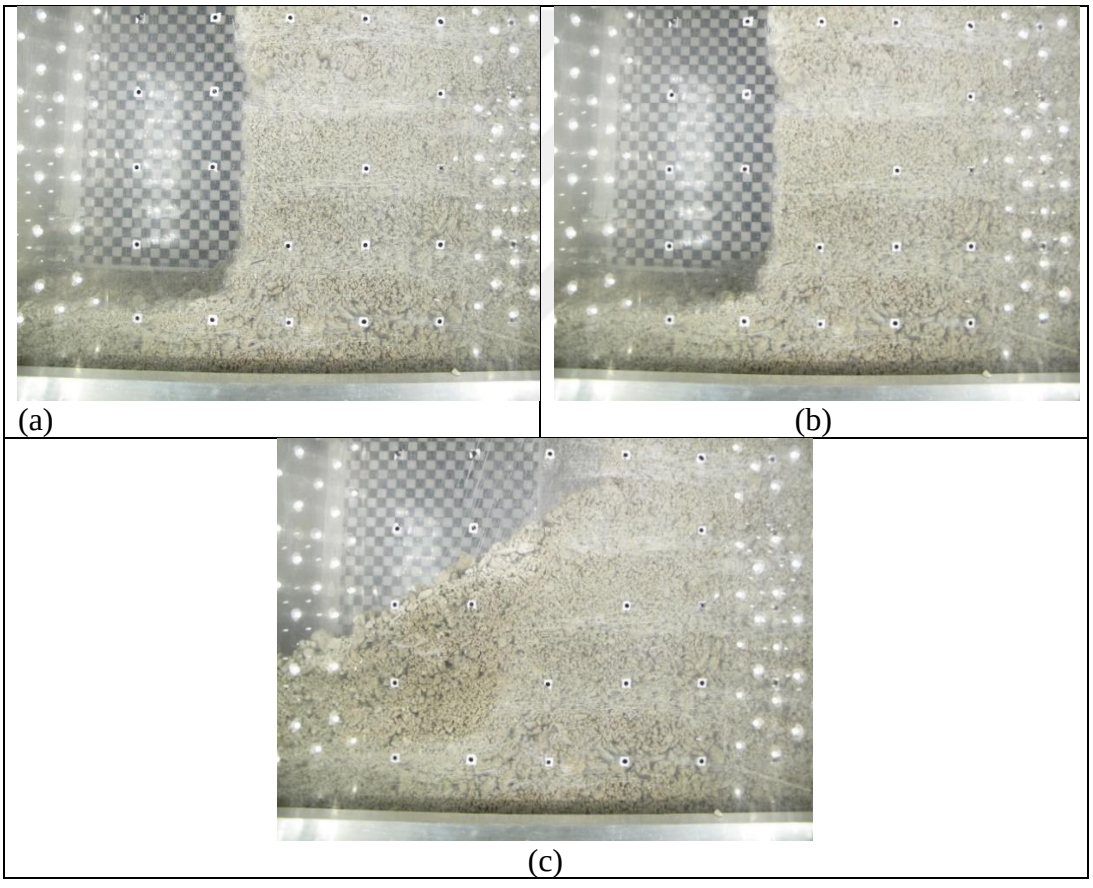

Figure 5.22 : Soil model at a) start of the test, b) 10 seconds before the failure, and c) failure.

Since the displacement amount is very little in this test, vectorial displacements are not clear. (Figure 5.23)

The results of this test are affected by some experimental error. The Plexiglass is dirty and unclear is some parts, that effected the results of this experiment.

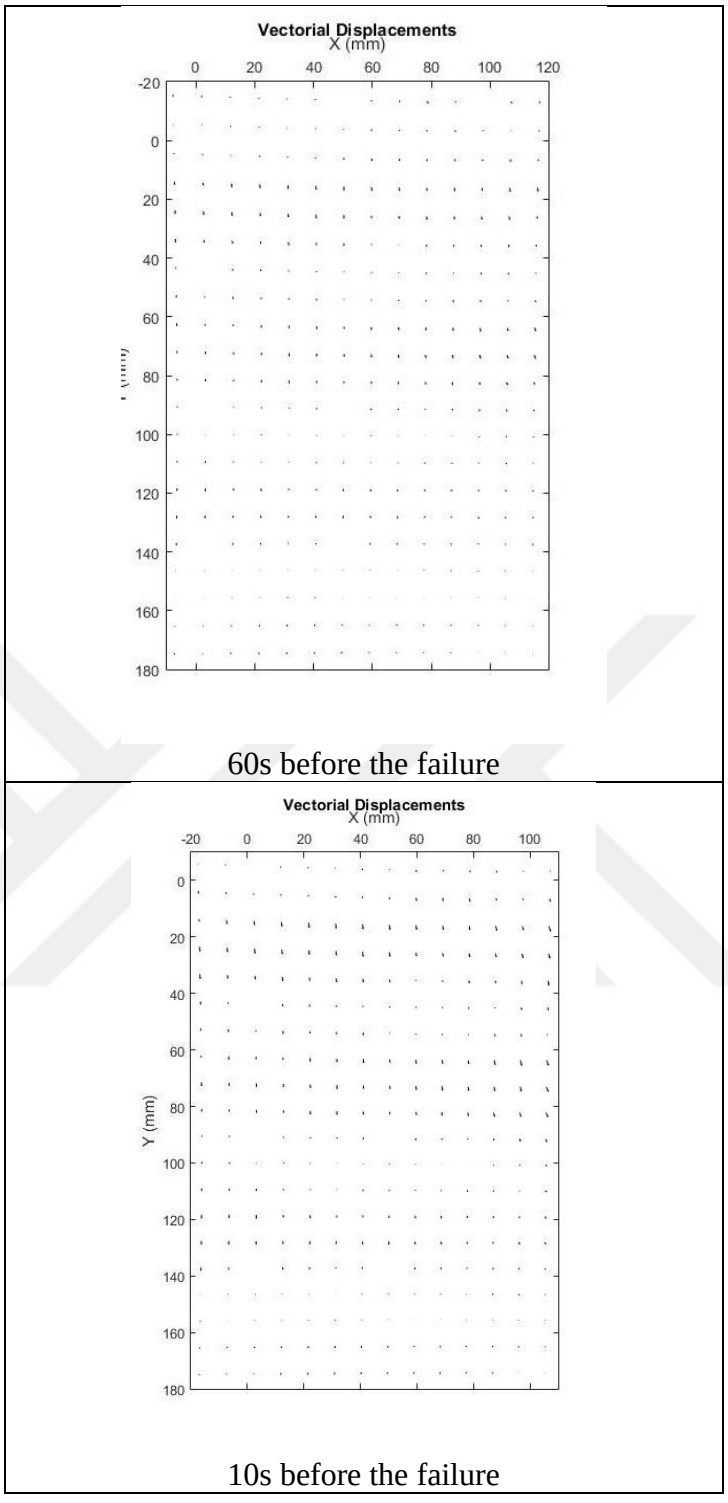

Figure 5.23 : Vector field of soil displacement.

Horizontal and vertical contours of displacements at maximum acceleration are shown in Figure 5.24. The displacements are mostly vertical. Figure 5.25 shows the contours of shear strain of the slope. According to Figures 5.23, 5.24 and 5.25, the displacements are significant in some layers and in some layers the minimum displacements were occurred. The reason is that dirt on the plexiglass. However,

according to Figure 5.25, shear strains with maximum amount of 2 mms were happened in this test and the displacements were mostly at upper side of the slope. Strain concentration is at upper part of slope.

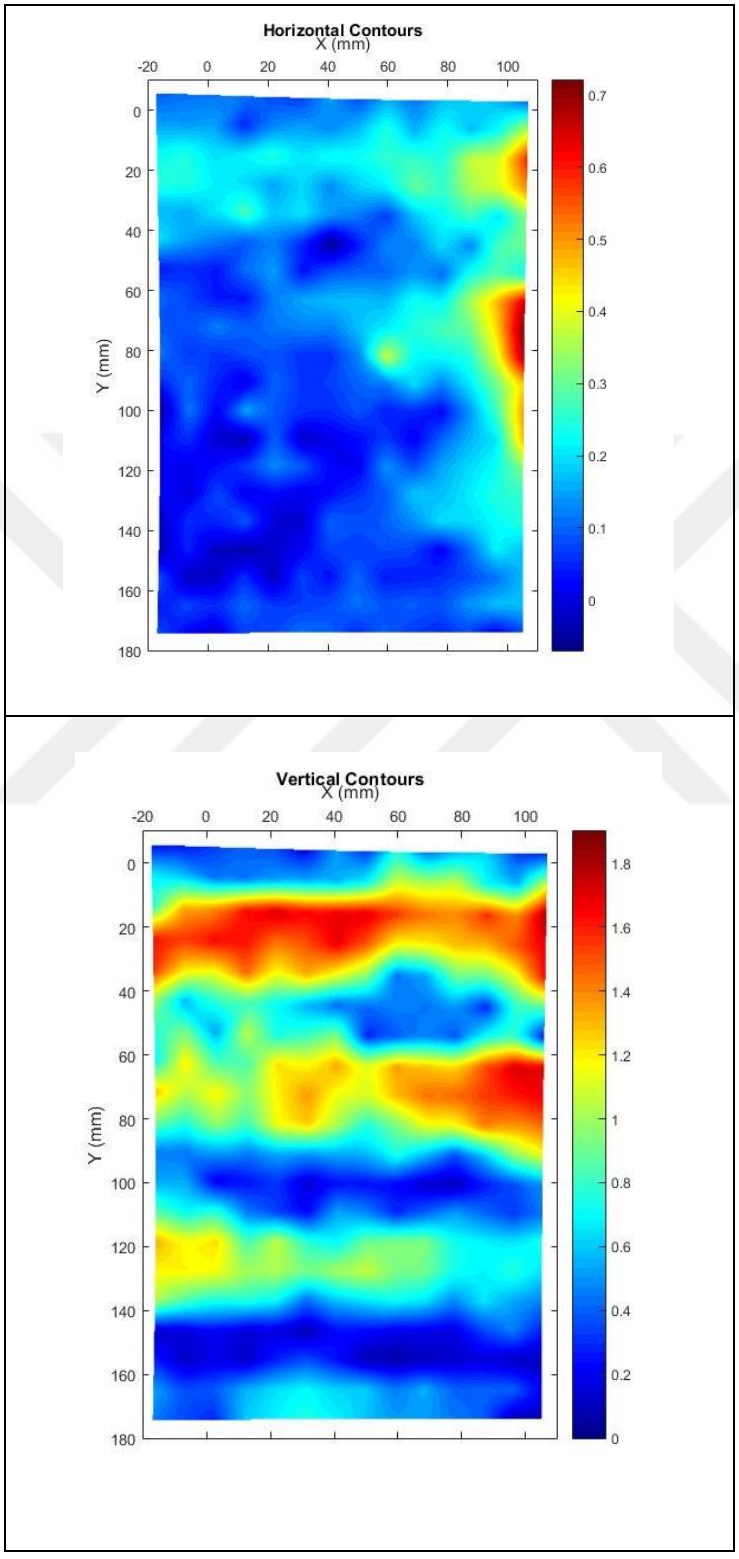

Figure 5.24 : Contours of vertical and horizontal displacement.

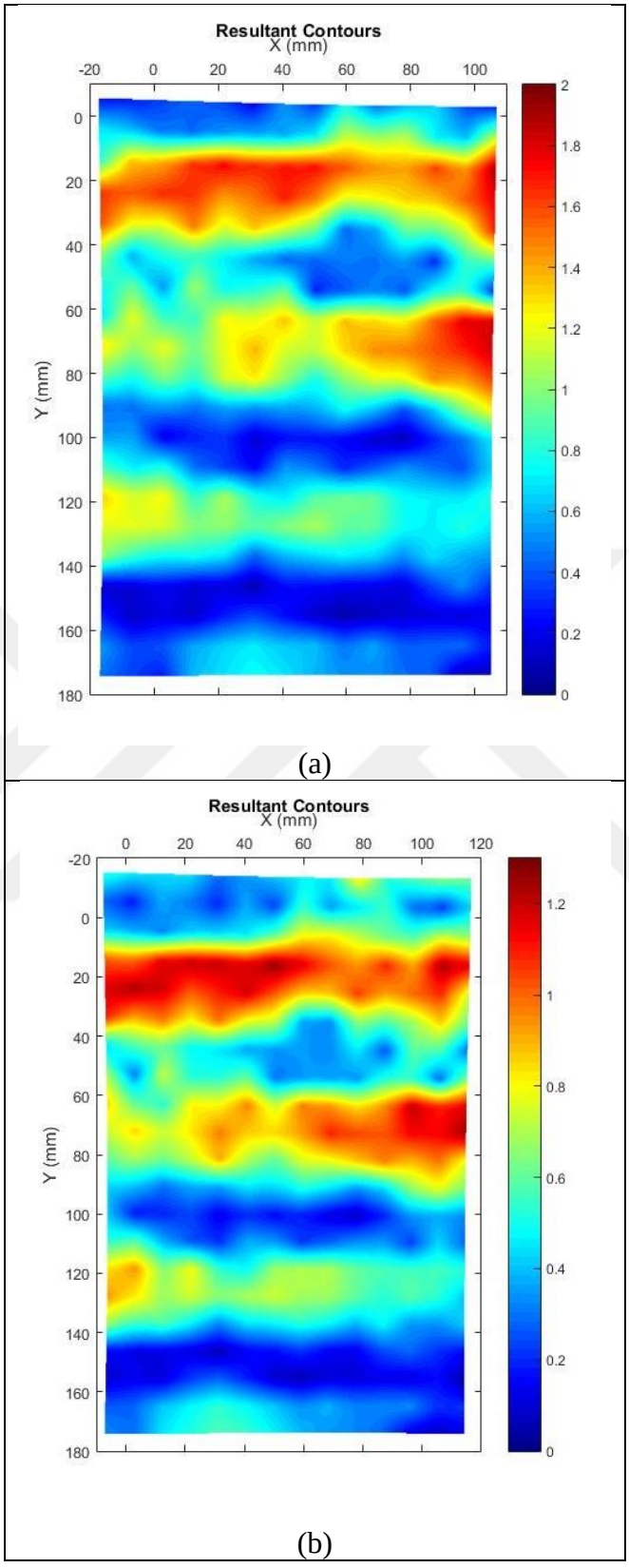

Figure 5.25 : Contours of shear strains at, a) maximum acceleration of 95g, and b) 60s before maximum acceleration.

5.2.2.2 Experiment 5

The properties of experiment 5 is shown in Table 5.8.

Table 5.8 : The properties of experiment 5.

Test No.	Soil Type	Cement content (%)	Water content (%)	Slope model height (cm)	Relative Density (%)	slope inclination	Acceleration at Failure (g)
5	S1	3	6.7	30	72	90°	59.5

The first frame, the last frame (10 seconds before the failure.), and frame of failure are shown in Figure 5.26.

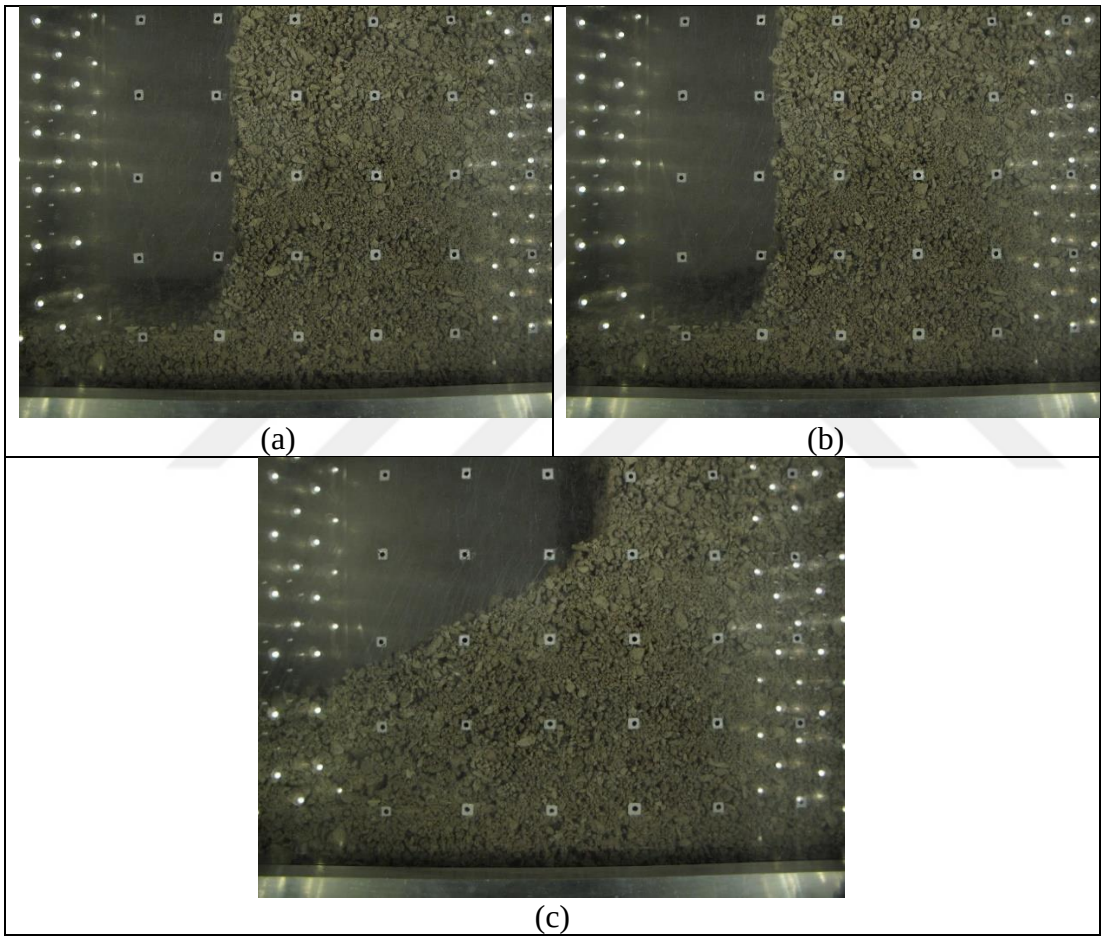

Figure 5.26 : Soil model at a) start of the test, b) 10 seconds before the failure, and c) failure.

In order to observe the displacements, the vectors of displacement at slope crest were magnified and was shown in Figure 5.27. Horizontal and vertical contours of displacements (10 seconds before the failure) are shown in Figure 5.28. In both horizontal and vertical displacement contours, the maximum displacements have occurred at upper side of the slope near the slope surface and slope crest. The

coordinates of the maximum vertical displacements are between 60-120 mm in X direction and between -10-60 mm in Y direction.

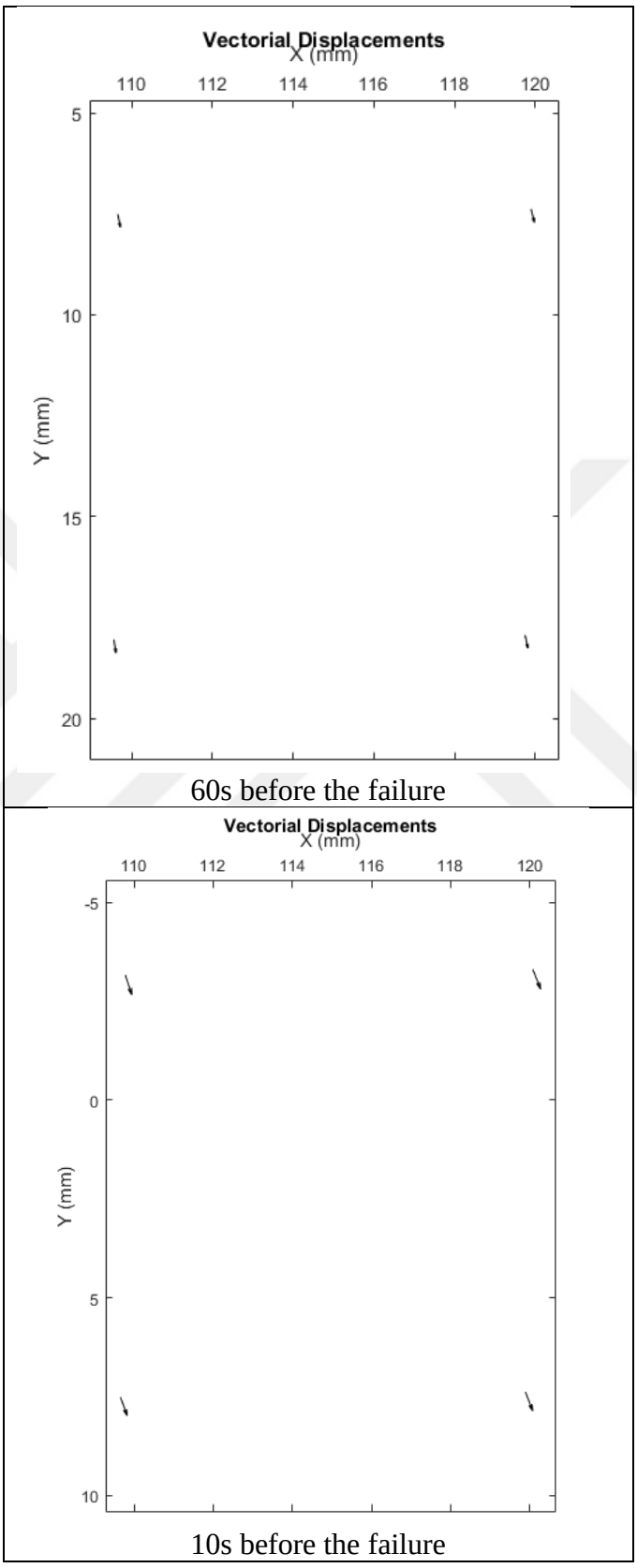

Figure 5.27 : Magnified vector field of soil displacement.

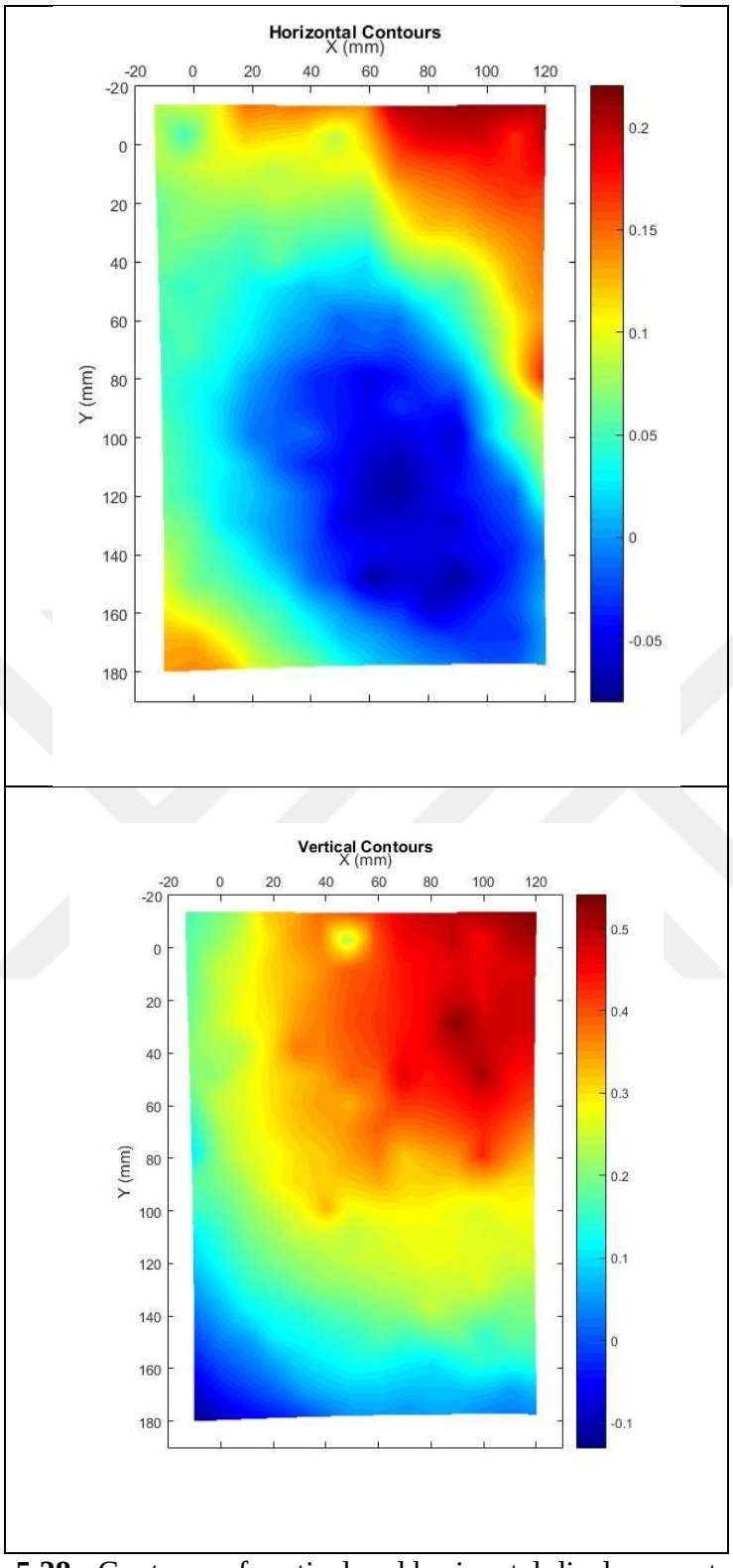

Figure 5.28 : Contours of vertical and horizontal displacement.

Figure 5.29 shows the contours of shear strain of the slope (10 seconds and 60 seconds before the failure). According to Figure 5.29 soil failure was initiated at slope crest and was developed in both X and Y directions.

Strain concentration is at upper part of slope, between 60-120 mms in X direction and between -20-40 mms in Y direction.

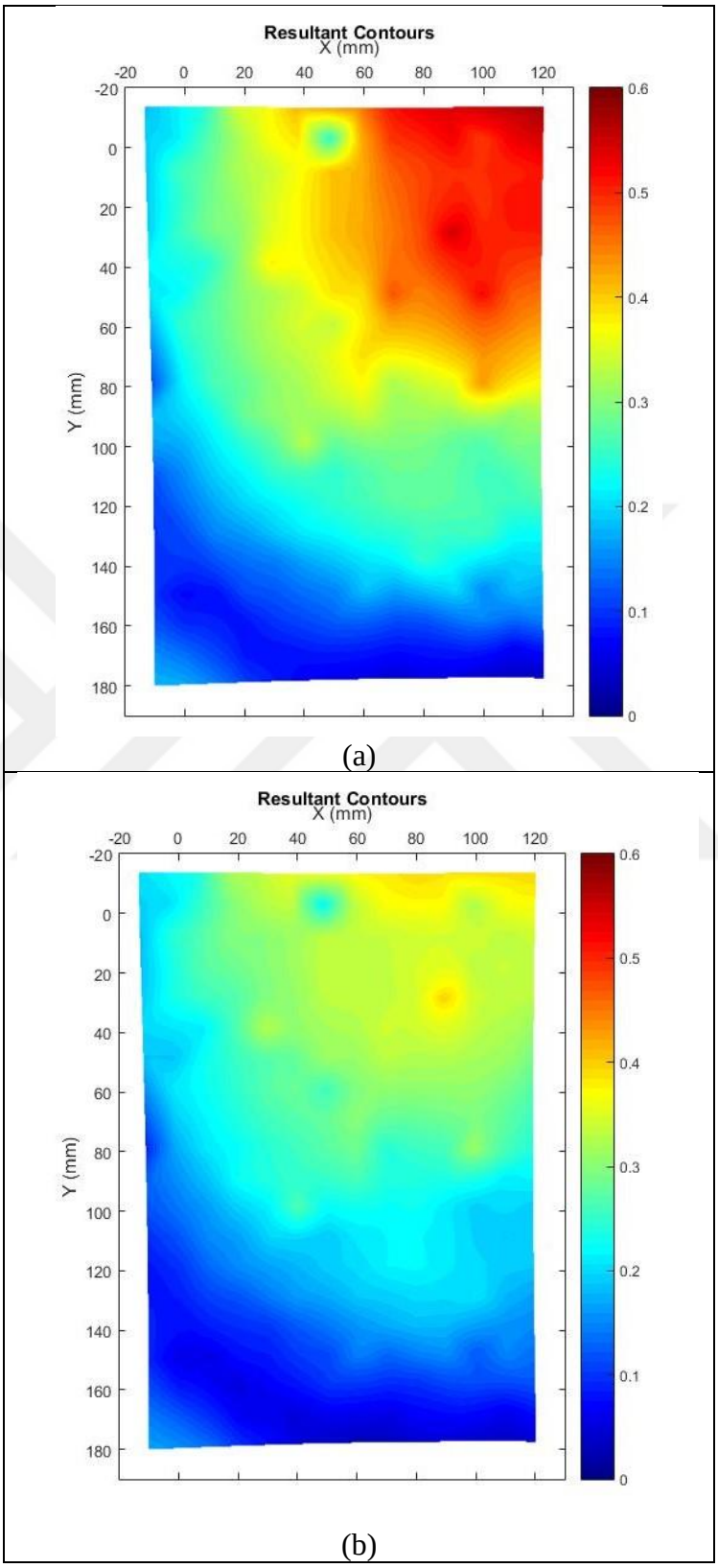

Figure 5.29 : Contours of shear strains at, a) 10s before the failure, and b) 60s before the failure.

5.2.2.3 Experiment 7

The properties of experiment 7 is shown in Table 5.9.

Table 5.9 : The properties of experiment 7.

Test No.	Soil Type	Cement content (%)	Water content (%)	Slope model height (cm)	Relative Density (%)	slope inclination	Acceleration at Failure (g)
7	S1	0	6.7	25	72	90°	12.8

The first frame, the last frame (10 seconds before the failure.), and frame of failure are shown in Figure 5.30.

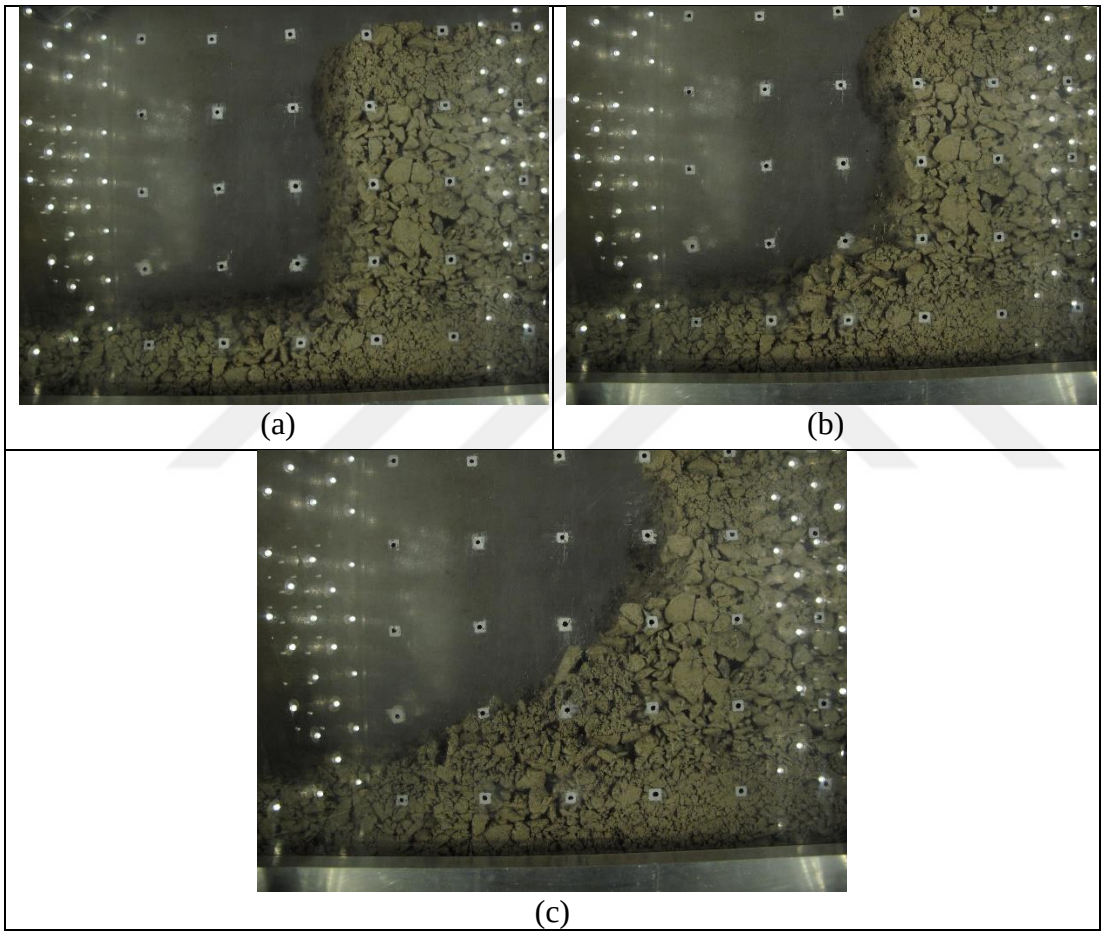

Figure 5.30 : Soil model at a) start of the test, b) 10 seconds before the failure, and c) failure.

In order to observe the displacements, the vectors of displacement at lower part of the slope, opposite side of slope surface were magnified and was shown in Figure 5.31. According to Figure 5.31, direction of the displacement vectors has changed.

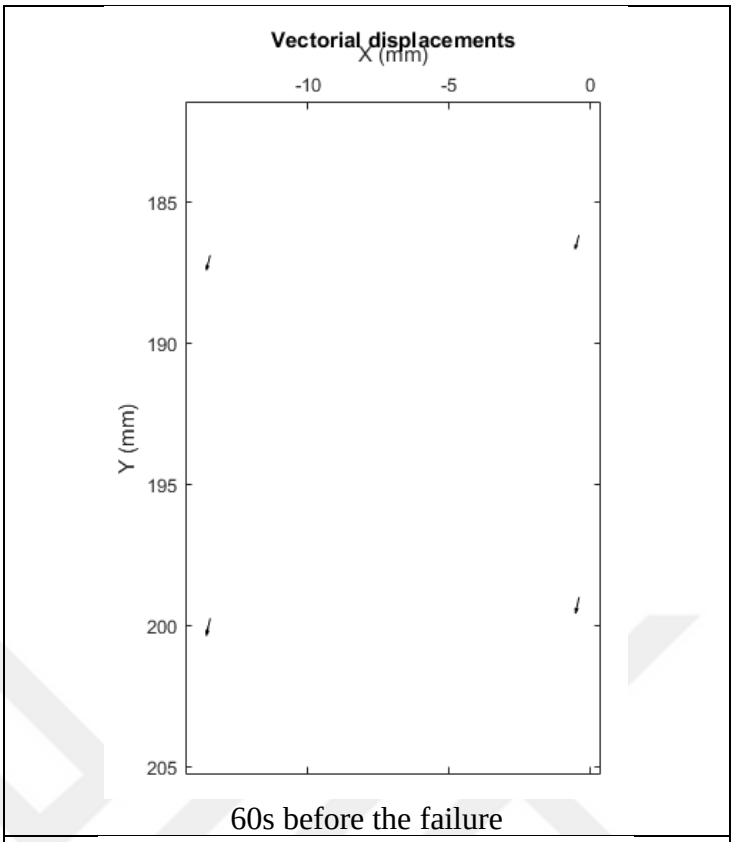

60s before the failure

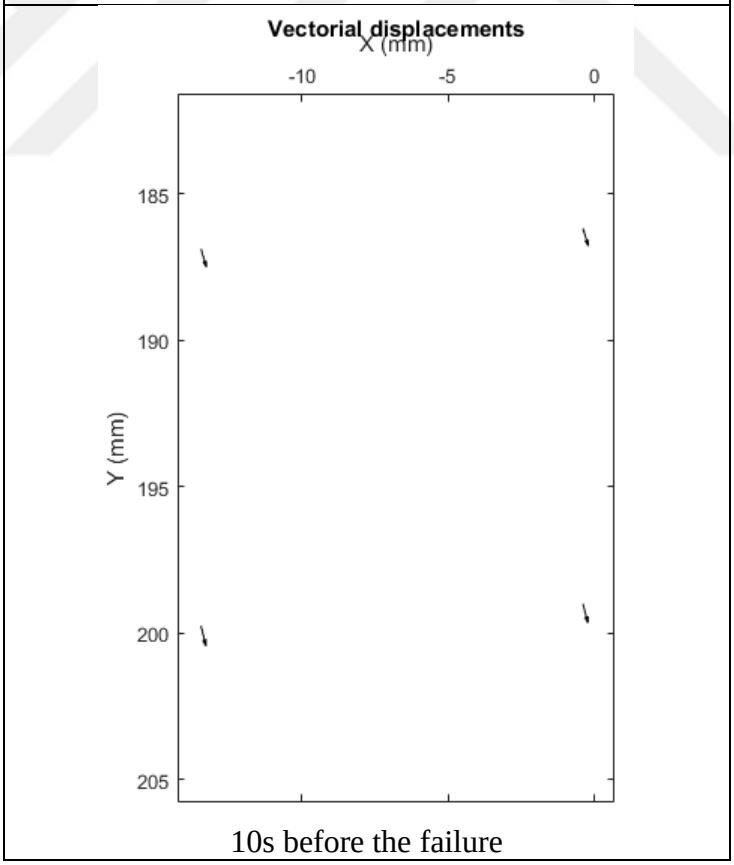

10s before the failure

Figure 5.31 : Magnified vector field of soil displacement.

Horizontal and vertical contours of displacements (10 seconds before the failure) are shown in Figure 5.32. Horizontal displacements have occurred mostly at slope crest. However, vertical displacements have occurred mostly at lower part of the slope, opposite side of slope surface. The displacements are mostly vertical and the coordinates of the maximum vertical displacements are between -60-20 mms in X direction and between 160-200 mms in Y direction.

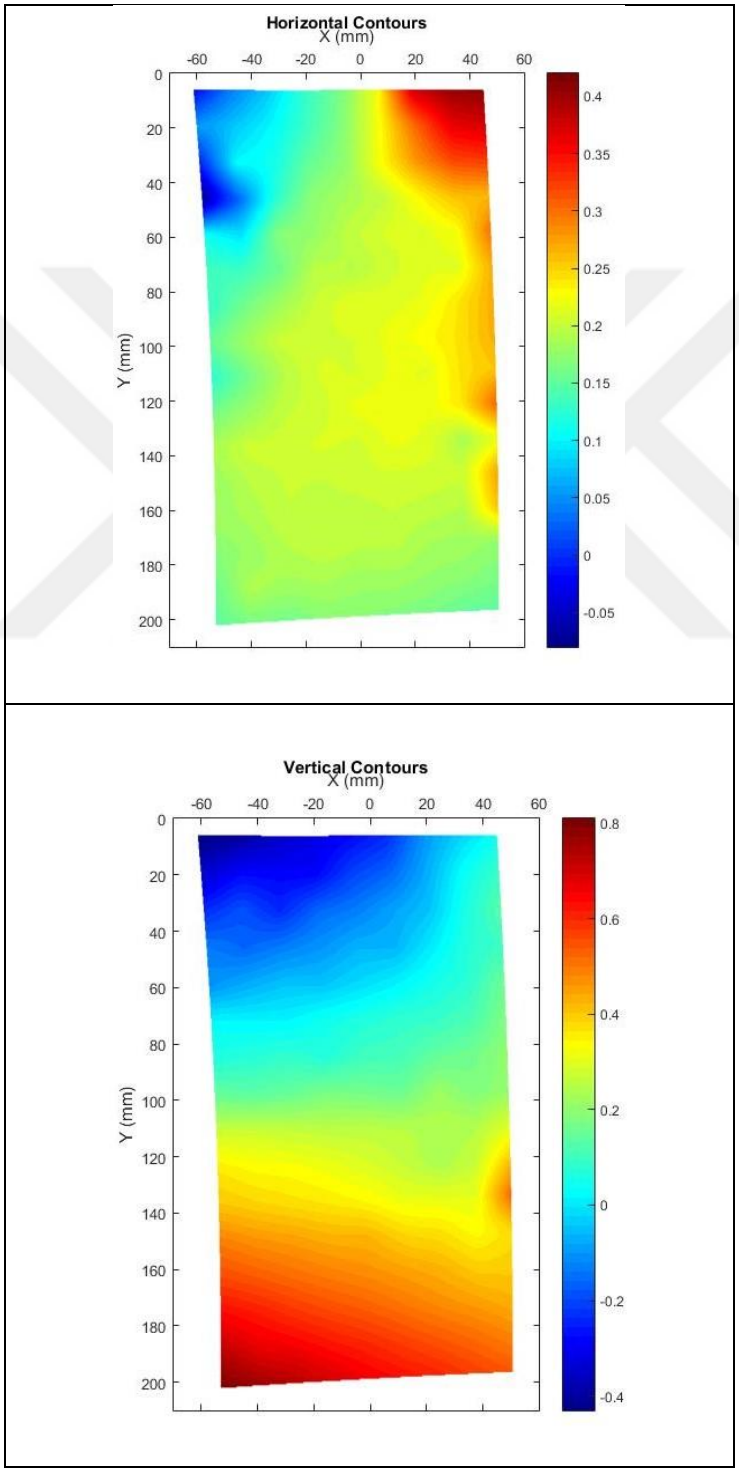

Figure 5.32 : Contours of vertical and horizontal displacement.

Figure 5.33 shows the contours of shear strain of the slope (10 seconds and 60 seconds before the failure). According to Figure 5.30, soil failure was initiated at lower part and at upper part of the slope, opposite side of slope surface. Strain concentration are mostly at lower part of the slope, opposite side of slope surface and at slope crest.

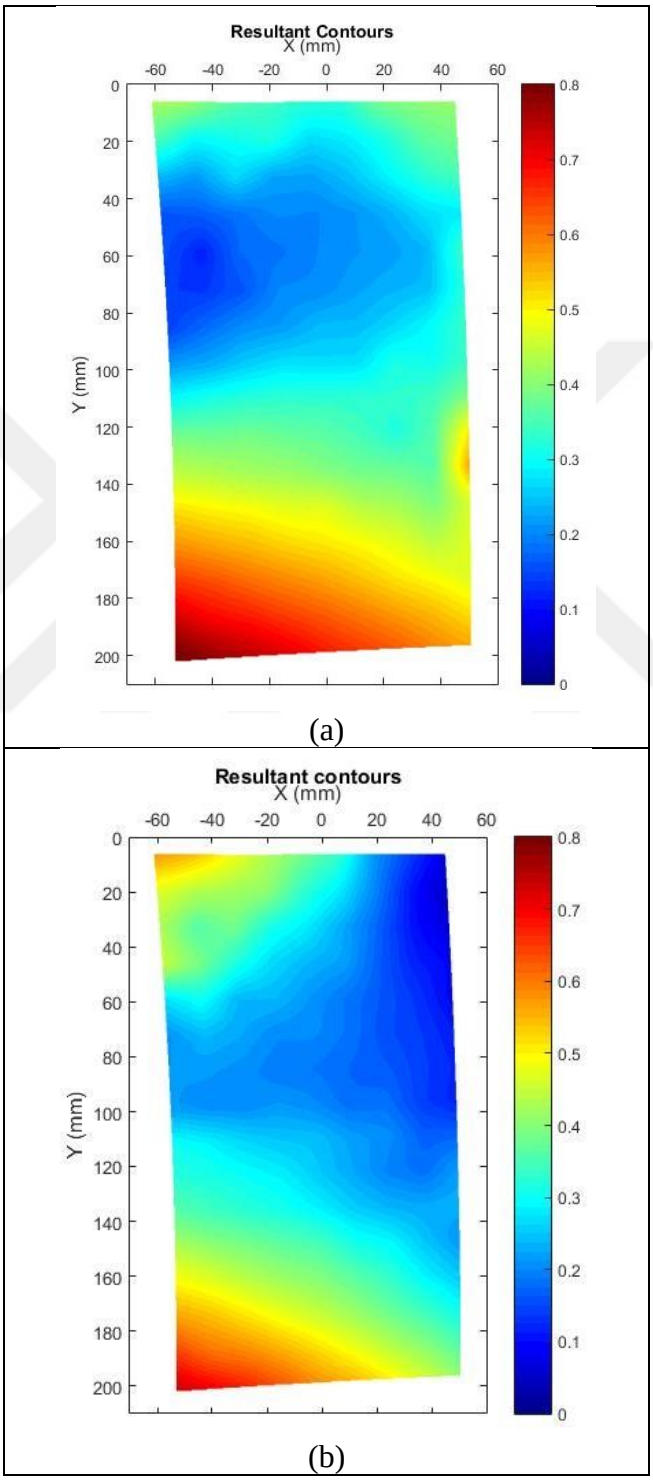

Figure 5.33 : Contours of shear strains, a) 10 seconds before the failure, and b) 60 seconds before the failure.

5.2.2.4 Experiment 8

The properties of experiment 8 is shown in Table 5.10.

Table 5.10 : The properties of experiment 8.

Test No.	Soil Type	Cement content (%)	Water content (%)	Slope model height (cm)	Relative Density (%)	slope inclination	Acceleration at Failure (g)
8	S2	3	5	30	40	90°	57.2

The first frame, the last frame (10 seconds before the failure.), and frame of failure are shown in Figure 5.34.

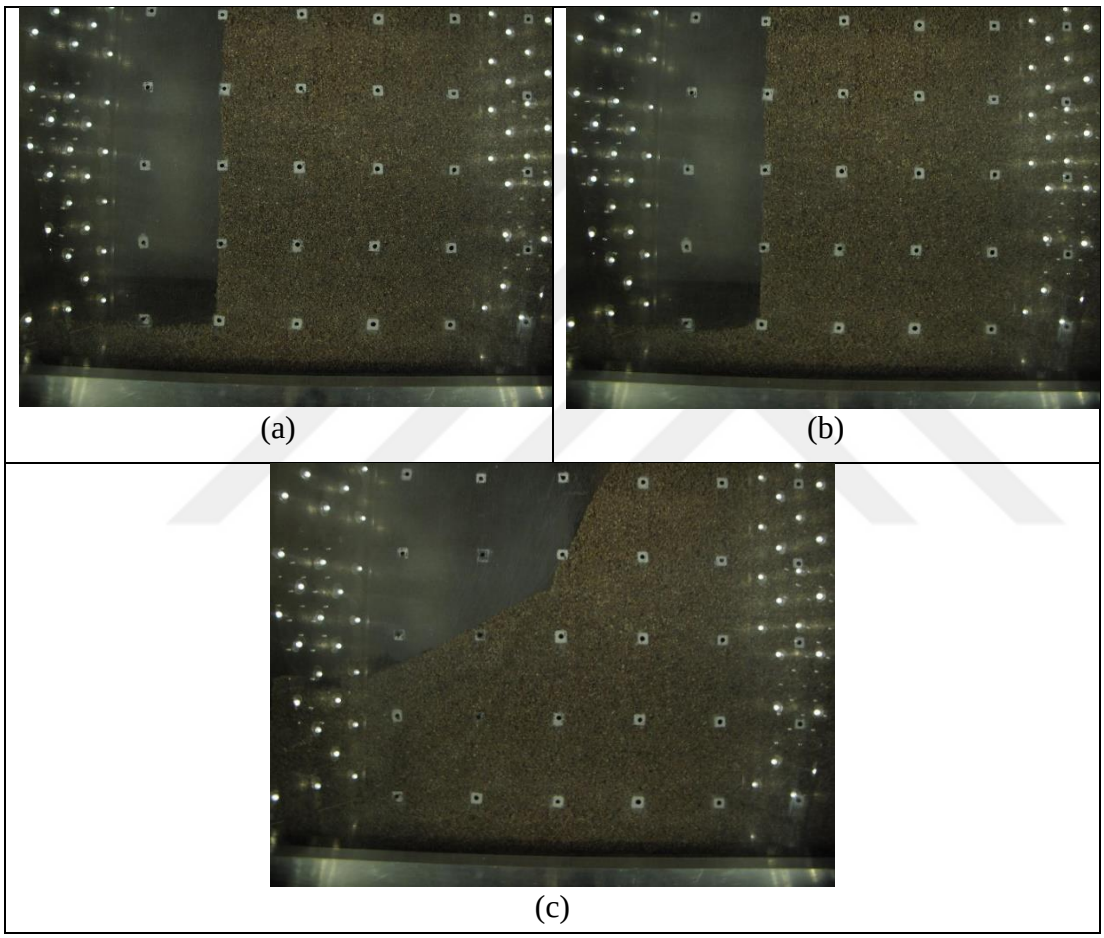

Figure 5.34 : Soil model at a) start of the test, b) 10 seconds before the failure, and c) failure.

In order to observe the displacements, the vectors of displacement at slope crest, near the slope surface were magnified and are shown in Figure 5.35.

Horizontal and vertical contours of displacements at maximum acceleration are shown in Figure 5.36. Maximum horizontal displacement has occurred at slope crest with a quantity of 0.47 mm. However, the maximum vertical displacement has occurred at upper layer of the slope between -20-0 mms in Y direction with a quantity of 0.9 mms.

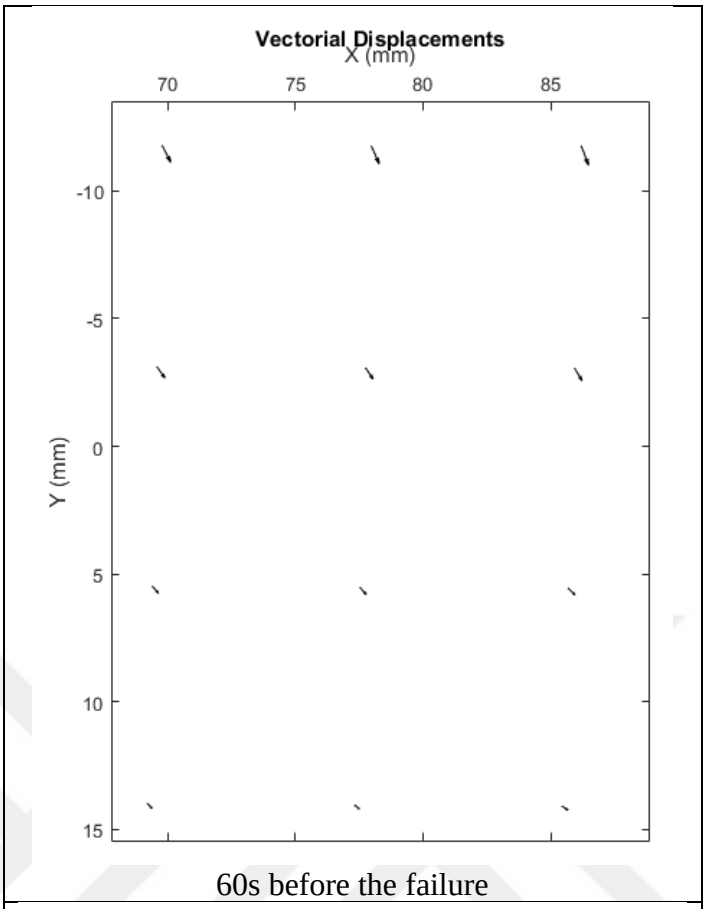

60s before the failure

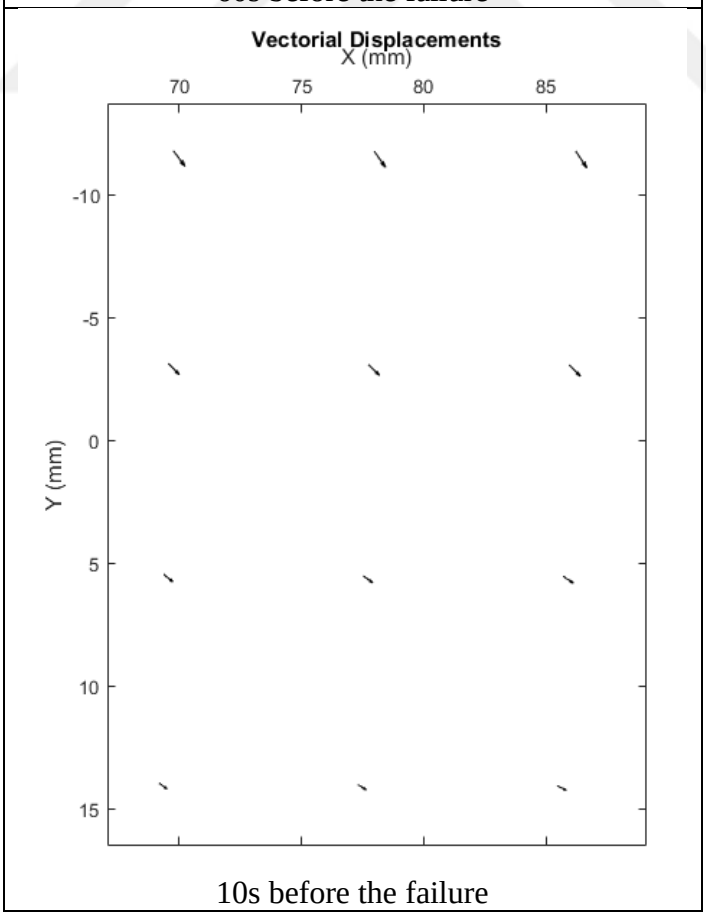

10s before the failure

Figure 5.35 : Magnified vector field of soil displacement.

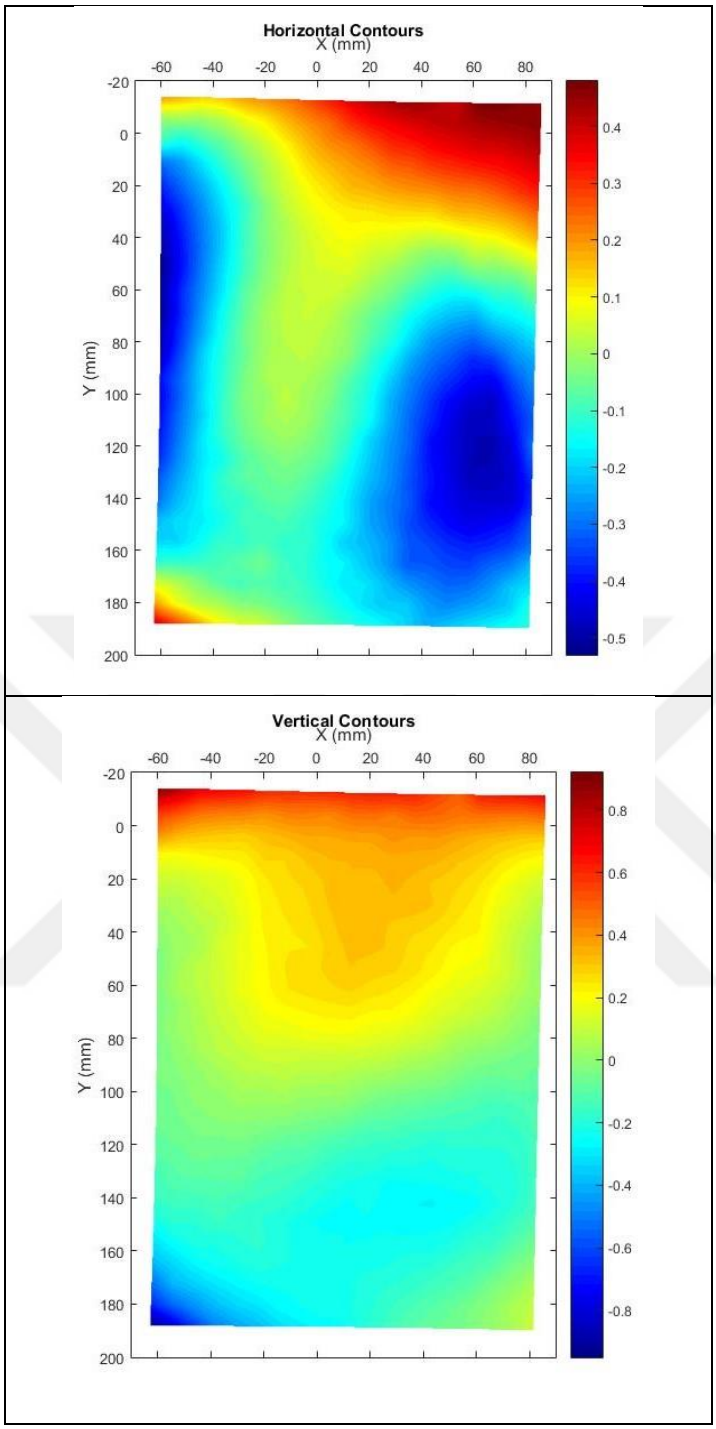

Figure 5.36 : Contours of vertical and horizontal displacement.

Figure 5.37 shows the contours of shear strain of the slope (10 seconds and and 60 seconds before the failure). The soil failures are close to the slope crest.

Strain concentration is at upper part of slope, between -60-85 mms in X direction and between -20-0 mms in Y direction.

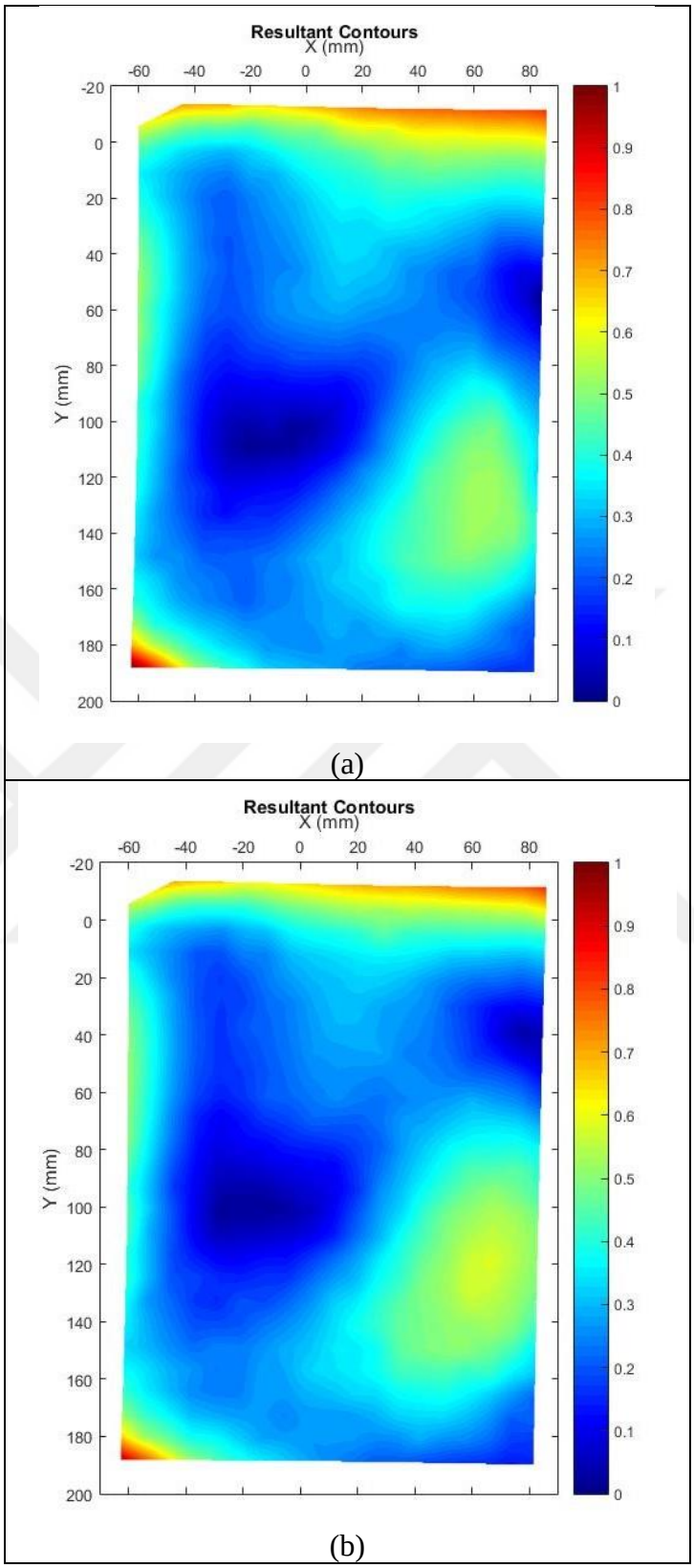

Figure 5.37 : Contours of shear strains, a) 10 seconds before the failure, and b) 60s before the failure.

5.3 Summary of Results

According to results, increasing slope inclination, decreased the required acceleration of centrifuge to cause failure of the slopes.

By comparing results of experiment 9 and 8 (slopes with S2 and different inclination), it can be easily seen that the failure of the slope is very much different from each other. By increasing slope inclination, displacements amount increased from 0.25 mm to 1 mm in slopes with S2. In addition, increasing the slope inclination caused failure of the slope; required acceleration of centrifuge to cause failure of the slope has reduced. Unlike test 9 (70° slope with S2), the displacements in test 8 (90° slope with S2), are mostly vertical. Slope models with S2 (both 70° and 90°) have failed catastrophically. Soil deformations of the slopes with S1 (both 70° and 90°) has the same properties. The deformations were observed along the slope crest. Below results for slopes with 70° and 90° inclination are summarized.

Slopes with 70° inclination

- By comparing results of experiment 6, which is non-cemented soil, by other experiments we can see that the soil displacement and shear strain were reduced in cemented soil slopes.
- By comparing the results of experiments 1 and 6, as the slope height is the same in both tests, it is observed that maximum shear strain reduced from 18 mm to 2.5 mm by adding 3% cement to the soil.
- In all the slope models with S1, the slope started to fail from the upper side of the slope, near to the slope crest and then it continues to the surface of the slope.
- In experiment 9 (slope model with S2), the slope started to fail from the middle height of the slope, near the slope surface.
- By comparing results of experiments 2 and 4, it is concluded that by increasing relative density, soil displacement and shear strain were reduced. The maximum shear strain was reduced from 0.57 mm to 0.1 mm, when the relative density of soil 1 (S1) was increased from 72% to 77%.
- The displacements amounts were less in slope model with S2, when compared to slope model with S1.

- The failure mechanism was same in all the slope models with S1. In addition, the location of the slope failures is not changing in cemented and non-cemented slope models.
- Comparing results of experiments 1 and 4, increasing the height of the slope by 10 cm, resulted failure in slope at lower acceleration of geotechnical centrifuge. The maximum displacement amount in experiment 4 is less, when compared to experiment 1. The reason is low maximum acceleration of experiment 4 (86G), when the acceleration in experiment 1 is 95G.
- By observing contours of vertical and horizontal displacement, it can be concluded that, the slope models with S1 and relative density of 72%, have mostly vertical displacements. However, the displacements in experiment 2 (S1 and relative density of 77%) were mostly horizontal. The maximum horizontal and vertical amount was same in experiment 9 (slope model with S2 and relative density of 40%).

Slopes with 90° inclination

- Despite the slopes with inclination of 70 degrees, soil displacement and shear strain were not reduced in cemented slopes. The reason is that acceleration at failure of non-cemented slope is too low (12.8 g), when compared to cemented tests. In addition, the height of slope in non-cemented slope model is less when compared to other tests.
- According to test 5 (slope model with S1), the slope started to fail from the slope crest and then it continues to the whole part of the slope. The displacements are more at upper part of the slope.
- According to experiment 7 (non-cemented slope with S1), slope started to fail from lower part and at upper part of the slope, opposite side of slope surface.
- Horizontal displacements in both cemented and non-cemented slopes with S1 are at slope crest and near to the slope surface.
- The direction of displacement vectors has changed in non-cemented slope with S1.
- In slope model with S2 (test 8), soil failures are close to slope crest. The horizontal displacements are close to slope crest. Vertical displacements have occurred at upper layer of slope; between -20-0cms in Y direction and tends to develop to lower parts of the slope.

- Horizontal displacement location in all slopes with S1 is same.
- Comparing results of experiments 3 and 5, increasing the model height of the slope by 5cm, reduced required acceleration of centrifuge at failure from 59.5 G to 48.2 G. In addition, increasing the slope height by 5cm, increased maximum displacement from 0.6 mms to 2 mms.
- By observing contours of vertical and horizontal displacement, it can be concluded that, in all slope models with inclination of 90 degrees, the amount of maximum vertical displacement is more than the amount of maximum horizontal displacement.
- Adding cement to slope increased the required acceleration of centrifuge at failure of the slope. In addition, cement stabilized displacements of soil particles; since direction of soil particle displacement is changed in non-cemented slope model.

6. CONCLUSIONS AND RECOMMENDATIONS

6.1 Interpretation of the Results

Particle Image Velocimetry (PIV) method was used in this research to reveal the failure mechanisms of the cemented soil slopes. The results are the visual observation of failure mechanism in 10 seconds intervals just before the failure of the slope. According to the analysis results, soil particle displacement was much lower in cement-stabilized models than in non-cemented models. By adding 3% cement to soil slope models, amount of soil particle displacements was decreased from 18mm down to 1.4 mm. In addition, using PIV method along with geotechnical centrifuge tests was found very valuable and useful to study displacement and deformation behavior of the soil slopes.

The variables of centrifuge testing of slope models are:

(1) slope inclination (70º and 90º)

(2) soil type (S1 and S2)

(3) relative density (77%, 72% and 40%)

(4) height of slope models (25, 30, 35 cm)

Table 6.1 presents the summary of experiment results. Maximum prototype displacements and prototype height were back-calculated according to maximum centrifuge acceleration that the model experienced.

Table 6.1 : Summary of experiment results.

Test No.	Soil Type	C (%)	W (%)	h_m (m)	Dr (%)	β	Centrifuge acceleration (g)	h_p (m)	MMD (mm)	MPD (m)	D/H (%)
1	S1	3	6.7	0.25	72	70°	95	23.75	2.5	0.237	1.000
2	S1	3	6.7	0.35	77	70°	95	33.25	0.1	0.010	0.029
3	S1	3	6.7	0.35	72	90°	48.2	16.87	2	0.096	0.571
4	S1	3	6.7	0.35	72	70°	85.9	30.07	0.57	0.049	0.163
5	S1	3	6.7	0.30	72	90°	59.5	17.85	0.6	0.036	0.200
6	S1	0	6.7	0.25	72	70°	35	8.75	18	0.630	7.200
7	S1	0	6.7	0.25	72	90°	12.8	3.20	0.8	0.010	0.320
8	S2	3	5	0.30	40	90°	57.2	17.16	1	0.057	0.333
9	S2	3	5	0.30	40	70°	95	28.50	0.3	0.029	0.100

h_m = slope model height, Dr= Relative Density, β = Slope inclination, h_p =Prototype height, C = cement content, W = water content, MMD= Max Model Displacement, MPD= Max Prototype Displacement, D/H= ratio of displacement to height.

Figure 6.1 shows the variation of acceleration of geotechnical centrifuge according to slope inclination, relative density and height of the slope model for cemented slopes with S1. (tests 1 to 5). According to Figure 6.1, required acceleration of centrifuge has decreased by increasing the slope height and inclination. The acceleration of centrifuge didn't change by increasing the relative density of soil; because the centrifuge acceleration was limited to 95g in this research. For the same reason, there was no failure in some slopes. However, by increasing the relative density the maximum displacements of soil have reduced from 0.5 mm to 0.1 mm.

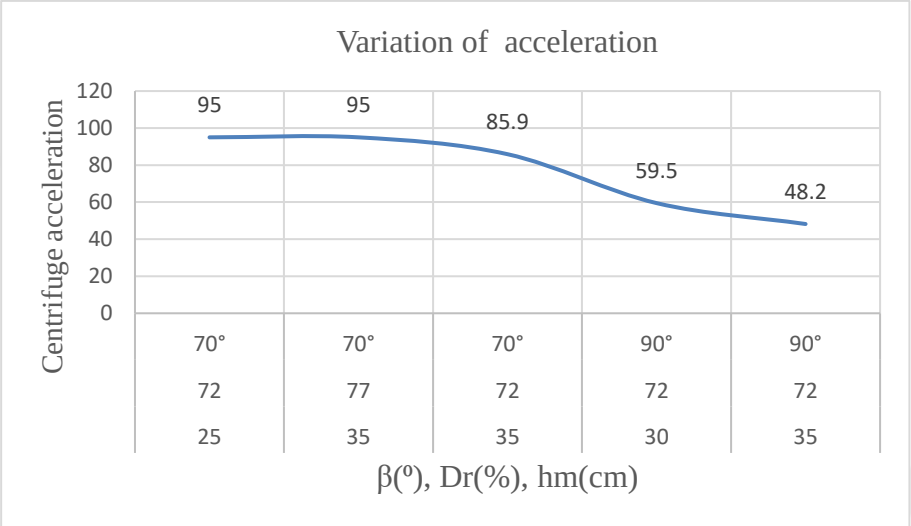

Figure 6.1 : Variation of centrifuge acceleration for the tests 1 to 5.

The obtained values of centrifuge acceleration in rpm are shown in Table 6.2. According to results, by increasing the height and slope inclination, the required acceleration of centrifuge has reduced. In addition, adding 3% cement to slopes delayed the time of failure of the slopes and increased the required acceleration of the centrifuge.

Table 6.2 : Centrifuge test results in RPM.

Test No.	Soil Type	Cement content (%)	Slope model height (cm)	Relative Density (Dr) (%)	slope inclination	Acceleration at Failure (rpm)
1	S1	3	25	72	70°	>274
2	S1	3	35	77	70°	>274
3	S1	3	35	72	90°	182
4	S1	3	35	72	70°	243
5	S1	3	30	72	90°	203
6	S1	0	25	72	70°	155
7	S1	0	25	72	90°	94
8	S2	3	30	40	90°	198.4
9	S2	3	30	40	70°	>274

6.2 Conclusions

A series of cemented soil slope models were tested in a geotechnical centrifuge to identify the possible failure mechanisms. The variables considered in the centrifuge study were the slope inclinations, soil type, relative density, and height of slope models. All the tests were conducted according to self-weight of the slopes by increasing the acceleration of geotechnical centrifuge. Acceleration was increased until the slope models failed. However, the maximum acceleration of centrifuge was 95g and in some tests, there was no failure. PIV method was used in this study. According to results:

- Soil displacement and shear strain have reduced in cemented soil slopes.
- Geotechnical centrifuge acceleration at failure has increased by adding cement in slope models.
- The required acceleration of the centrifuge at slope failure has decreased with increasing slope inclination.
- By increasing slope inclination, displacements amount has increased .
- Slope models with S2 and non-cemented slope models have failed catastrophically.
- Soil deformations of the slopes with S1 has the same properties. The deformations were observed along the slope crest.
- By increasing relative density, soil displacement and shear strain have reduced.
- In slopes with 70º inclination, the location of the slope failures is not changing in cemented and non-cemented slope models.
- Increasing the height of the slope, resulted failure in slope at lower acceleration of geotechnical centrifuge.
- By increasing the slope height, maximum displacements amount has increased.
- Using PIV method along with geotechnical centrifuge tests was found very valuable and useful to study displacement and deformation behavior of the soil slopes.

6.3 Future Researches

There was no failure in some of the slopes in this research. The reason is that the acceleration of geotechnical centrifuge was limited to 95g. Using a centrifuge with high acceleration value gives the possibility of failure, so that the exact dimensions of the prototypes can be obtained and compared with each other. In addition, it helps to find out more about the failure mechanism of the slopes. If the model is bigger, it can be a chance to see the deformation of the lower parts of slope in the PIV analysis. Cleaning the plexiglass is important for image analysis by PIV. In addition, if wire meshes or erosion mats or vegetation are applied over the slope face, the results would be better. For future researches:

- LVDT (Linear Variable Differential Transformer) Transducer can be used to measure axial displacements in slope models.
- Slopes can be loaded with different types of foundation loads and the results will be evaluated.
- The soils can be improved with fly ash, lime or geosynthetics.
- Slopes with different inclinations can be studied.
- The acceleration can be increased to a certain value and then a static load can be applied on slope to evaluate the slope behavior.

REFERENCES

Abramson, L., Lee, T., Boyce, G., & Sharma, S. (2002). *Slope stability and Stabilisation Methods*. John Wiley & Sons, Inc.

Aklik, Pelin. (2012). *Model tests of geosynthetic reinforced slopes in a geotechnical centrifuge*. (Doctoral dissertation). University of Natural Resources and Applied Life Sciences, VIENNA.

Aklik, P, & Wu, W. (2013). Centrifuge model tests on foundation on geosynthetic reinforced slope. *Proceedings of the 18th International Conference on Soil Mechanics and Geotechnical Engineering*, 875–878.

Ansaripour, M. (2014). *Investigation of load deflection behavior in sand soil using PIV technique and zero extension line mesh*. (Master's thesis). Shiraz University, SHIRAZ.

Arya, I. W., Wiraga, I. W., & Suryanegara, I. G. A. G. (2018). Effect of cement injection on sandy soil slope stability, case study: slope in Petang district, Badung regency. *Journal of Physics: Conference Series*, *953*(1), 012103. https://doi.org/10.1088/1742-6596/953/1/012103

Azzouz, A., Baligh, M., & Ladd, C. (1981). Three-dimensional stability analysis of four embankment failures. *Proceedings of the 10th International Conference on Soil Mechanics and Foundation Engineering*, 343–346.

Baba, K., Bahi, L., Ouadif, L., & Akhssas, A. (2012). Slope Stability Evaluations by Limit Equilibrium and Finite Element Methods Applied to a Railway in the Moroccan Rif. *Open Journal of Civil Engineering*, *02*(01), 27–32. https://doi.org/10.4236/ojce.2012.21005

Barbir, O., & Mathews, J. (2016). Investigation of the influence of gravity on granular flow using silo centrifuge model. *25th European Young Geotechnical Engineers Conference.*

Chen, R. H., & Chameau, J. L. (1983). Three-dimensional limit equilibrium analysis of slopes. *Géotechnique*, *33*(1), 31–40. https://doi.org/10.1680/geot.1983.33.1.31

Cheng, Z., Ding, J., Rao, X., Cheng, Y., & Xu, H. (2013). Physical model tests of expansive soil slope. *Geotechnical Special Publication*, *231 GSP*, 731–740.

Collins, B. D., & Sitar, N. (2011). Stability of Steep Slopes in Cemented Sands. *Journal of Geotechnical and Geoenvironmental Engineering*, *137*(1), 43–51. https://doi.org/10.1061/(ASCE)GT.1943-5606.0000396

Costa, C. M. L., Zornberg, J. G., & Costa, Y. D. J. (2013). Failure of Geotextile-Reinforced Walls in Centrifuge Model Tests. *Advanced Materials Research*, *831*, 321–325. https://doi.org/10.4028/www.scientific.net/AMR.831.321

Daraei, A., Herki, B. M. A., Sherwani, A. F. H., & Zare, S. (2018). Slope Stability in Swelling Soils Using Cement Grout: A Case Study. *International Journal of Geosynthetics and Ground Engineering*, *4*(1), 10. https://doi.org/10.1007/s40891-018-0127-9

Duncan, J. M., Wright, S. G., & Brandon, T. L. (2014). *Soil Strength and Slope Stability*. John Wiley & Sons, Inc.

Elfass, S. A., Aczel, R., Norris, G. M., & Jacobson, E. (2006). Physical and Numerical Modeling of Rock Joints and Slope Stability. *GeoCongress 2006: Geotechnical Engineering in the Information Technology Age*, 274. https://doi.org/10.1061/40803(187)274

Ertan, T. (2012). *The investıgatıon of stabılity of tunnels and settlements with centrifuge modelling*. (Master's thesis). Istanbul Technical University, ISTANBUL.

Ertan, T, Wu, W., Erken, A., & Idinger, G. (2012). The investıgatıon of stability of tunnels and settlements with centrifuge modelling. *ISCE - International Student Conference of Civil Engineering.*

Evirgen, B., Tuncan, M., & Fırat, M. (2017). Modelling Study on the Geotextile, Geogrid and Steel Strip Reinforced Slopes. *Çukurova University Journal of the Faculty of Engineering and Architecture*. *32*, 227–240.

Han, J., Sheth, A. R., Porbaha, A., & Shen, S.-L. (2004). Numerical Analysis of Embankment Stability over Deep Mixed Foundations. *Geotechnical Engineering for Transportation Projects*, 1385–1394. https://doi.org/10.1061/40744(154)128

Hayward, T., Lees, A. S., Powrie, W., Richards, D. J., & Smethurst, J. (2000). Centrifuge modelling of a cutting slope stabilised by discrete piles. (Report No. 471). Berkshire : Transport Research Laboratory.

Hedayati, M. K. (2012). *Study on the effect of use of geosynthetics on the failure mechanism and bearing capacity of surface foundation by using of centrifuge model tests*. (Master's thesis). Tehran University, TEHRAN.

Heikkila, J., & Silven, O. (1997). A four-step camera calibration procedure with implicit image correction. *Proceedings of IEEE Computer Society Conference on Computer Vision and Pattern Recognition*, 1106–1112. https://doi.org/10.1109/CVPR.1997.609468

Hovland, H. J. (1978). Three-dimensional slope stability analysis method. *International Journal of Rock Mechanics and Mining Sciences & Geomechanics Abstracts*, *15*(1), A17. https://doi.org/10.1016/0148-9062(78)90889-6

Idinger, G. (2016). *Experimental study on failure initiation in partially saturated slopes*. (Doctoral dissertation). University of Natural Resources and Applied Life Sciences, VIENNA.

Idinger, G., Aklik, P., Wu, W., & Borja, R. I. (2011). Centrifuge model test on the face stability of shallow tunnel. *Acta Geotechnica*, *6*(2), 105–117. https://doi.org/10.1007/s11440-011-0139-2

Kitazume, M., & Takeyama, T. (2013). Centrifuge Model Tests on Influence of Slope Height on Stability of Soft Clay Slope. *Geo-Congress 2013*, *231 GSP*, 2094–2097. https://doi.org/10.1061/9780784412787.212

Knappett, J. A., Haigh, S. K., & Madabhushi, S. P. G. (2006). Mechanisms of failure for shallow foundations under earthquake loading. *Soil Dynamics and Earthquake Engineering*, *26*(2–4), 91–102.

https://doi.org/10.1016/j.soildyn.2004.11.021

Koerner, R. M., & Soong, T.Y. (2001). Geosynthetic reinforced segmental retaining walls. *Geotextiles and Geomembranes*, *19*(6), 359–386.

Li, B., Yu, W., Gong, B., & Cheng, Z. (2013). Centrifugal and Numerical Modeling of High and Steep Geosynthetic-Reinforced Slopes. *Geo-Congress 2013, 231 GSP*, 482–488. https://doi.org/10.1061/9780784412787.050

Ling, H., & Ling, H. I. (2012). Centrifuge model simulations of rainfall-induced slope instability. *Journal of Geotechnical and Geoenvironmental Engineering*, *138*(9), 1151–1157. https://doi.org/10.1061/(ASCE)GT.1943-5606.0000679

Ling, H. I., Wu, M.-H., Leshchinsky, D., & Leshchinsky, B. (2009). Centrifuge Modeling of Slope Instability. *Journal of Geotechnical and Geoenvironmental Engineering*, *135*(6), 758–767. https://doi.org/10.1061/(ASCE)GT.1943-5606.0000024

Ling, H. I., Xu, L., Leshchinsky, D., Collin, J. G., & Rimoldi, P. (2016). Centrifugal Modeling of Reinforced Soil Retaining Walls Considering Staged Construction. *Geosynthetics, Forging a Path to Bona Fide Engineering Materials*, *1*, 95–105. https://doi.org/10.1061/9780784480182.009

Luo, F., Huang, R., & Zhang, G. (2018). Centrifuge modeling of the geogrid reinforced slope subjected to differential settlement. *Acta Geotechnica.*

Mamaghanian, J., Razeghi, H. R., Viswanadham, B. V. S., & Manikumar, C. H. S. G. (2018). Behaviour of geogrid reinforced soil walls with marginal backfills with and without chimney drain in a geotechnical centrifuge. *9th International Conference in Physical Modelling in Geotechnics*,

Mandal, J. N., Kumar, S., & Meena, C. L. (2005). Centrifuge Modeling of Reinforced Soil Slopes Using Tire Chips. *Geotechnical Special Publication*, *52*(10), 2695–2702. https://doi.org/10.1061/40787(166)7

Nasiri, M. (2015). *Experimental study of earth slope reinforced using geotextileencased stone column*. (Master's thesis). Razi University, KERMANSHAH.

Nayler, J., & Frazer, R. (1917). Vortex motion. Preliminary report upon an experimental method of investigating, by the aid of cinematographic photography, the history of eddying flow past a model immersed in water, Rep. *Memo. Advis. Comm. Aeronaut*, 18-25.

Park, D. S., & Kutter, B. L. (2012). Centrifuge Tests for Artificially Cemented Clay Slopes. *Geotechnical Special Publication*, 2027–2036. https://doi.org/10.1061/9780784412121.208

Schofield, A. N. (1980). Cambridge Geotechnical Centrifuge Operations. *Géotechnique*, *30*(3), 227–268. https://doi.org/10.1680/geot.1980.30.3.227

Schofield, A. N. (1981). Dynamic and Earthquake Geotechnical Centrifuge Modelling. *International Conferences on Recent Advances in Geotechnical Earthquake Engineering and Soil Dynamics*, 1081–1100.

Seed, R. B., Mitchell, J. K., & Seed, H. B. (1990). Kettleman Hills Waste Landfill

Slope Failure. II: Stability Analyses. *Journal of Geotechnical Engineering*, *116*(4), 669–690. https://doi.org/10.1061/(ASCE)0733-9410(1990)116:4(669)

Sitar, N., Clough, G. W., & Bachus, R. G. (1980). Behavior of weakly cemented soil slopes under static and seismic loading conditions (Final Report). Stanford: John A. Blume Earthquake Engineering Center.

Stanier, S. A., Blaber, J., Take, W. A., & White, D. J. (2016). Improved image-based deformation measurement for geotechnical applications. *Canadian Geotechnical Journal*, *53*(5), 727–739. https://doi.org/10.1139/cgj-2015-0253

Taylor, R. N. (1995). *Geotechnical centrifuge technology*. Blackie Academic & Professional.

Terzaghi, K. (1943). *Theoretical Soil Mechanics*. Wile.

Tsuchida, T., & Athapaththu, A. M. R. G. (2014). Practical slip circle method of slices for calculation of bearing capacity factors. *Soils and Foundations*, *54*(6), 1127–1144. https://doi.org/10.1016/j.sandf.2014.11.008

Ugai, K. (1988). Three dimensional slope stability analysis by slice methods. *6th International Conference on Numerical Methods in Geomechanics*, 1369–1374.

Viswanadham, B. V. S. (2019). Centrifuge Model Studies on the Performance of Geosynthetic-Reinforced Soil Structures. In M. Latha G. (Ed.), *Coastal Engineering* (Vol. 3, pp. 157–182). Springer Singapore. https://doi.org/10.1007/978-981-13-5871-5_9

Viswanadham, B. V. S., & König, D. (2009). Centrifuge modeling of geotextile-reinforced slopes subjected to differential settlements. *Geotextiles and Geomembranes*, *27*(2), 77–88. https://doi.org/10.1016/j.geotexmem.2008.09.008

Viswanadham, B. V. S., & Mahajan, R. (2004). Modeling of Geotextile Reinforced Highway Slopes in a Geotechnical Centrifuge. *Geotechnical Engineering for Transportation Projects*, 637–646. https://doi.org/10.1061/40744(154)50

Viswanadham, B. V. S., & Mahajan, R. R. (2007). Centrifuge model tests on geotextile-reinforced slopes. *Geosynthetics International*, *14*(6), 365–379. https://doi.org/10.1680/gein.2007.14.6.365

White, D., & Take, A. (2002). GeoPIV: Particle Image Velocimetry (PIV) software for use in geotechnical testing. *Cambridge University Engineering Department Technical Report*, *322*(October), 15.

White, D., Take, A., & Bolton, M. (2001). Measuring soil deformation in geotechnical models using digital images and PIV analysis. *10th International Conference on Computer Methods and Advances in Geomechanics*.

White, D., Take, A., & Bolton, M. (2003). Soil deformation measurement using particle image velocimetry (PIV) and photogrammetry. *Géotechnique*, *53*(7), 619–631. https://doi.org/10.1680/geot.53.7.619.37383

Yamamoto, K., & Kusuda, K. (2001). Failure mechanisms and bearing capacities of reinforced foundations. *Geotextiles and Geomembranes*, *19*(3), 127–162. https://doi.org/10.1016/S0266-1144(01)00003-6

Zhao, Y., Zhang, G., Hu, D., & Han, Y. (2018). Centrifuge Model Test Study on Failure Behavior of Soil Slopes Overlying the Bedrock. *International Journal of Geomechanics*, *18*(11), 04018144. https://doi.org/10.1061/(ASCE)GM.1943-5622.0001292

Zornberg, J. G., & Arriaga, F. (2003). Strain Distribution within Geosynthetic-Reinforced Slopes. *Journal of Geotechnical and Geoenvironmental Engineering*, *129*(1), 32–45. https://doi.org/10.1061/(ASCE)1090-0241(2003)129:1(32)

CURRICULUM VITAE

Name Surname **: Hesam Ebrahimisadr**

Place and Date of Birth **: Tabriz, Iran 1993.03.14**

E-Mail **: ebrahimisadr17@itu.edu.tr**

EDUCATION **:**

- **B.Sc.** **:** 2016, IAUT, Civil Engineering Department

PROFESSIONAL EXPERIENCE AND REWARDS:

- 2014-2015 Azad University of Tabriz, American Concrete Institute competitions.
- 2015-2016 Civil Engineer at Isargaran Company. Tabriz, Iran

PUBLICATIONS, PRESENTATIONS AND PATENTS ON THE THESIS:

- **Ebrahimisadr H.** Stability Analysis of Cemented Soil Slopes In A Geotechnical Centrifuge. Graduate Thesis And Project Research Poster Day, July 1, 2020 Istanbul, Turkey.